

Two-Dimensional Separation via Hybrid Liquid Chromatography and Differential Ion Mobility Spectrometry for PFAS Characterization

by

Christopher Robbin Makanakealoha Ryan

A thesis
presented to the University of Waterloo
in fulfillment of the
thesis requirement for the degree of
Master of Science
in
Chemistry

Waterloo, Ontario, Canada, 2024

© Christopher Robbin Makanakealoha Ryan 2024

Author's Declaration

This thesis consists of material all of which I authored or co-authored: see Statement of Contributions included in the thesis. This is a true copy of the thesis, including any required final revisions, as accepted by my examiners. I understand that my thesis may be made electronically available to the public.

Statement of Contributions

Chapter 4 and **Appendix A** incorporate sections of a manuscript which is ready for submission titled

“Two-Dimensional Hybrid LC×DMS Analysis of 34 PFAS Compounds” with coauthors as listed:

Christopher R. M. Ryan

Emir Nazdrajić

J. Larry Campbell

Kati Bell

Domenico Santoro

W. Scott Hopkins

Abstract

This thesis details the development and implementation of differential mobility spectrometry (DMS) methods for the separation of per- and polyfluoroalkyl substances (PFAS). PFAS have become ubiquitous environmental pollutants, posing significant risks to ecosystems and human health. The complexity of PFAS matrices in environmental samples necessitates separation prior to mass spectrometric analysis because co-elution of compounds can cause ion suppression and compromise analyte identification and quantification accuracy. Although liquid chromatography (LC) is commonly used in PFAS analyses, some PFAS species co-elute and could benefit from an additional orthogonal dimension of separation.

In **Chapter 3** I explore the effects of solvent modifier on DMS behaviour for 224 compounds in negative mode electrospray ionization (ESI) mass spectrometry (MS). The data procured from these measurements will be used for machine learning (ML) purposes to predict the DMS behaviour of emerging environmental pollutants. Prior to this study, our library of DMS data was composed entirely of compounds that were measured in positive mode ESI MS and the distribution of observed dispersion behaviour was heavily skewed towards one behaviour type. Incorporation of the negative mode ESI data not only provided a better overall distribution of dispersion behaviour, but also allows for future ML models to be applicable for anions and cations alike. The results of this chapter also provide insight into the ion-neutral interactions that occur as analytes transit the DMS cell. From this it can be determined how different classes of compounds interact with various solvent modifiers, and how their analytical separation is influenced by the choice of modifier. This allowed us to determine the instrument conditions that lead to the optimal separation of the studied PFAS.

In **Chapter 4**, I utilize the optimal separation conditions determined in **Chapter 3** in a hybrid LC×DMS-MS² method. Here, I employ DMS following LC separation to analyse 34 PFAS species. Upon incorporating DMS in a 2D separation scheme, I observed baseline resolution of 29 compounds in the 2D space, with only two and three compounds co-eluting, respectively. In comparison, only 5

compounds were baseline resolved in 1-dimensional LC experiments. Because DMS measurements are acquired within seconds, targeted 2D LC×DMS-MS² analyses operate on the same timescale as 1D LC-MS² analysis. Additionally, limits of quantitation approach those observed in state-of-the-art LC-MS² methods. Moreover, distinct trends observed in the 2D separation space for the various PFAS subclasses could enable analyte identification in future non-targeted analyses.

Acknowledgements

Completing this degree has been a transformative journey, made possible by the support and guidance of several individuals who have enriched my academic path.

First and foremost, I extend my deepest gratitude to my supervisor and mentor, Prof. W. Scott Hopkins. Your support, guidance, and leadership have been instrumental throughout this degree. Your mentorship has not only shaped my understanding of DMS but has also inspired me to pursue excellence in every aspect of my academic and professional endeavors. I am also thankful to my committee members, Dr. Richard Smith and Prof. Anh Pham. Your expertise and commitment to academic excellence have been crucial in refining my research.

Dr. J. Larry Campbell, your knowledge of DMS and MS has been pivotal in shaping the technical aspects of my work. Your insights and advice have been invaluable. Dr. Emir Nazdrajić, your technical expertise and willingness to fix broken instruments have been a lifesaver. Your friendship and support have been immensely appreciated.

Dr. Alexander Haack, your mentorship and friendship from my undergraduate days have been sources of constant inspiration and encouragement. Your belief in my abilities has propelled me forward and strengthened my resolve to achieve academic excellence. Dr. Christian Ieritano, your comprehensive knowledge of DMS and patient teaching have been fundamental to my technical development and research success.

Special thanks to Anish Arjuna, and Carys Soulsby for their contributions to data collection in **Chapter 3**. Anish, your efforts and work ethic ensured thorough and reliable data. Carys, your foundational work set a strong basis for our research.

To my amazing friends in the lab, I owe you my deepest gratitude. Shannon Lemmens, your positive attitude has made all the difference in the last year. Patrick Thomas, your wise counsel has helped immensely, especially throughout the writing of this thesis. Cailum Stienstra, your advice and coding

ability has been most helpful. Arthur Lee, your IT support throughout this degree has been crucial. Justine Bissonnette, your help with data collection was invaluable.

To my wonderful parents, your unwavering love, encouragement, and sacrifices have sustained me throughout my academic pursuits. Your belief in me has been a constant source of strength and motivation.

Lastly, I would like to acknowledge Mike Stammler (Stam), my high school chemistry teacher. Your passion for chemistry ignited my own and set me on this academic path.

To all these exceptional individuals, thank you for your unwavering support, invaluable contributions, and belief in my potential. This thesis is a reflection of your collective guidance and encouragement, for which I am profoundly grateful.

Table of Contents

Author's Declaration	ii
Statement of Contributions	iii
Abstract	iv
Acknowledgements	vi
List of Figures	ix
List of Tables	xi
List of Equations	xii
List of Abbreviations	xiii
Quote	xv
Chapter 1 Introduction	1
1.1 What are PFAS?	1
1.2 Current Methods for PFAS Analysis.....	2
1.3 Scope of this Thesis.....	3
Chapter 2 Analytical Background.....	5
2.1 Liquid Chromatography	5
2.2 Fundamentals of Ion Mobility Spectrometry and Differential Mobility Spectrometry.....	7
Chapter 3 DMS Behaviour of Anions.....	13
3.1 Introduction	13
3.2 Materials and Methods	14
3.2.1 Materials	14
3.2.2 Methods	14
3.3 Results	15
3.3.1 Organic Acids and Other Small Molecules	15
3.3.2 PFAS in N ₂ and Modified Environments	25
3.4 Conclusions	30
Chapter 4 Two-Dimensional Hybrid LC×DMS Analysis of 34 PFAS Compounds	32
4.1 Introduction	32
4.2 Materials and Methods	32
4.2.1 Materials	32
4.2.2 DMS-MS ² Methods	33
4.2.3 LC-MS ² Methods.....	34
4.2.4 LC×DMS-MS ² Methods.....	34
4.3 Results and Discussion.....	36
4.3.1 LC-MS ² Separation	36
4.3.2 DMS-MS ² Separation.....	39
4.3.3 LC×DMS-MS ² Separation.....	41
4.3.4 Instrument Quantitation Limits	46
4.4 Conclusions	48
Chapter 5 Conclusions and Outlook	50
References	54
Appendix A Supplementary Information	71

List of Figures

- Figure 2.1.** Schematic depicting the CCS between a spherical ion (A) and a spherical neutral (B). The CCS of this pair can be calculated using Eq 2.2..... 8
- Figure 2.2.** A schematic showing the DMS-MS² instrument setup and the trajectory of an ion as it passes through a DMS cell. The red zig-zag trace represents an un-stable ion trajectory which occurs when the incorrect CV is applied for a given SV. The blue zig-zag trace represents a stable ion trajectory when the correct CV is applied. The purple trace represents the shape of the SV waveform as a function of time..... 10
- Figure 2.3.** DMS dispersion curves depicting Type A (red), Type B (blue) and Type C (black) behaviour. Type A behaviour is associated with strong ion-solvent clustering, Type B is associated with weak ion-solvent clustering, and Type C is associated with hard-sphere scattering or non-clustering environments. 12
- Figure 3.1.** Distribution of DMS dispersion types for 205 anionic compounds measured in a pure N₂ environment..... 17
- Figure 3.2.** Distribution of DMS dispersion types for 198 anionic compounds measured in a 1.5 mol% MeOH modified environment. 17
- Figure 3.3.** Chemical structure of deprotonated taurocholic acid..... 18
- Figure 3.4.** DMS dispersion behaviour of deprotonated pterostilbene (red), deprotonated vanillin (light blue), deprotonated hexanoic acid (purple), and deprotonated 1,5-naphthalenedisulfonic acid (green) in pure N₂ (solid line) and in N₂ containing 1.5 mol% MeOH (dashed line). The structure of each compound is shown on the right..... 19
- Figure 3.5.** Distribution of DMS dispersion types for 738 cations measured in both pure N₂ and a 1.5 mol% MeOH modified environment..... 20
- Figure 3.6.** Distribution of DMS dispersion types for 403 anions measured in both pure N₂ and a 1.5 mol% MeOH modified environment..... 20
- Figure 3.7.** Distribution of DMS dispersion types for 1141 compounds measured in both pure N₂ and a 1.5 mol% MeOH modified environment. 21
- Figure 3.8.** DMS dispersion curves for deprotonated 4-mercaptobenzoic acid measured in pure N₂. The red trace corresponds to the O-deprotomer and the yellow trace corresponds to the S-deprotomer.... 23
- Figure 3.9.** Ionogram taken at SV = 3200 V showing the two separation of the O- (red) and S- (yellow) deprotomers of 4-mercaptobenzoic acid in pure N₂. Note that the peak positions are shifted from those of the dispersion curves shown in Figure 3.8; this measurement was recorded on another DMS system several months later..... 23
- Figure 3.10.** Product ion spectra of the mobility-selected deprotomers of 4-mercaptobenzoic acid. The S-deprotomer (Panel A) has a smaller fragment-to-parent ratio than the O-deprotomer (Panel B)..... 25
- Figure 3.11.** DMS dispersion curves measured in pure N₂ for (A) PFCA species, (B) PFSA species, (C) FTCA and FTS species, and (D) fourteen PFAS from other chemical classes. Compounds whose curves abruptly end prior to the SV = 4000 V instrument limit undergo field-induced fragmentation within the DMS cell. 27
- Figure 3.12.** DMS dispersion curves measured in 1.5 mol% MeOH modifier for (A) PFCA species, (B) PFSA species, (C) FTCA and FTS species, and (D) fourteen PFAS from other chemical classes.

Compounds whose curves abruptly end prior to the SV = 4000 V instrument limit undergo field-induced fragmentation within the DMS cell. 28

Figure 3.13. DMS dispersion curves measured in 1.5 mol% IPA modifier for (A) PFCA species, (B) PFSA species, (C) FTCA and FTS species, and (D) fourteen PFAS from other chemical classes. Compounds whose curves abruptly end prior to the SV = 4000 V instrument limit undergo field-induced fragmentation within the DMS cell. The transparent area surrounding each dispersion curve represents the FWHM of the extracted ionogram at the measured SV value. In the case of panel B, the upper portion of this transparent area divided by a factor of two is displayed for ease of viewing. 29

Figure 4.1. Chromatograms showing (A) the 38 detected PFAS by monitoring total ion current, (B) the PFCA species, (C) the PFSA species, (D) the FTCA and FTS species, and (E) fourteen PFAS from other chemical classes. Note that the intensity scales are not equal across different panels. 37

Figure 4.2. Relationship between the LC retention time and the carbon chain length of the PFCA species (blue) and the PFSA species (red). 38

Figure 4.3. Ionograms taken at an SV of 3800 V showing the separation of (A) the 34 detected PFAS by monitoring total ion current, (B) the PFCA species, (C) the PFSA species, (D) the FTCA and FTS species, and (E) eleven PFAS from other chemical classes. Note that the intensity scales are not equal across panels. 40

Figure 4.4. Ionograms measured at SV = 3800 V for PFOA (left) and PFOS (right) with varying mobile phase B (MPB) composition. The optimal CV value for PFOA remains relatively constant as MPB increases, whereas that of PFOS gradually shifts to more positive values. 43

Figure 4.5. 2D LC×DMS plot showing the separation for 34 PFAS compounds. The ovals are a guide to the eye which highlight the approximate trend lines for the PFSA species (red), the PFCA species (blue), the FTS species (green), and the FTCA species (orange). Features corresponding to branched isomers (denoted by *B*) of three PFASs (PFHxS, PFHpS, and PFOS) are distinguishable from the linear species (denoted by *L*). 44

Figure 4.6. Full width at half maximum (FWHM) values for ionograms of the PFCA species (blue) and the PFSA species (red) as a function of chain length. Note that there is a linear increase in FWHM for the PFCA species, however there is a significant outlier in the PFSA trend. This outlier occurs at the 8 carbon-long chain (i.e. PFOS) and is attributed to the presence of multiple isomers which are slightly separated in DMS measurements. 46

Figure A.1. Electrostatic potential (ESP) surfaces of PFOS (left) and PFOA (right) calculated with Gaussian16 using B3LYP 6-31G(D). Note that the CO₂ headgroup of PFOA exhibits much more electron density (i.e. deeper red) than the SO₃ headgroup of PFOS. 90

List of Tables

Table 4.1 LC mobile phase gradient for PFAS analysis.....	34
Table 4.2 Instrument LOQs for 33 PFAS as determined for the 2D LC×DMS-MS ² method. LOQs were determined via seven replicate measurements.....	47
Table A.1 List of anion compound names, molecular weights, parent and fragment <i>m/z</i> and dispersion behaviour measured in N ₂ or MeOH.	71
Table A.2 List of PFAS compound classes, names, abbreviations, and which chemical standard(s) each compound is found in.	78
Table A.3 Multiple Reaction Monitoring (MRM) table of PFAS for DMS and LC experiments.....	79
Table A.4 CV-labeled MRM transitions of PFAS for LC×DMS experiments.....	81
Table A.5 CV shifts of PFAS between LC×DMS and DMS measurements.	91

List of Equations

Eq 2.1	5
Eq 2.2	7
Eq 2.3	7
Eq 2.4	9
Eq 2.5	9

List of Abbreviations

11Cl-PF3OUdS	11-chloroeicosafluoro-3-oxaundecane-1-sulfonic acid
9Cl-PF3ONS	9-chlorohexadecafluoro-3-oxanone-1-sulfonic acid
ACN	Acetonitrile
CCS	Collision cross section
CCS(T_{eff})	Effective temperature-dependent collision cross section
CV	Compensation voltage
CV _{opt}	Optimal CV for ion transmission
Da	Dalton
DMS	Differential mobility spectrometry
DTIMS	Drift tube ion mobility spectrometry
EPA	Environmental Protection Agency
ESI	Electrospray ionization
FAIMS	High-field asymmetric-waveform ion mobility spectrometry
FOSA	Perfluorosulfonamide
FOSAA	Perfluorosulfonamidoacetic acid
FTCA	Fluorotelomer carboxylic acid
FTS	Fluorotelomer sulfonate
FTUCA	Fluorotelomer unsaturated carboxylic acid
FWHM	Full width at half maximum
GenX	2,3,3,3-Tetrafluoro-2-(heptafluoropropoxy)propanoic acid
HRMS	High-resolution mass spectrometry
IMS	Ion mobility spectrometry
IPA	Isopropanol
kDa	kilo-Dalton
LC	Liquid chromatography
LC-MS	Liquid chromatography-mass spectrometry
LC-MS ²	Liquid chromatography tandem mass spectrometry
LOQ	Limit of quantitation
m/z	Mass-to-charge ratio
MeOH	Methanol
ML	Machine learning
MPA	Mobile phase A
MPB	Mobile phase B
MRM	Multiple reaction monitoring
MS	Mass spectrometry
NEtFOSA	N-Ethylperfluoro-1-octanesulfonamide
NFDHA	Nonafluoro-3,6-dioxahexanoic acid
NMeFOSA	N-Methylperfluoro-1-octanesulfonamide
PABA	Para-aminobenzoic acid
PFAS	Per- and polyfluoroalkyl substances
PFBA	Perfluorobutanoic acid
PFBS	Perfluorobutane sulfonate
PFCA	Perfluorocarboxylic acid
PFDA	Perfluorodecanoic acid
PFDoS	Perfluorododecane sulfonate
PFDS	Perfluorodecane sulfonate

PFHpS	Perfluoroheptane sulfonate
PFHxDA	Perfluorohexadecanoic acid
PFHxS	Perfluorohexane sulfonate
PFMPA	2,2,3,3-tetrafluoro-3-(trifluoromethoxy)propanoic acid
PFNA	Perfluorononanoic acid
PFOA	Perfluorooctanoic acid
PFOS	Perfluorooctane sulfonate
PFPeA	Perfluoropentanoic acid
PFPeS	Perfluoropentane sulfonate
PFSA	Perfluorosulfonic acid
PFTDA	Perfluorotetradecanoic acid
psi	Pounds per square inch
QQQ-MS	Triple quadrupole mass spectrometry
RT	Retention time
S/N	Signal-to-noise ratio
SPE	Solid phase extraction
SV	Separation voltage
SV _{pp}	Separation voltage (peak-to-peak) - used interchangeably with SV
Td	Townsend
<i>T_{eff}</i>	Effective temperature
TIC	Total ion chromatogram
TWIMS	Travelling wave ion mobility spectrometry
wB97X-D3BJ	DFT functional

Quote

*Always two there are, no more, no less.
A master and an apprentice.*

Yoda, The Phantom Menace

Chapter 1

Introduction

1.1 What are PFAS?

Per- and polyfluoroalkyl substances (PFAS) are a vast group of synthetic chemicals that have garnered global attention as pollutants in recent years. Owing to the strength of their numerous C-F bonds, PFAS display remarkable thermodynamic and chemical stability.¹ Additionally, the possession of both hydrophilic headgroups and hydrophobic tails give PFAS simultaneous water- and oil-repellant properties.^{2,3} The combination of their stability and repellant properties have made PFAS highly useful in consumer and industrial applications, most notably in non-stick cookware, food packaging materials, weather resistant clothing, stain-repellants, and aqueous film-forming foams.^{1,4,5} However, their extensive usage since the 1950s owing to these useful properties has led to unintended consequences, with PFAS accumulating in ecosystems and contaminating groundwater and drinking water sources in regions around the world.⁶⁻⁹ The environmental impact of PFAS is concerning because of their slow-degradation and bioaccumulation in living organisms.¹⁰⁻¹² The accumulation of PFAS in smaller organisms is especially concerning for humans, as they tend to magnify through the trophic chain.^{13,14} In fact, PFAS are seemingly unavoidable, as reports suggest that the blood from 98.5% of Canadians contains at least three PFAS: perfluorooctane sulfonate (PFOS), perfluorooctanoic acid (PFOA) and perfluorohexane sulfonate (PFHxS).¹⁵ Concerningly, emerging research suggests potential health risks associated with PFAS exposure, including an onslaught of adverse health effects in human reproduction, child development, and increased cancer risks.^{10-12,16-23}

In January 2024, the U.S. Environmental Protection Agency (EPA) finalized a rule preventing companies from beginning or resuming the production of 329 PFAS without EPA review.²⁴ Similarly, PFOS, PFOA, and long chain PFAS (> 8 carbons) have been banned in Canada under the Prohibition of Certain Toxic Substances Regulations, 2012.²⁵ Health Canada has also implemented maximum acceptable concentration guidelines for both PFOS and PFOA as well as screening values for a short

list of other PFAS which are commonly found in drinking water.⁷ Further to this, Health Canada has recently proposed a limit of 30 ng L⁻¹ sum of total PFAS in drinking water.⁸ Although the direct production and import of PFAS are currently regulated in both the United States and Canada, they continue to enter North America in imported products without proper regulation (*e.g.* textiles, food packaging, fertilizer).^{26,27}

1.2 Current Methods for PFAS Analysis

PFAS are typically analysed using techniques such as mass spectrometry (MS), liquid chromatography (LC), and ion mobility spectrometry (IMS), often coupled in hybrid formats with each technique contributing uniquely to the comprehensive analysis of these compounds. Mass spectrometry, particularly high-resolution mass spectrometry (HRMS) and triple quadrupole mass spectrometry (QQQ-MS), is central in PFAS analysis. HRMS provides accurate mass measurements and high sensitivity, making it ideal for identifying and quantifying a wide range of PFAS compounds, including those at trace levels.^{28–30} The use of QQQ-MS is prevalent in targeted analysis due to the ability to conduct multiple reaction monitoring (MRM) experiments using this platform, which enhances the specificity and sensitivity of the analysis by focusing on specific precursor-product ion transitions.^{30–32}

Often coupled with MS (*i.e.*, LC-MS), LC is crucial for separating PFAS compounds before MS detection. Techniques such as reverse-phase LC and hydrophilic interaction liquid chromatography (HILIC) are commonly employed to achieve efficient separation of PFAS from complex matrices.^{33–42} LC-MS² (tandem mass spectrometry) is particularly effective in quantifying trace levels of PFAS in environmental and biological samples, owing to its high sensitivity and specificity. LC-MS² is often coupled with solid-phase extraction (SPE), a sample preparation technique that helps clean-up dirty matrices and allows for pre-concentration of samples. This combination is outlined and recommended by the EPA as per method 1633 for the analysis of PFAS in liquid and solid samples.⁴³

Ion mobility spectrometry (IMS) and its numerous variants are emerging as techniques for PFAS analysis given their ability to rapidly separate ions based on shape, size, and charge. While simple drift tube IMS (DTIMS) has proven effective for PFAS samples,⁴⁴⁻⁴⁸ some researchers have turned to more advanced mobility techniques including travelling wave IMS (TWIMS),⁴⁹⁻⁵¹ trapped IMS (TIMS),⁵²⁻⁵⁴ and differential mobility spectrometry (DMS).⁵⁵ The latter of these techniques, DMS, is of particular interest since the ion carrier gas can be doped with solvent vapours which can enhance separation. To date, though, reports of the application of DMS to PFAS characterization have been sparse.

While the techniques described here are robust and pertinent for PFAS analysis, each has its own limitations. MS may be suitable for measuring and monitoring PFAS species with unique mass-to-charge (m/z) ratio, but it is incapable of differentiating between structural isomers and fails to differentiate isobaric species (*i.e.*, species with identical mass at the chosen MS resolution, but different elemental composition). In some cases, MS² may reveal unique fragmentation pathways for isomers and isobars though it has been documented that PFAS isomers often produce identical fragmentation spectra.⁵⁵ LC-MS² tends to be the most common separation technique for complex PFAS matrices, however these methods require relatively lengthy runtimes which inhibit high-throughput analysis. IMS techniques allow for the rapid gas-phase separation of PFAS, but resolution of all compounds is challenging for rich mixtures – recall that the number of PFAS species exceeds 12,000.⁵⁶ In this thesis, I explore the combination of orthogonal techniques to improve chemical separation and uncover multidimensional trends for a variety of PFAS classes. These trends could be leveraged for non-targeted analysis of emerging and unknown PFAS species.

1.3 Scope of this Thesis

This thesis explores the capabilities of DMS for anion separation and characterization prior to MS detection. DMS is a specialized form of IMS which employs an asymmetric waveform for ion separation. In DMS experiments the carrier gas is often doped with a volatile chemical modifier to

improve analytical separation. Here, I investigate how different modified DMS environments affect ion behaviour and how DMS can be coupled with LC and MS to improve separation.

Chapter 2 describes the theory and background for the experimental techniques employed throughout the thesis. A brief description of LC is discussed, but the focus of the chapter is ion mobility. The fundamentals of IMS are described and the differences between drift-tube IMS and DMS are highlighted. Additionally, I discuss the types of interactions that occur between ions and solvent modifier molecules within the DMS cell and how these interactions can influence separation.

Chapter 3 discusses the development of a comprehensive database of DMS dispersion curves for anionic species. The goal of this work is two-pronged in nature, aiming to generate sufficient data for training predictive machine learning (ML) models while also garnering insight into the impact of solvent modifiers on the DMS behaviour of anions. DMS measurements of anions are important because most studies to date have been of cations (which limits ML model generalizability), and the majority of PFAS species are measured as anions (and a detailed understanding of anion behaviour in DMS will benefit PFAS studies).

Chapter 4 describes the integration of DMS into an LC workflow to enhance the separation of 34 PFAS compounds, achieving improved resolution while maintaining a similar run time to traditional LC-MS analysis. This is a novel separation technique for PFAS and my work establishes a foundation for future non-targeted analyses employing two-dimensional hybrid LC×DMS-MS², which could improve the identification and quantification of complex mixtures, including those that contain unknown PFAS compounds.

Chapter 2

Analytical Background

2.1 Liquid Chromatography

Analytical separation prior to MS detection is essential when working with complex sample matrices. Liquid chromatography (LC) is the gold-standard in separation and has been used to separate everything from small organic molecules,⁵⁷⁻⁶⁰ to peptides,⁶¹⁻⁶⁴ to kDa proteins.⁶⁵⁻⁶⁹ In LC, analytes are separated based on their affinity for a stationary phase as they are carried by a mobile phase. The stationary phase consists of silica beads tightly packed within the LC column; the surface of the beads are normally chemically modified with short, polar functional groups. Practitioners refer to this as normal-phase LC and when used for separation, the most non-polar compounds will elute off the column first.^{70,71} The polar compounds however will have increased interactions with the column and will elute more slowly. The time it takes the analyte to transit the column and reach the MS detector is known as the retention time (RT). In reverse-phase LC, the surfaces of the silica beads are modified with alkyl chains such as C18 (a chain containing 18 carbon atoms).^{70,71} Because these chains are highly hydrophobic, and thus non-polar, the elution order is from the most-to-least polar. While analyte interactions with the stationary phase primarily influence elution, interactions with the mobile phase also play a role. Ultimately, the elution time depends on the partition coefficient K_d per **Eq 2.1**:

$$K_d = \frac{C_s}{C_m} \quad \text{Eq 2.1}$$

where C_s is the concentration of the analyte in the stationary phase and C_m is the concentration of the analyte in the mobile phase.^{72,73} K_d can be affected by modifying the composition of the mobile phase. Often in LC experiments, the total mobile phase is a combination of at least two separate mobile phases where one is mostly aqueous, and the other is mostly organic. For example, in normal-phase LC the polar analytes have a strong affinity for the stationary phase, but if one were to increase the percentage of aqueous mobile phase (*i.e.*, making the overall mobile phase more polar) then the analytes will have a lower partition coefficient and will elute faster. The opposite is true for reverse-phase LC, where

increasing the organic phase will diminish analyte interactions with the column and results in faster elution of non-polar compounds. The flow of the mobile phase through the column can be isocratic where the composition is consistent throughout the LC run, or gradient where the amounts of aqueous and organic phases are varied. Isocratic elution is useful for separating well-defined mixtures and is simpler given the minimal amount of optimization required.^{74,75} Gradient elution is more commonly used for complex mixtures since it offers the ability to enhance separation by varying the mobile phase composition throughout the run.^{73,75}

Depending on the MS mode being used, various additives can be included in the mobile phases to aid in ionization. Formic acid is often added when running positive mode MS, as it provides protons and increases the conductivity of the solvent for better ionization. In the same vein, ammonium acetate is often used when operating in negative mode MS. A large benefit of employing LC prior to MS detection is the reduction in ion-suppression. Should a complex sample be introduced into the MS without separation, it is possible that certain compounds will inhibit the ionization of others. This has consequences for quantitation efforts, because the signal of the inhibited ions will be less than that if they were measured in the absence of competing species, and thus the apparent intensity of these ions will not be representative of their true concentration in the sample.⁷⁶⁻⁷⁹ Additionally, isobaric interferences may present a problem for LC analyses, especially in instances where two compounds share the same fragmentation pathways.⁸⁰⁻⁸³ A further downside to LC is the runtime which, depending on the complexity of the sample in question, can extend to over 30 minutes. Long runtimes limit throughput and increase the supplies required (*e.g.* mobile phases solvents) for analysis. To avoid these sorts of runtimes, one can sometimes replace LC with ion mobility, which operates in the gas phase and takes only seconds.

2.2 Fundamentals of Ion Mobility Spectrometry and Differential Mobility Spectrometry

Ion mobility spectrometry (IMS) is a common analytical separation method that is employed in mass spectrometric analyses, and which temporally separates analytes based on their shape, size, mass, and charge. In a typical drift-tube IMS (DTIMS) setup, ions are pulsed into a region filled with an inert bath gas (*e.g.* N₂ or He) and a fixed electric field is applied to the cell which drags analyte ions through the bath gas.^{84,85} The overall drift time of an analyte depends on its mobility as it moves through the cell. The mobility itself is dictated by the ion's collision cross section (CCS) which is defined as the orientationally averaged area around a molecule that is involved in momentum transfer with a bath gas particle (see **Figure 2.1**). Ions with a larger CCS will experience more collisions moving through the length of the cell, resulting in a decreased mobility and longer drift time relative to ions with smaller CCS. For a spherical ion interacting with a spherical bath gas particle, the CCS (Ω) can be calculated through **Eq 2.2**,

$$\Omega = \pi(r_A + r_B)^2 \quad \text{Eq 2.2}$$

where r_A is the radius of the ion of interest and r_B is the radius of the bath gas.⁸⁶ However, for non-spherical species, the calculation of CCS is not straightforward. Normally, one measures the ion mobility (K) using DTIMS, then converts that to CCS using the Mason-Schamp equation (**Eq 2.3**). These measurements can then be compared to computed theoretical CCS values to assign molecular geometry. Software such as MobCal-MPI, which employs molecular dynamics simulations of ion-neutral (*i.e.*, with a bath gas particle) collisions, can be used to determine CCS *in-silico*.⁸⁷

$$K = \frac{(18\pi)^{1/2}}{16} \left(\frac{1}{m_i} + \frac{1}{m_g} \right)^{1/2} \frac{ze}{\Omega N (k_B T)^{1/2}} \quad \text{Eq 2.3}$$

Here, m_i is the mass of the ion, m_g is the mass of the bath gas molecule, z is the ion's charge, e is the elementary charge, N is the density of the bath gas, and T is the temperature of the gas. The ion is assumed to be in equilibrium with the bath gas temperature which, stated in another way, means that the Mason-Schamp equation is valid only if the field-induced heating of the ion is negligible compared

to the gas temperature.^{88,89} This is referred to this as the low field limit, under which an ion's mobility responds linearly to changes in the applied field. In DTIMS experiments, the field strengths used are relatively low (ca. < 10 Td), thus the Mason-Schamp equation linearly relates an ion's mobility to its CCS.⁸⁹

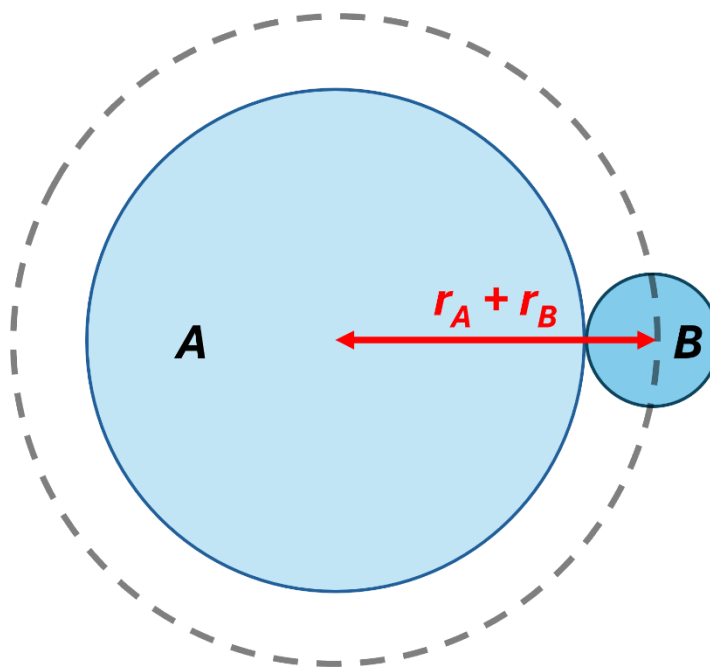


Figure 2.1. Schematic depicting the CCS between a spherical ion (A) and a spherical neutral (B). The CCS of this pair can be calculated using **Eq 2.2**.

Differential mobility spectrometry (DMS), also known as high-field asymmetric-waveform ion mobility spectrometry (FAIMS), is a specialized form of IMS.^{90,91} In DMS, ions and carrier gas particles are pulled through the mobility cell by the vacuum of the MS. The cell consists of two parallel electrodes across which an asymmetric waveform is applied. This waveform, known as the separation voltage (SV) has two distinct regions: a high-field and a low-field (see **Figure 2.2**). During the high-field portion of the SV waveform, an ion travelling through the cell is susceptible to field-induced heating which increases its local temperature. In DMS, the experimental field strengths exceed the low-field limit, inducing a change in the ion's effective temperature (T_{eff}) which can be described by two-temperature theory (2TT) in **Eq 2.4**,^{92,93}

$$T_{eff} = T_{gas} + T_{field} \quad \text{Eq 2.4}$$

where T_{gas} is the temperature of the carrier gas (*i.e.* the temperature of the system) and T_{field} is the temperature induced by the applied field. The increase in T_{eff} results in an apparent increase in the carrier gas viscosity, and consequently a decrease in ion mobility.⁹⁴ This can be incorporated back into the Mason-Schamp equation (see **Eq 2.5**).

$$K = \frac{(18\pi)^{1/2}}{16} \left(\frac{1}{m_i} + \frac{1}{m_g} \right)^{1/2} \frac{ze}{\Omega(T_{eff})N(k_B T_{eff})^{1/2}} \quad \text{Eq 2.5}$$

Due to the asymmetry of the SV waveform, ions will experience a change in mobility during the high-field portion that is not linearly proportional to that during the low-field portion. This causes the ion to continually migrate off the transmission axis (*i.e.* off the axis leading to the detector) with every iteration of the SV duty cycle. To correct for this, a static potential known as the compensation voltage (CV) is applied, the magnitude of which depends on how far off-axis the ion migrates during the SV cycle. As the overall peak-peak amplitude of the SV waveform (SV_{pp}) increases, ions will migrate further off axis and will require CVs of larger magnitude to correct their trajectory. The CV value required for transmission at a given SV is specific to the ion in question depending on its CCS.

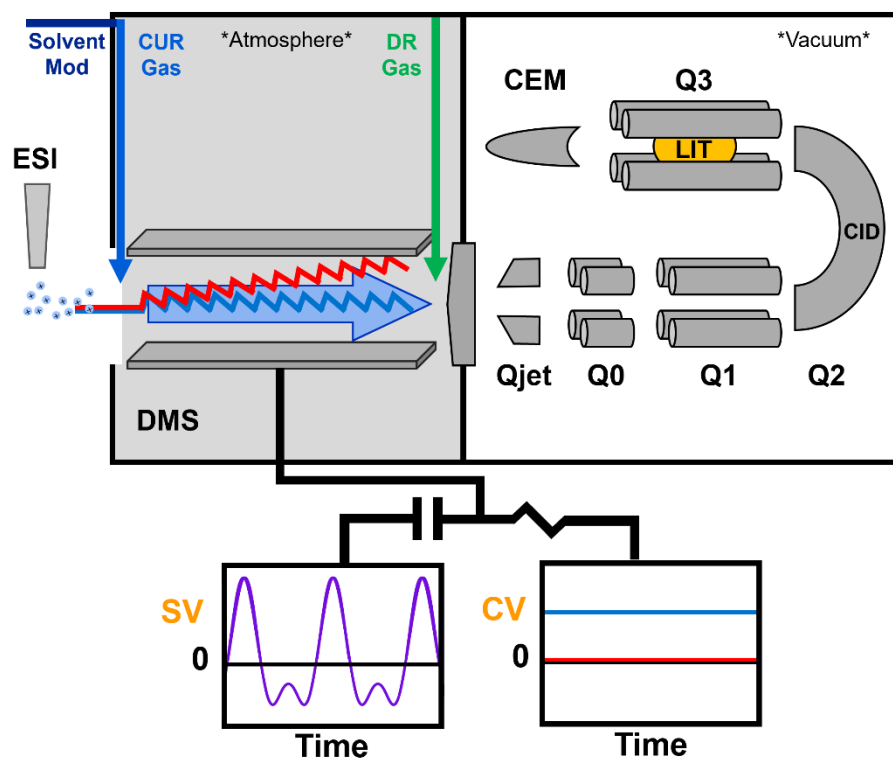


Figure 2.2. A schematic showing the DMS-MS² instrument setup and the trajectory of an ion as it passes through a DMS cell. The red zig-zag trace represents an un-stable ion trajectory which occurs when the incorrect CV is applied for a given SV. The blue zig-zag trace represents a stable ion trajectory when the correct CV is applied. The purple trace represents the shape of the SV waveform as a function of time.

The relation between CV and SV is influenced by the composition of the collision environment and how the ions of interest interact with it across the SV duty cycle. Additionally, how the optimal CV for transmission evolves with increasing SV_{PP} is also dictated by ion-neutral interactions. One can often classify the CV / SV (or dispersion) behaviour of an ion as one of three types: A, B, or C (see **Figure 2.3**). The latter, Type C, is used to describe a non-clustering environment. Here, ion-neutral interactions are comprised of hard sphere scattering, where the ion experiences an increased number of collisions during the high-field portion of the SV waveform, resulting in a diminished mobility relative to the low-field portion.^{89,94} The relative mobility between both field regions continually decreases with increasing SV_{PP} and as such, an increasingly positive CV value is required to correct the ion's trajectory.

Oftentimes in DMS experiments, a volatile solvent modifier will be incorporated into the carrier gas to improve analytical separation.⁹⁵⁻⁹⁸ In Type A behaviour, which is referred to as strongly clustering, ion-solvent clusters form under low-field conditions, followed by some amount of evaporation under high-field conditions. This results in a decreased effective CCS during the high-field portion of the SV duty cycle and an increase in the ion's mobility. In this case, the ion will migrate off axis in the opposite direction compared to Type C behaviour, and thus requires a negative CV for axial correction. As the SV_{PP} increases, so too does T_{eff} which drives solvent evaporation at high field conditions. This leads to a further increase in mobility and increasingly negative CV for transmission. Type B behaviour is considered an intermediate to Types A and C and is observed within weakly clustering environments. The initial portion of the dispersion curve is analogous to Type A behaviour up until some SV_{PP} value. At this point, all solvent adducts decluster from the ion during high-field conditions, and the local heating of the ion is significant enough that further clustering during low-field conditions is not thermodynamically favorable. Because the ion is now bare throughout the SV waveform, hard sphere scattering takes over and Type C-like behaviour is observed for all SV beyond this point. Since the apparent changes in CCS of similar ions are inflated through micro-solvation processes, solvent-modified DMS can be extremely useful for analytical separation. Additionally, the choice of solvent modifier can lead to drastically different extents of separation which makes DMS a selective analytical method.

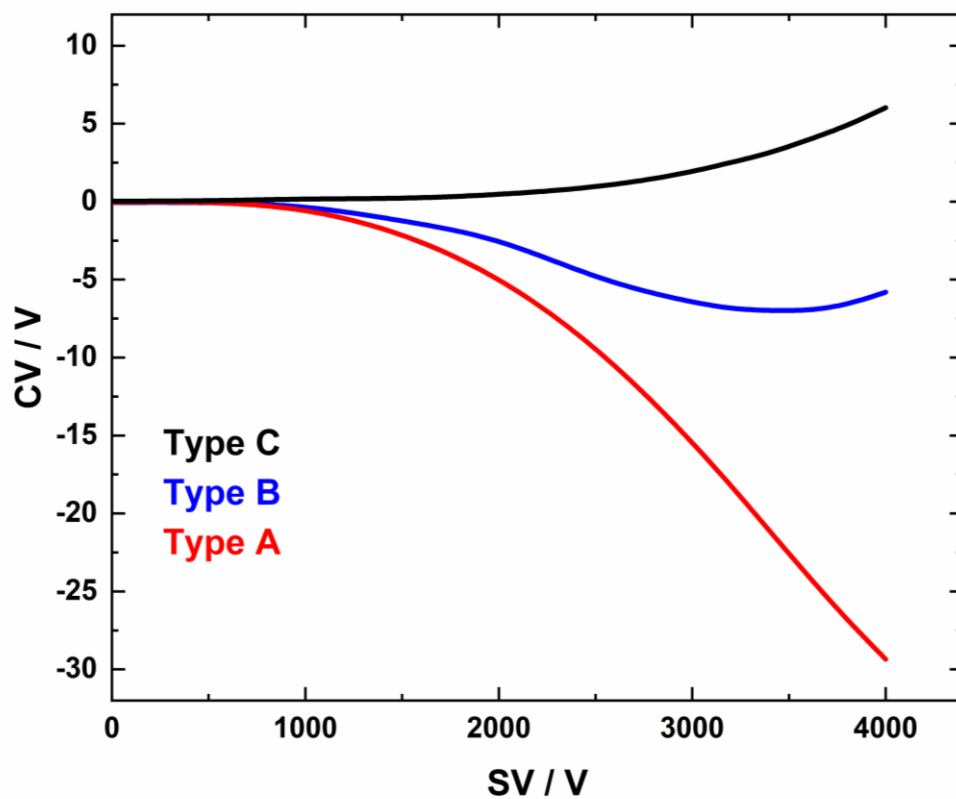


Figure 2.3. DMS dispersion curves depicting Type A (red), Type B (blue) and Type C (black) behaviour. Type A behaviour is associated with strong ion-solvent clustering, Type B is associated with weak ion-solvent clustering, and Type C is associated with hard-sphere scattering or non-clustering environments.

Chapter 3

DMS Behaviour of Anions

3.1 Introduction

A key aspect of DMS analysis of PFAS (and other classes of compounds) is the ability to predict an analyte's DMS behaviour in advance of conducting experiments to limit the parameter space (*e.g.*, SV, CV) that must be searched. Over the past several years, the Hopkins research group has developed a first-principles model of DMS behaviour, but simulating an analyte's dispersion curve can take days-to-weeks – far too long to be effective in most situations.^{92,99,100} Utilizing ML to predict DMS behaviour is therefore desirable since ML models can generate predictions in seconds-to-minutes. Previous work has shown that ML can be leveraged to predict physicochemical properties of compounds based on DMS data.^{101,102} However, a substantial amount of experimental data is needed to train an accurate ML model. Although the Hopkins laboratory has accumulated dispersion data for hundreds of compounds in positive mode (*i.e.*, cationic species) electrospray ionization (ESI), we had yet to introduce anionic species to the database. To remedy this situation, and to ensure the applicability of the ML model to compounds which may ionize in either positive or negative mode ESI, 224 compounds were selected for analysis in negative mode (*i.e.*, anionic species) ESI and their DMS behaviours were measured in pure N₂ and in N₂ modified with MeOH (1.5 mol%). This collection of analytes included various PFAS, organic acids, amino acids, various dyes, and small drug molecules that could be deprotonated. In addition to pure N₂ and MeOH modifier, the DMS behaviours of 41 PFAS were also measured in a 1.5 mol% isopropanol (IPA) environment. This work not only provided additional data (*i.e.*, anions) which would offer a better understanding of ion behaviour in various DMS environments, but also enabled exploration of the DMS behaviour of anionic PFAS as a first-step in developing a hybrid LC×DMS-MS² method.

3.2 Materials and Methods

3.2.1 Materials

Many of the compounds studied here were previously obtained for use in our laboratory and many others were sourced from within the chemistry department at the University of Waterloo. This analyte library was supplemented with several compounds that were purchased from Enamine (Kyiv, Ukraine), and others that were provided by Yves Le Blanc, Mircea Guna and Brad Schneider from SCIEX (Ontario, Canada). HPLC-grade methanol (MeOH), and isopropanol (IPA) were purchased from Sigma-Aldrich (Missouri, USA). Ultrapure water was obtained from a Milli-Q system (Millipore, 18.2 $\text{m}\Omega\text{ cm}^{-1}$). Mixtures containing five to ten analytes each were prepared in MeOH containing 0.5% (v/v) ammonium hydroxide at a working concentration of 500 ng mL^{-1} . Mixtures were prepared such that the m/z of each component differed by at least 2 Da from all other components. This procedure was necessary to ensure that each analyte could be easily distinguished by m/z in the SCIEX 5500 triple quadrupole mass spectrometer.

The molecules chosen for this study were carefully selected to ensure that ionization via negative mode ESI was feasible. Compounds containing hydroxyl-, carboxyl-, sulfo-, and amide groups were targeted as these groups tend to deprotonate easily under basic conditions. Sodium salt species were also included given their ability to readily ionize in solution. In total, 224 unique compounds were investigated as anions. Most of these compounds were measured in both pure N_2 and in MeOH-modified DMS environments; full dispersion curves were not obtainable for some compounds owing to field-induced fragmentation, charge scavenging by the solvent modifier, or ion suppression. A full list of compounds is available in **Table A.1**.

3.2.2 Methods

A planar SelexION differential mobility spectrometer with a 1 mm gap height was placed between the sampling orifice of a QTRAP 5500 hybrid triple quadrupole linear ion trap mass spectrometer and a Turbospray ion source (SCIEX). Refer to the schematic shown in **Figure 2.2** in **Section 2.2**. All data

were obtained via direct infusion of analyte mixtures into the ESI source. Desolvation of the analyte during electrospray ionization (ESI) was aided by application of a nebulizing gas (50 psi) and an auxiliary gas (40 psi). Data acquisition was performed by MRM, the transitions of which are provided in N₂ was used as the DMS carrier gas (20 psi), the collision gas for collision-induced dissociation (*ca.* 7 mTorr), and the nebulizing/auxiliary gases used to aid desolvation during ESI. All remaining settings for the ion optics, as defined by the controlling software (Analyst 1.7), were as follows: collision gas (CAD) setting of high, entrance potentials of -10 V, DMS offset potential of -3 V, and collision cell exit potentials of -15 V. The declustering potential was optimized for each compound to maximize signal response. Experiments were completed with the DMS heater set to $T = 150\text{ }^{\circ}\text{C}$, which corresponds to a measured bath gas temperature of $T = 100\text{ }^{\circ}\text{C}$.¹⁰³ DMS measurements were obtained by incrementing the SV from 0 V to 3000 V in steps of 500 V and from 3000 V to 4000 V in steps of 200 V. For each discrete SV value, the ion current was monitored as a function of the CV over the range of -100 V to 20 V in steps of 0.25 V to produce an ionogram. Ionogram peaks were fit to a Gaussian function, where the peak of this distribution corresponds to the optimal CV for ion transmission at a given SV value. Optimal CVs were plotted against the corresponding SV values to produce dispersion plots for the analytes.

3.3 Results

3.3.1 Organic Acids and Other Small Molecules

When working with DMS environments comprised of pure N₂, one typically observes only Type C behaviour. However, Type B behaviour is sometimes observed for small molecules with m/z less than 200 Da. Rather than being indicative of ion-N₂ clustering, which is unlikely owing to the inertness of the N₂, Type B behaviour for these species arises from the temperature dependency of their CCS. Recall **Eq 2.5** for calculating mobility, where the temperature dependent CCS ($\Omega_{T_{eff}}$) and the effective temperature (T_{eff}) terms both appear in the denominator. Increases in either of these terms result in a decrease in mobility. As the effective ion temperature increases, the glancing collisions between the

ion and the carrier gas particles become less “glancing” and thus there is an apparent decrease in the ion CCS.⁸⁷ Because the T_{eff} term has a square-root dependence, in some situations the apparent decrease in CCS can outweigh the increase in T_{eff} , and the ion’s mobility actually increases under the high-field condition. Eventually, as the SV_{PP} increases further, T_{eff} becomes large enough to overcome the decrease in CCS at which point hard-sphere scattering is adopted.

Because most of the compounds that I investigated were small organic acids, a substantial number of the measured dispersion curves exhibited Type B behaviour in the pure N_2 environment. In fact, there was a near-even split between Types C and B for the 205 dispersion curves measured in N_2 (see **Figure 3.1**). Unsurprisingly, no instances of Type A behaviour were observed under these conditions. Conversely, most species when measured in a 1.5 mol% MeOH modified environment exhibited Type A dispersion curve behaviour. As seen in **Figure 3.2**, 69.2% of the dispersion curves in MeOH modifier displayed Type A behaviour, while only 29.3% showed Type B behaviour. Three compounds (1.5% of the total dataset) exhibited Type C behaviour in the MeOH-modified DMS environment. This behaviour is common for larger molecules because the adduction of a solvent molecule does not significantly impact the CCS of ion and so the field-dependent differential mobility driven by dynamic clustering is negligible. In this case, though, the three compounds were relatively small, ranging from 514 Da to 633 Da. I attribute the observed Type C behaviour for one of these compounds (taurocholic acid; see **Figure 3.3**) to its overall bulkiness; given the size of the multiple ring moieties opposite of the headgroup, dynamic clustering is unlikely to result in significant differences in CCS (and thus mobility) between the high- and low-field conditions. In the case of the other two compounds, the observed Type C behaviour is less apparent. These species, 9-chlorohexadecafluoro-3-oxanone-1-sulfonic acid (9Cl-PF3ONS) and 11-chloroeicosafluoro-3-oxaundecane-1-sulfonic acid (11Cl-PF3OUdS), are PFAS compounds whose sizes are less than that of the largest perfluorosulfonic acid (PFSA), perfluorododecane sulfonate (PFDoS), which exhibits Type B behaviour. Structurally, these compounds are analogous to the PFSA class, as both consist of fluorinated chains with sulfonate headgroups. The

only differences between the PFSA and the two compounds in question are the presence of ether linkages in the gamma position (relative to the headgroup), and the presence of a single chlorine atom on the terminal carbon (furthest from the headgroup). These differences in molecular composition and structure change the associated interaction potential of the molecule compared with the PFSA and result in little-to-no dynamic clustering between the ions and the MeOH modifier.

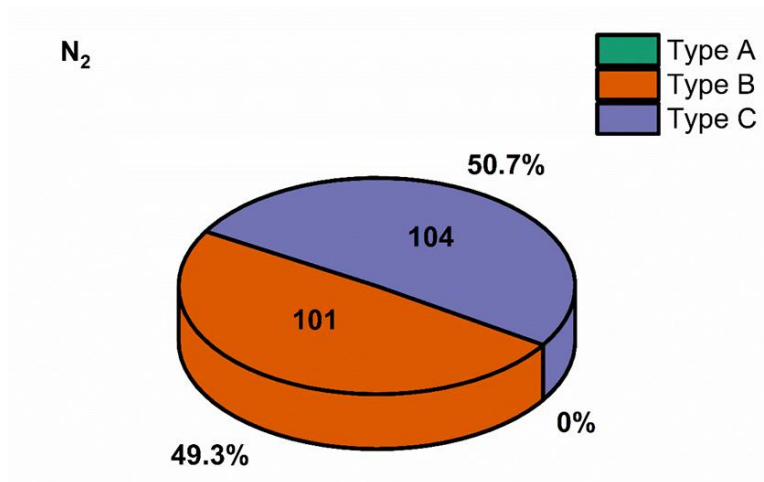


Figure 3.1. Distribution of DMS dispersion types for 205 anionic compounds measured in a pure N₂ environment.

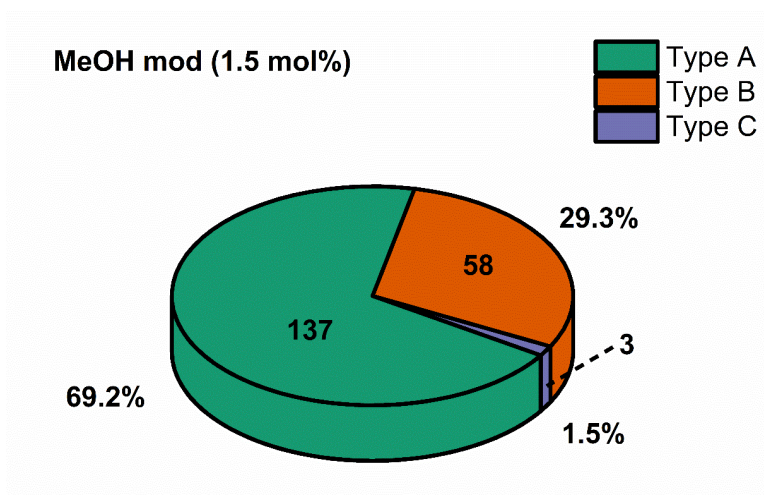


Figure 3.2. Distribution of DMS dispersion types for 198 anionic compounds measured in a 1.5 mol% MeOH modified environment.

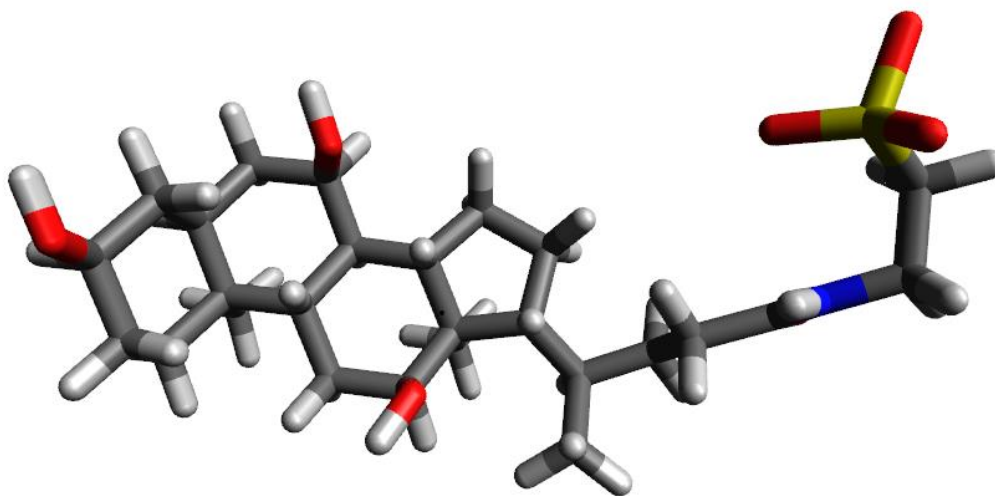


Figure 3.3. Chemical structure of deprotonated taurocholic acid.

Though two ions might exhibit similar (or even indistinguishable) Type C behaviour in N_2 , their behaviours in modified environments may be completely different. For example, **Figure 3.4** shows DMS dispersion curves for pterostilbene, vanillin, hexanoic acid, and 1,5-naphthalenedisulfonic acid. Although the dispersion behaviours for these four ions is relatively similar in a pure N_2 environment (solid lines), in the MeOH-modified environment (dashed lines) the ions significantly different behaviours; deprotonated vanillin and 1,5-naphthalenedisulfonic acid exhibit Type B behaviours with significantly different minima, and deprotonated pterostilbene and hexanoic acid exhibit Type A behaviours with substantially different curvatures. The differences in dispersion behaviour for these compounds is associated with their respective ion-solvent clustering propensities. The Type B behaviour observed in the MeOH-modified environment for deprotonated 1,5-naphthalenedisulfonic acid, for instance, is a result of the weak clustering that is typically observed between sulfonic acids and solvent modifiers. In contrast, the clustering between MeOH and the deprotonated hydroxyl group of pterostilbene is quite strong during low-field conditions and continues at higher SV_{PP} , leading to Type A behaviour. Comparing deprotonated vanillin (blue curves) and 1,5-naphthalenedisulfonic acid (green curves), both ions exhibit Type B behaviour in the MeOH-modified environment, but the CV

values for vanillin are consistently more negative compared to those for 1,5-naphthalenedisulfonic acid. The difference in their dispersion curves is a result of the different sizes of the molecules; clustering with MeOH causes a more substantial relative change in apparent CCS for deprotonated vanillin. This results in a larger mobility increase during high-field conditions for deprotonated vanillin compared to deprotonated 1,5-naphthalenedisulfonic acid, and thus a more negative CV is required to correct the trajectory of vanillin. A similar argument can be made to rationalize the differences in dispersion behaviour for deprotonated hexanoic acid (purple curves) and deprotonated pterostilbene (red curves).

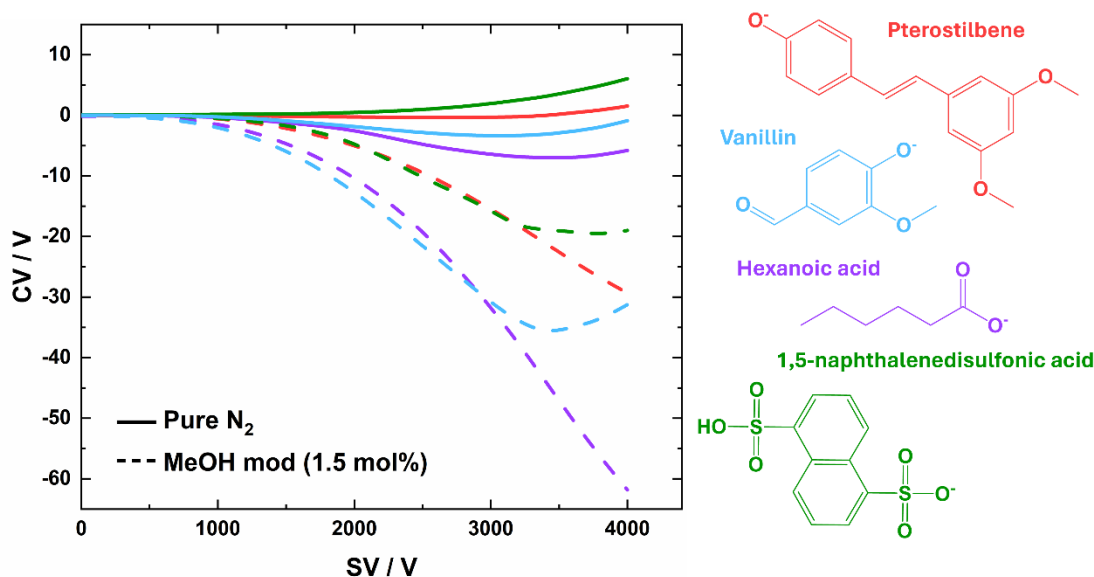


Figure 3.4. DMS dispersion behaviour of deprotonated pterostilbene (red), deprotonated vanillin (light blue), deprotonated hexanoic acid (purple), and deprotonated 1,5-naphthalenedisulfonic acid (green) in pure N₂ (solid line) and in N₂ containing 1.5 mol% MeOH (dashed line). The structure of each compound is shown on the right.

By measuring these anionic species, I have expanded the existing database and I have introduced additional chemical diversity. This will enable others in the Hopkins laboratory to train more robust and accurate ML models for predicting molecular properties and DMS dispersion curves. Prior to data collection, the lab's dispersion curve library consisted entirely of cationic species. As shown in **Figure 3.5**, 55.0 % of the dispersion curves measured for cations in both N₂ and MeOH displayed Type C

behaviour, and 27.6 % exhibited Type A. Only 17.3 % of cations exhibited Type B behaviour. In comparison, **Figure 3.6** shows that 39.5 % of the measured anions displayed Type B behaviour and 26.5 % exhibited Type C behaviour. Combining the anion and cation data yields a more balanced distribution of dispersion types: 45.0 % Type C, 29.9 % Type A, and 25.2 % Type B (see **Figure 3.7**).

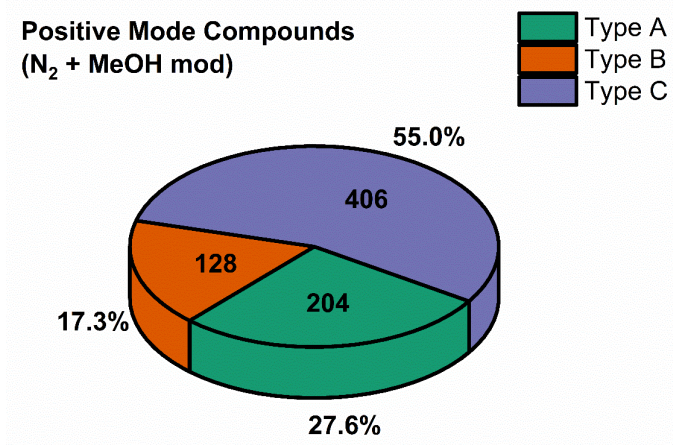


Figure 3.5. Distribution of DMS dispersion types for 738 cations measured in both pure N₂ and a 1.5 mol% MeOH modified environment.

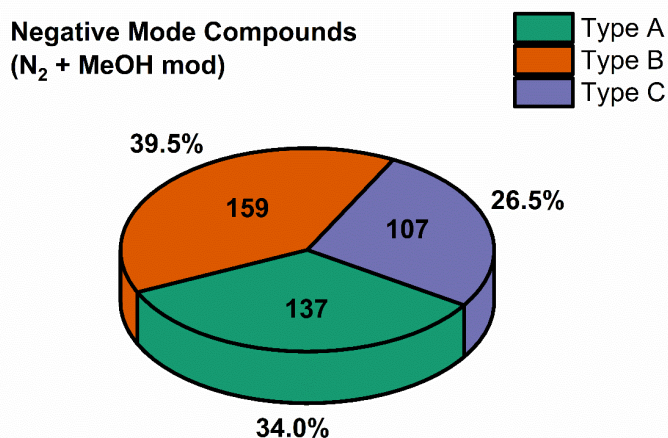


Figure 3.6. Distribution of DMS dispersion types for 403 anions measured in both pure N₂ and a 1.5 mol% MeOH modified environment.

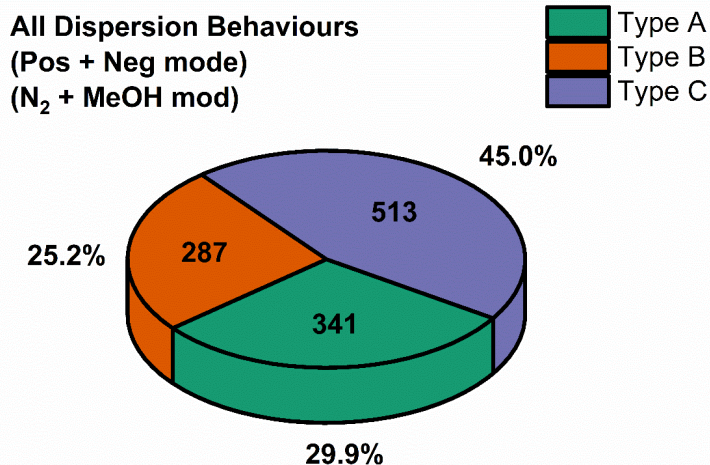


Figure 3.7. Distribution of DMS dispersion types for 1141 compounds measured in both pure N₂ and a 1.5 mol% MeOH modified environment.

Except for a few amino acid samples which were D/L mixtures, and a few PFAS samples which contained multiple isomeric forms, all the analytes were purchased as pure analytical standards containing a single molecular structure. Nevertheless, in several cases, “pure” compounds exhibited multiple ionogram peaks and thus yielded multiple dispersion curves over the measured SV range. Upon further consideration, I realized that several compounds in the database were susceptible to (de)protonation at multiple sites, which yielded multiple (de)prototropic isomers (*i.e.*, (de)protomers) that were separable by DMS. This phenomenon is well-documented.^{98,104–109} Differences in dispersion behaviour between (de)protomers are driven by differences in CCS following removal of a proton from two different sites on the molecule, by differences in the interaction potentials of the (de)protomers with the gaseous collision environment, and by differences in the effective CCSs of the (de)protomers as influenced by solvent binding at the various charge locations. For example, **Figure 3.8** shows the dispersion curves measured for deprotonated 4-mercaptobenzoic acid; depending on the site of deprotonation, I observe two different dispersion curves. This scenario is like that of *para*-aminobenzoic acid (PABA), which exhibits two protomers that can be separated *via* DMS in pure N₂ and subsequently characterized spectroscopically.¹⁰⁵ In the case of deprotonated 4-mercaptobenzoic acid, I observe two Type B dispersion curves in N₂. Drawing analogy with protonated PABA, I expect

that one curve is associated with deprotonation of the carboxylic acid and the other with deprotonation at the mercapto group. However, it is not readily apparent which structure corresponds to which dispersion curve. Examining the ionogram measured at $SV = 3200$ V reveals a significant disparity in the intensities of the two peaks (see **Figure 3.9**). To explore the relative energies (and thus populations) of the O- and S-deprotomers of 4-mercaptobenzoic acid, I used the ORCA software to compute their optimal geometries and relative Gibbs energies at the wB97X-D3BJ level of theory.¹¹⁰ This approach yielded an O-deprotomer that is 9.19 kJ mol^{-1} higher in energy than the S-deprotomer. These relative energies imply that the ionogram peak at $CV = -1.3$ V (Figure 3.8) corresponds to the S-deprotomer. However, in their study of protonated PABA, Coughlan *et al.* reported significant ESI solvent-dependent changes in the relative formation of the N- and O-protomers. They showed that when employing pure water, the protomers were generated in approximately equal populations. In contrast, a 50:50 $\text{H}_2\text{O}:\text{MeOH}$ mixture favoured O-protonation, and a 95:5 $\text{MeCN}:\text{H}_2\text{O}$ mixture favoured N-protonation.¹⁰⁵ It was rationalized that protic ESI solvents enabled proton transfer between the amine and carboxylic acid moieties. By increasing the MeOH content in the solvent the proton transfer between the N-protomer (which is favoured in solution) and the O-protomer (which is favoured in the gas phase) is enabled. Because proton transfer is also possible between deprotomers, and because the ESI solvent I used was pure MeOH, deprotomer assignment based on Gibbs energy is insufficient.

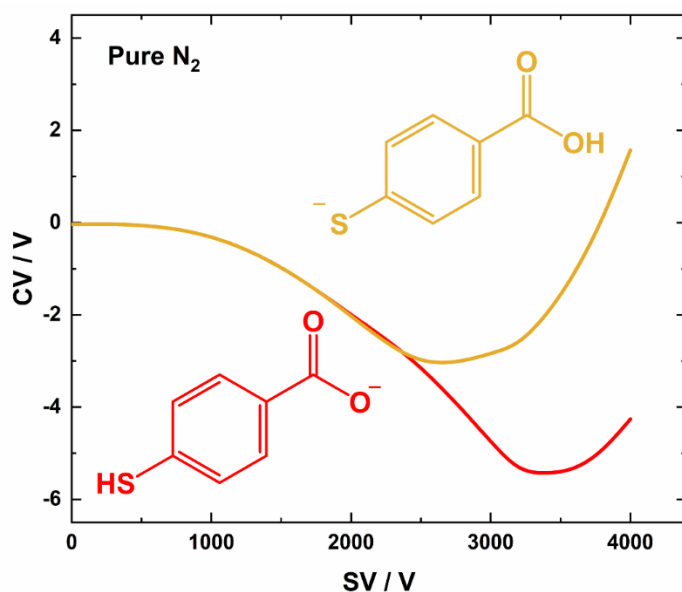


Figure 3.8. DMS dispersion curves for deprotonated 4-mercaptobenzoic acid measured in pure N_2 . The red trace corresponds to the O-deprotomer and the yellow trace corresponds to the S-deprotomer.

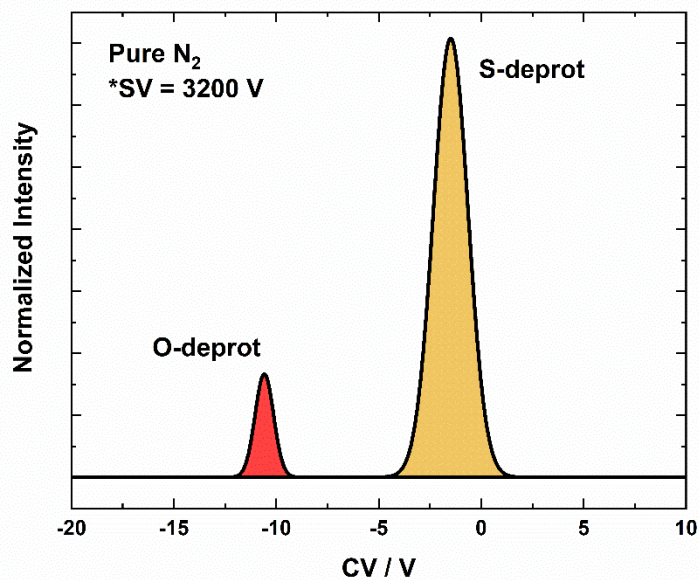


Figure 3.9. Ionogram taken at $SV = 3200$ V showing the two separation of the O- (red) and S- (yellow) deprotomers of 4-mercaptobenzoic acid in pure N_2 . Note that the peak positions are shifted from those of the dispersion curves shown in **Figure 3.8**; this measurement was recorded on another DMS system several months later.

My initial interpretation is supported by the product ion spectra for each ionogram peak recorded at $SV = 3200$ V (see **Figure 3.10**). Both features show a parent peak at $m/z = 153$ and both form a fragment at $m/z = 109$, which corresponds to a loss of CO_2 . Panel A, which corresponds to the ionogram peak at $CV = -1.3$ V, shows a 1.7:1 intensity ratio between fragment and parent peaks, whereas panel B, which corresponds to the ionogram peak at $CV = -10.5$ V, exhibits a 9.1:1 ratio. The fact that CO_2 occurs more readily for the peak at $CV = -10.5$ V implies that this feature is associated with the O-deprotomer. An interesting direction for future research would be exploring how ESI solvent composition influences deprotomer populations for 4-mercaptobenzoic acid (*i.e.*, does ESI solvent composition promote deprotonation at one site over the other).

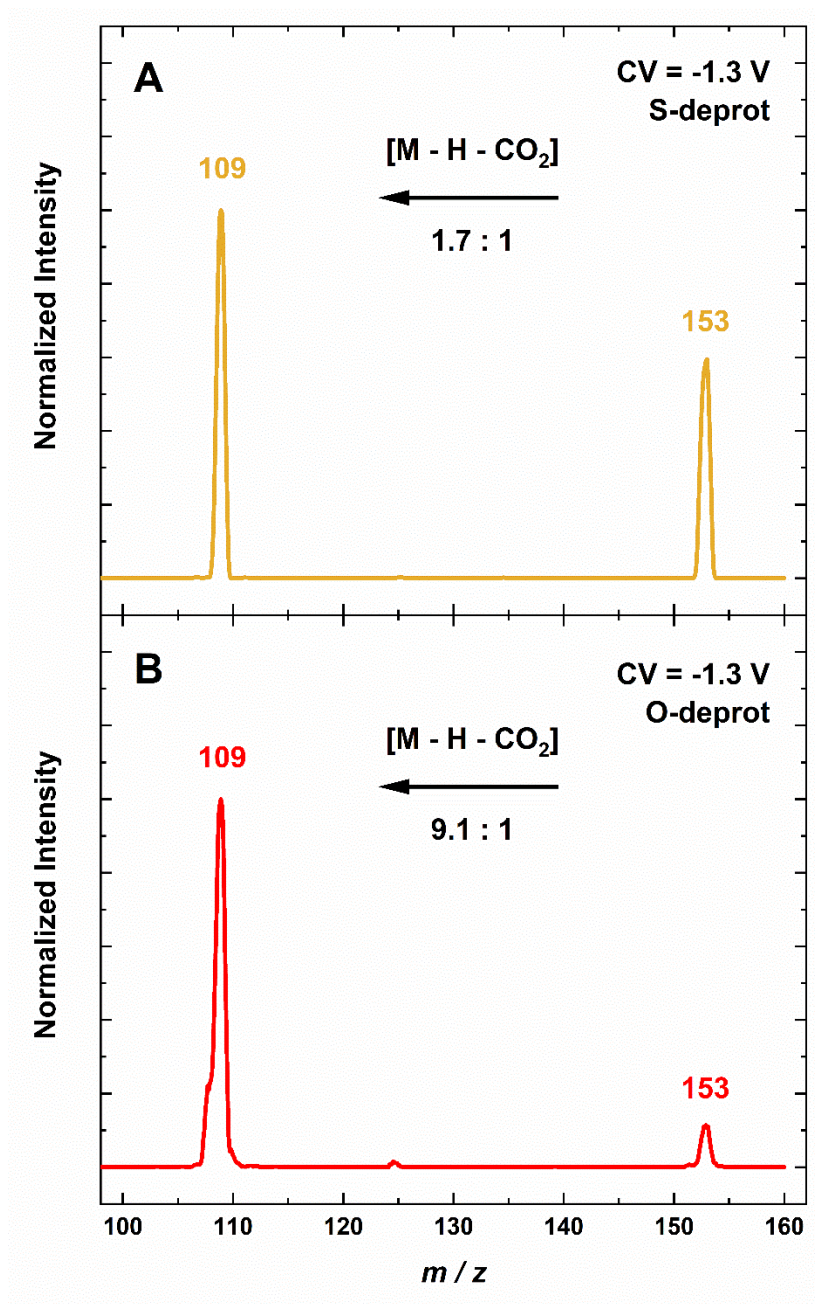


Figure 3.10. Product ion spectra of the mobility-selected deprotonomers of 4-mercaptobenzoic acid. The S-deprotonomer (Panel A) has a smaller fragment-to-parent ratio than the O-deprotonomer (Panel B).

3.3.2 PFAS in N₂ and Modified Environments

Although acquiring dispersion data for a variety of anions is helpful for expanding the DMS database, an accurate predictive ML model for DMS is yet to be developed and I must still record the behaviour of a collection of PFAS species in various environments to gain insight into optimal separation

conditions. **Figure 3.11** shows experimental DMS dispersion curves measured in pure N₂ for deprotonated PFAS molecules associated with different chemical classes. As might be expected, the pure N₂ environment was not ideal for separating the 41 target PFAS species. Most of the observed dispersion behaviour under these conditions is Type C, and most of the longer chain species co-elute at all SV values. Notably, some shorter chain perfluorocarboxylic acids (PFCAs) and fluorotelomer carboxylic acids (FTCAs) exhibit Type B behaviour in the pure N₂ environment and can be resolved at higher SV values. The dispersion curves for a several compounds (*e.g.* PFBA, PFPeA, PFMPA) suddenly cease at SVs lower than 4000 V. In these cases, the energy imparted by the SV field leads to field-induced fragmentation within the DMS cell (prior to MS detection). This phenomenon is well known and often affects smaller ions at lower SVs.¹⁰³

To improve resolution, small amounts of solvent vapour can be doped in the DMS N₂ carrier gas. Given the poor separation of PFAS species in pure N₂, I tested the impact of a MeOH modifier; it has a high vapour pressure, it is inexpensive, and it can potentially interact with the PFAS anions *via* hydrogen bond formation. The fact that the cation data set had also been measured in a MeOH-modified environment was an additional impetus. **Figure 3.12** shows the dispersion behaviour of 41 PFAS anions measured in a 1.5 mol% MeOH-modified N₂ environment. Unlike in the pure N₂ environment, the MeOH-modified environment generated an appreciable amount of ion separation and well-resolved dispersion curves could be measured for most compounds. Type A behaviour is observed for all PFCAs except PFTDA (**Figure 3.12**; top left panel), and Type B behaviour is observed for all PFSAAs (**Figure 3.12**; top right panel). Although the PFCA Type A curves appear to be approaching a CV minimum, only PFTDA reaches that minimum and has an increase in CV during the final SV measurement. This highlights an important question regarding behaviour type: what are the criteria for Type A/B classification? Inherently, all Type A ions are actually Type B ions whose dispersion curves have been truncated, either owing to instrument limitations or field-induced dissociation of the parent. In this work, I define Type A behaviour as dispersion data wherein the CV values are increasingly negative

with increasing SV. I define Type B behaviour as dispersion data wherein CV values reach a minimum at some $SV > 0$ V, and Type C behaviour as dispersion data wherein the CV values are increasingly positive with increasing SV.

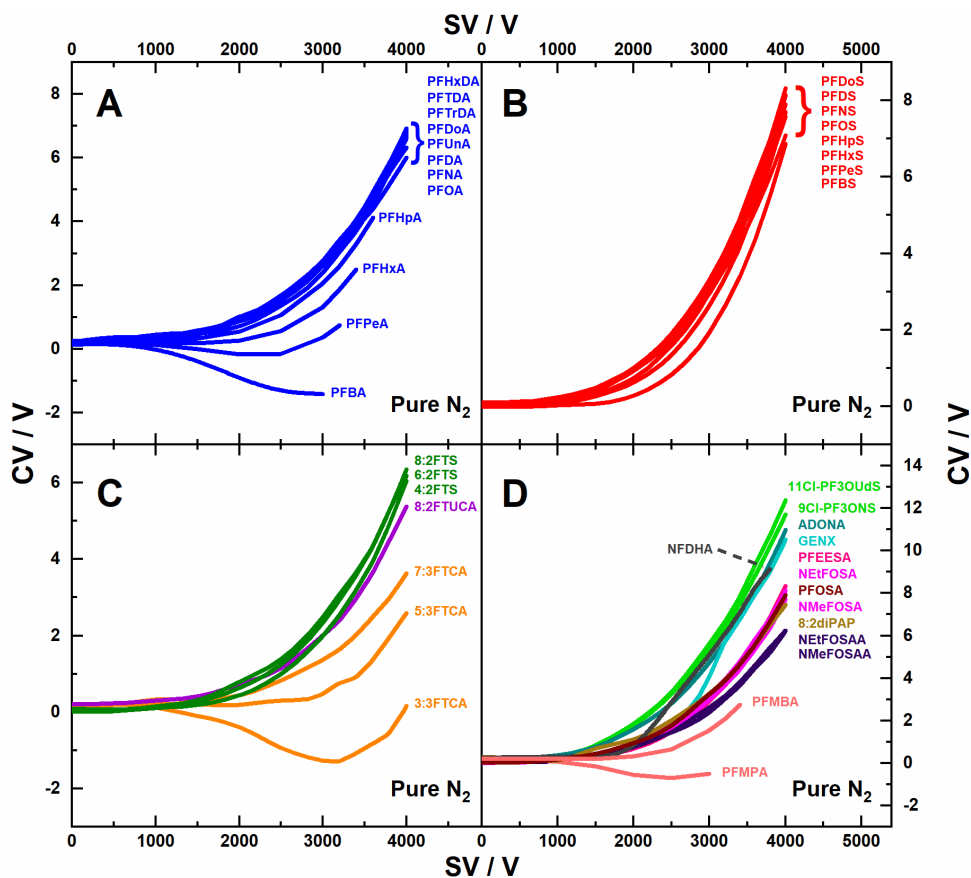


Figure 3.11. DMS dispersion curves measured in pure N₂ for (A) PFCA species, (B) PFSA species, (C) FTCA and FTS species, and (D) fourteen PFAS from other chemical classes. Compounds whose curves abruptly end prior to the SV = 4000 V instrument limit undergo field-induced fragmentation within the DMS cell.

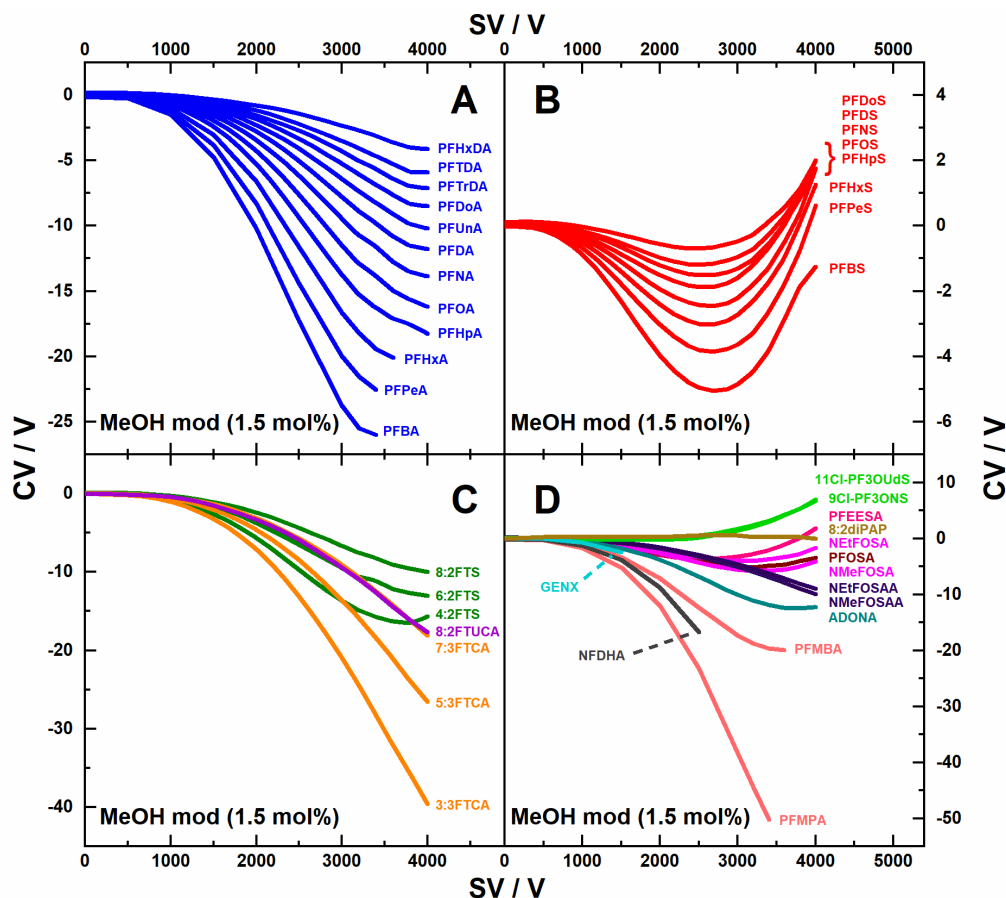


Figure 3.12. DMS dispersion curves measured in 1.5 mol% MeOH modifier for (A) PFCA species, (B) PFSA species, (C) FTCA and FTS species, and (D) fourteen PFAS from other chemical classes. Compounds whose curves abruptly end prior to the SV = 4000 V instrument limit undergo field-induced fragmentation within the DMS cell.

Although the addition of MeOH to the DMS carrier gas enhances separation (compared to the pure N₂ environment), the PFSA species were still poorly resolved – most of the PFSA species exhibited partial separation at relatively low SV_{PP} and their dispersion curves re-converged at higher SV_{PP}. Recalling that the size of a solvent modifier can impact an ion's apparent CCS (see Section 3.3.1), I decided to also test a larger solvent modifier. I selected isopropanol (IPA) because it is slightly larger than MeOH but should exhibit similar chemistry (with respect to ion-solvent interactions). **Figure 3.13** shows the DMS dispersion data recorded for the 41 target PFAS compounds in a 1.5 mol% IPA modified environment. Compared to the MeOH-modified environment (**Figure 3.12**), the IPA modifier

dramatically shifts the dispersion behaviour of the PFCA and fluorotelomer sulfonate (FTS) species (note the scale in each panel of **Figure 3.13**). Curiously, the IPA-modifier had a relatively small impact on PFSA dispersion behaviour, though at high SV_{PP} the CVs for individual species were better resolved. This suggests that neither MeOH nor IPA bind strongly with the PFSA compounds and that CV differences between the two environments are predominantly associated with the differential mobility arising from dynamic clustering with the two differently sized solvent molecules. Since IPA provides good separation of most PFAS in the mix, it will be used for all future experiments.

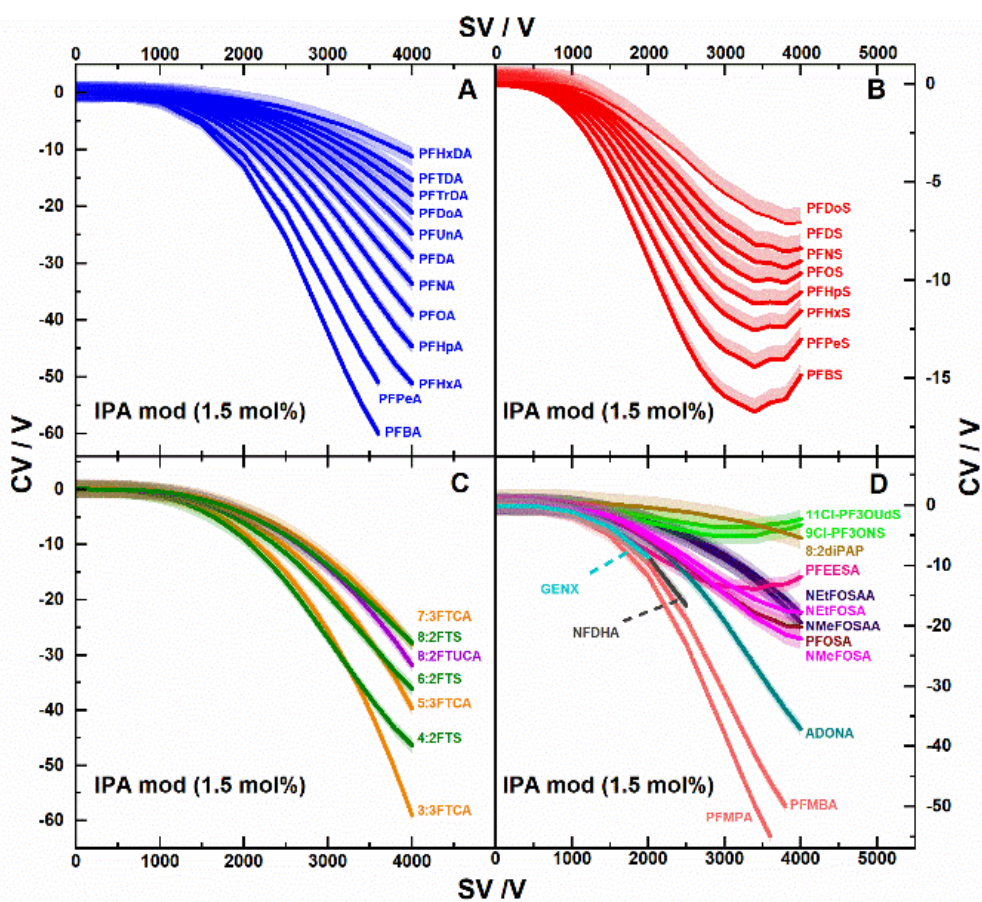


Figure 3.13. DMS dispersion curves measured in 1.5 mol% IPA modifier for (A) PFCA species, (B) PFSA species, (C) FTCA and FTS species, and (D) fourteen PFAS from other chemical classes. Compounds whose curves abruptly end prior to the $SV = 4000$ V instrument limit undergo field-induced fragmentation within the DMS cell. The transparent area surrounding each dispersion curve represents the FWHM of the extracted ionogram at the measured SV value. In the case of panel B, the upper portion of this transparent area divided by a factor of two is displayed for ease of viewing.

3.4 Conclusions

DMS dispersion data was measured for 224 unique negative mode compounds, which yielded a total of 403 dispersion curves; 205 in the N₂ environment and 198 in the MeOH-modified environment. By combining this data with the existing cation database, I now have data for anionic species, thus enabling the future development of a predictive ML model for DMS behaviour.

Something to consider when developing predictive models for DMS behaviour is the effect of charge location. An interesting case was discovered while processing data for the anion study: 4-mercaptobenzoic acid, analogous to para-aminobenzoic acid (PABA), exhibited multiple features in its ionogram at SV > 2500 V. While multiple peaks typically point to isobaric interferences or structural isomers, the culprit here is evidence of multiple deprotomers, especially considering that PABA is known to have two protomers. By mobility-selecting each feature in the ionogram and performing product ion scans, I was able to identify the corresponding deprotomers. A possible direction for future study is how ESI solvent effects relative formation of each deprotomer.

Importantly, and in contrast with the cationic species measured to date, many of the anionic species exhibited Type B dispersion curves. These measurements have thus resulted in a more even distribution of dispersion types for the entire dataset. Also importantly, when selecting the anion library, I included 41 PFAS molecules that are monitored by the Environmental Protection Agency. Consequently, I have garnered important insight regarding how PFAS anions behave in mass spectrometric environments and their thermodynamic stabilities. Furthermore, this data will be used to train predictive ML models that will be used in the analysis of emerging PFAS (*i.e.*, those for which chemical standards are not currently available), reducing the need for broad survey scans.

The dispersion behaviour, and therefore DMS resolution, of the PFAS species varied significantly between the pure N₂ environment, the MeOH-modified environment, and the IPA-modified environment. Pure N₂ yielded essentially no separation between most of the PFAS, and MeOH modifier provided reasonable separation of PFCAs and FTSS, but the PFSA species remained unresolved.

However, introducing IPA modifier significantly enhanced the separation of PFCA and FTS, and offered a slightly improved resolution for PFASs. Ultimately, these experiments demonstrated that PFASs do not interact strongly with alcohol modifiers; in the future, it might be useful to explore other non-protic modifiers (*e.g.*, acetone, acetonitrile) to improve the resolution of PFASs. For the purposes of this work, though, IPA modifier was deemed as a reasonable choice for future experiments as it provides a degree of separation for compounds in all the studied PFAS classes.

Chapter 4

Two-Dimensional Hybrid LC×DMS Analysis of 34 PFAS Compounds

4.1 Introduction

In the analysis of environmental samples that contain PFAS, analytical separation prior to MS detection is crucial. PFAS-containing matrices are often diverse, and the varying acidity among co-eluting compounds can suppress ionization.^{41,111-114} This suppression negatively affects ion signal response, compromising quantitation and characterization efforts. Furthermore, isobaric interferences with PFAS MRM fragmentation pathways complicate analyses, particularly when employing low resolution MS.¹¹⁵ Ensuring drinking water quality and the effectiveness of wastewater treatment systems relies on accurate quantitation and characterization of PFAS, further underscoring the importance of effective analytical separation techniques.

LC-MS is often used in PFAS analyses,^{34,46,111} as it allows for chemical separation prior to detection, aiding in instrument sensitivity and ion signal response. In some instances, LC can also provide separation of isomeric species which are otherwise indistinguishable by MS. While useful for bench-scale analyses where samples consist of only a select handful of PFAS, LC alone may not be capable of separating all desired PFAS in drinking and wastewater samples. Thus, an additional method of pre-detection separation could be useful for targeted analysis.

Here, I introduce DMS following LC and investigate this two-dimensional separation method in the context of PFAS analysis. Because LC and DMS achieve separation based on different physicochemical properties, I hypothesize that the combination of the two techniques will provide improved analyte resolution and may reveal trends for homologous PFAS species.

4.2 Materials and Methods

4.2.1 Materials

EPA methods 1633-2 and 1633-4, and the International Organization for Standardization (ISO) Native PFAS method standards were purchased as a 2 µg mL⁻¹ solutions in methanol from Accustandard

(Connecticut, United States of America). In total, these standards contain 41 PFAS which are commonly found in ground, tap, and waste waters. This ensemble is diverse and includes perfluorocarboxylic acids (PFCAs), perfluorosulfonic acids (PFSAs), perfluorosulfonamides (FOSAs), perfluorosulfonamido acetic acids (FOSAAAs), fluorotelomercarboxylic acids (FTCAs), fluorotelomer sulfonates (FTSs), and several compounds containing ether linkages. A full list of chemical names and abbreviations is available in the supporting information (see **Table A.2**). HPLC-grade acetonitrile (ACN), MeOH, and IPA were purchased from Sigma-Aldrich (Missouri, United States of America). Ammonium acetate was purchased as a solid from VWR (Pennsylvania, United States of America). Ultrapure water was obtained from a Milli-Q system (Millipore, $18.2 \text{ m}\Omega \text{ cm}^{-1}$). Standards were diluted in MeOH to working concentrations of 100 ng mL^{-1} and 600 ng mL^{-1} ; the lower concentration solution was used for method development with DMS-MS² experiments and the higher concentration was used for all other method development experiments.

4.2.2 DMS-MS² Methods

DMS-MS² experiments were performed using a SelexION DMS cell with a 1 mm gap-height placed between a Turbospray electrospray ionization (ESI) source and the sampling orifice of a QTRAP 5500 hybrid triple quadrupole linear ion trap mass spectrometer (SCIEX, Canada). The mix of standards was directly infused into the ESI source at a flow rate of $15 \mu\text{L min}^{-1}$. A nebulizing gas (N_2 , 50 psi) and an auxiliary gas (N_2 , 40 psi) were applied to desolvate the analytes. A curtain gas (N_2 , 20 psi) was applied to carry analytes through the DMS cell and into the mass spectrometer. N_2 was also used as the gas for collision-induced dissociation (CAD gas, *ca.* 7 mTorr) and was set to high *via* the controlling software (Analyst 1.7). The DMS heater was set to 150°C , and the ion source temperature was set to 35°C . IPA was introduced into the curtain gas line (1.5 mol%) as a chemical modifier to aid in analyte separation. Data was collected via MRM for the two most prominent fragments of individual compounds. MRM transitions and their respective collision energies, declustering potentials, entrance potentials, and cell exit potentials are provided in **Table A.3**. DMS measurements were taken as described in **Section 3.2.2**.

An SV_{PP} of 3800 V provided the most separation for the PFAS in the mixture and was used for all subsequent DMS experiments.

4.2.3 LC-MS² Methods

LC-MS² experiments were conducted using an Agilent 1100 system coupled to the QTRAP 5500 instrument. Analyte separation was achieved on a Phenomenex Luna Omega 3 μ m Polar C18 column (100 \times 3.0 mm). The mobile phases used were 95:5 H₂O:ACN with 2 mM ammonium acetate (A) and 95:5 ACN:H₂O with 2 mM ammonium acetate (B). The mobile phase gradient employed is described in **Table 4.1**. The flow rate remained constant throughout the experiment at 350 μ L min⁻¹. To ensure desolvation of the LC effluent, the ESI source temperature was increased to 350°C. Data was collected in MRM mode using the same transitions identified in the DMS-MS² experiment. Initial LC-MS² runs were performed to visualize analyte separation, and to assess experimental reproducibility. At no point was the LC-MS² method modified to enhance analyte separation. Blanks (MeOH) were injected between standard runs to minimize analyte carry-over.

Table 4.1 LC mobile phase gradient for PFAS analysis.

Time (min)	Mobile Phase A (%)	Mobile Phase B (%)	Flow Rate (μ L min ⁻¹)
0.00	90.0	10.0	350
0.10	90.0	10.0	350
22.00	46.0	54.0	350
22.10	5.0	95.0	350
25.00	5.0	95.0	350
25.10	90.0	10.0	350
30.00	90.0	10.0	350

4.2.4 LC \times DMS-MS² Methods

A major challenge in running a tandem LC \times DMS experiment arises from the time required to scan large CV ranges. Previous work has shown that a combinatory LC and DMS method can be easily achieved on a QTOF instrument.¹¹⁶ Modifying the curtain gas with IPA improves analyte separation in the DMS, but requires CV scans that span 70 V, which can result in a total scan time on the order of minutes when monitoring several MRM channels. Because peak widths in LC experiments are

approximately 6 – 10 s, it is not possible to scan the full CV range on a QTRAP instrument while monitoring each analyte. To circumvent this issue, MRM channels were modified to include a CV parameter, the value of which corresponds to the ionogram peaks obtained in DMS-MS² experiments. Doing so with short dwell times (*viz.* 5 ms for each MRM + 5 ms between scans) allows the instrument to cycle CV quickly, resulting in analyte transmission at any retention time. However, by specifying only the optimal CV value for ion transmission (CV_{opt}) for a given MRM, resulting data will be void of dimensionality in the CV space. Additionally, slight shifts in CV_{opt} would likely go undetected, as any amount of transmitted analyte will produce an instrument response. Large shifts in CV_{opt} would prevent the analyte from being detected at all. To avoid this, multiple MRM channels were created for a given analyte, each with a unique CV value. By specifying CV_{opt} , as well as six points on either side (*i.e.*, 0.5 V steps for a total window of 6 V), the CV landscape surrounding an analyte feature can be adequately sampled. A full list of CV-labeled MRM transitions for this experiment can be found in **Table A.4**.

LC×DMS-MS² experiments were conducted by modifying the LC-MS² method to include the expanded list of CV-labeled MRM channels. DMS-MS² experimental conditions were emulated by introducing IPA (1.5 mol%) into the curtain gas and setting the SV_{PP} to 3800 V. Data acquired from the experiment was processed via a series of in-house python scripts. Thirteen chromatograms were produced for most analytes, corresponding to the thirteen MRM channels across the 6 V range of CV values for each analyte. Nineteen chromatograms were produced for isomer containing compounds (*i.e.* PFHxS, PFHpS and PFOS) which accounts for three additional 0.5 V steps on either side of CV_{opt} . Compound-specific normalization was done to better visualize those species that have relatively low peak intensities due to concentration or ionization efficiency, and a Gaussian smooth was applied to the CV data. The chromatograms were then compiled into a matrix of RT×CV and rendered as a contour plot.

4.3 Results and Discussion

4.3.1 LC-MS² Separation

Figure 4.1 illustrates the LC separation for the 41 PFAS. Several unresolved peaks are present in the TIC (**Figure 4.1A**) as various compounds experience coelution (*e.g.*, PFOS and PFDA *ca.* 14.80 min). Looking at the extracted ion chromatograms, it can be seen that most analytes within a subclass (*e.g.*, PFCAs, PFSAs, *etc.*) are baseline-separated. For PFCAs and PFSAs (**Figure 4.1B** and **Figure 4.1C**, respectively) there are polynomial relationships between retention time and analyte chain length. It can be seen for both the PFCAs and PFSAs that the increase in RT is minimized with increasing carbon chain length (**Figure 4.2**). Interestingly, the shortest PFCAs begin to deviate from the 2nd order polynomial trend and appear to asymptote. This asymptote likely corresponds to the time in which it takes an analyte that has no interaction with the stationary phase to move through the column. The plateau at the high-end of the PFCA trend may be skewed due to PFHxDA eluting after the sharp increase in mobile phase B (MPB) which causes the analytes remaining on the column to be flushed out.

Observations for the fluorotelomer species (FTSs and FTCAs, **Figure 4.1D**) are limited because relatively few of these compounds are present in the chemical standards. However, the fluorotelomers that I did measure are well separated and elute long before the spike in MPB. The distinguishing feature of the fluorotelomers compared to the PFCAs and PFSAs are the two CH₂ units adjacent to the headgroup. This structural difference has an observable impact on the fluorotelomer polarity. For example, 4:2 FTS has a much shorter retention time (4.99 min) than the perfluorinated analogue, PFHxS (11.20 min). However, the differences in retention time seem to diminish with increasing fluorotelomer chain length. For example, 7:3 FTCA and PFDA have near-identical retention times (*ca.* 15.50 min).

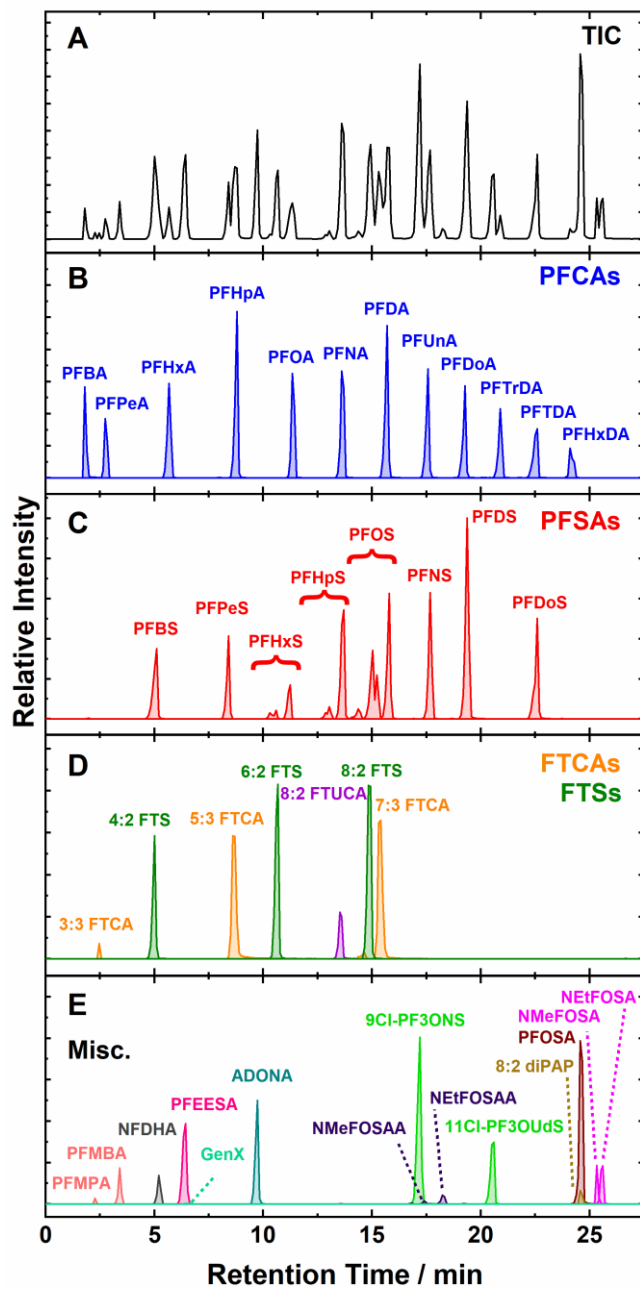


Figure 4.1. Chromatograms showing (A) the 38 detected PFAS by monitoring total ion current, (B) the PFCA species, (C) the PFSA species, (D) the FTCA and FTS species, and (E) fourteen PFAS from other chemical classes. Note that the intensity scales are not equal across different panels.

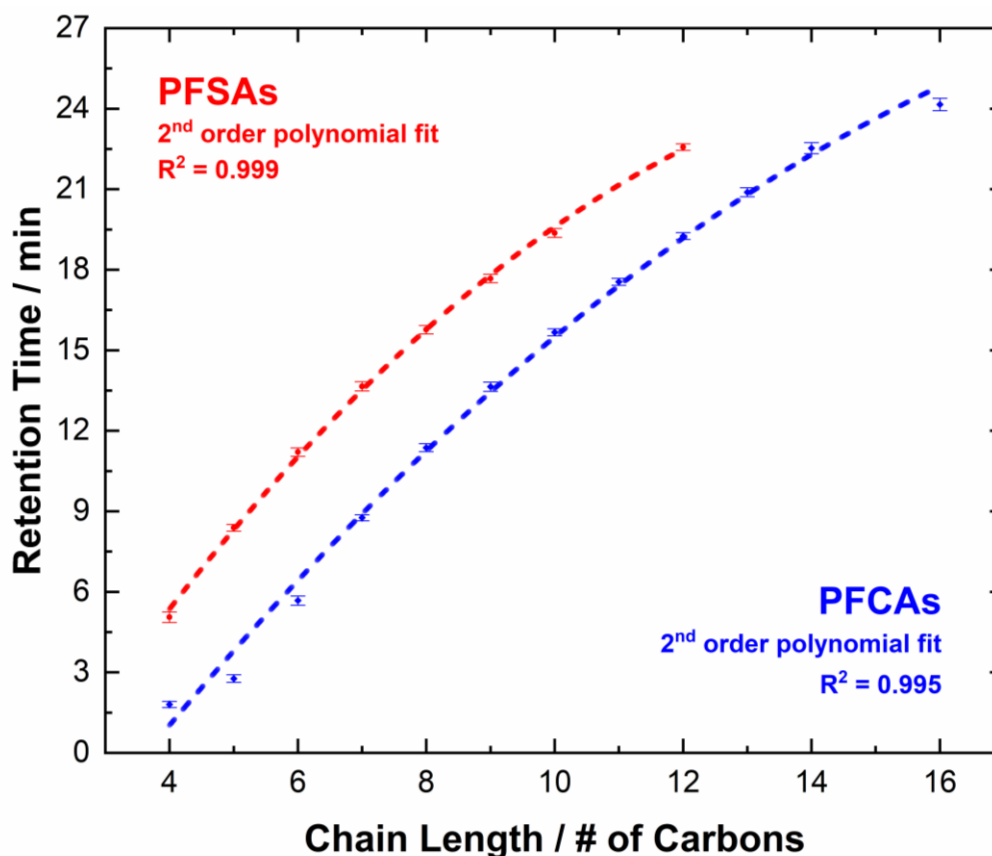


Figure 4.2. Relationship between the LC retention time and the carbon chain length of the PFCA species (blue) and the PFSA species (red).

Near co-elution of NMeFOSA and NEtFOSA (**Figure 4.1E**, *ca.* 25.45 min, $R = 1.19$) is also attributed to the sharp increase in MPB. Furthermore, partially resolved peaks corresponding to isomeric forms of PFHxS, PFHpS, and PFOS are observed around 10.50, 12.90, and 15.10 min, respectively. Convolution of these isomers arises due to the simple mobile phase gradient and the brevity of the method, coupled with their chemical similarity. Although fine-tuning and extending the LC method could potentially improve isomer separation and compound coelution, the incorporation of a DMS dimension offers a more streamlined solution without necessitating an increase in the overall runtime.

4.3.2 DMS-MS² Separation

Figure 4.3 illustrates the DMS separation of 36 of the 41 PFAS species studied. GenX, NFDHA, PFBA, PFPeA and PFMPA identified in the LC measurements undergo field-induced dissociation within the DMS cell at SVs greater than 2000 V (GenX), 2500 V (NFDHA), and 3600 V (PFBA, PFPeA and PFMPA) rendering these molecules undetectable at higher SVs via MS² analysis. Like LC, DMS facilitates effective separation of PFCAs and fluorotelomers, as shown in **Figure 4.3B** and **Figure 4.3D**, respectively. Although the elution order of PFCAs is analogous to that in LC, DMS separation tends to be less effective as chain length increases. This behaviour is a consequence of the micro-solvation process that drives separation in the DMS cell. For small PFAS there is a substantial change in the effective CCS when the analyte molecules undergo dynamic clustering with IPA. However, as the analyte size increases, the effective CCS change imparted by ion-solvent clustering diminishes, resulting in reduced separation between sequential homologues.

Although the elution order in DMS experiments is the same as was observed in LC experiments, DMS separation of the PFSA is poorer. The reduced separation power for PFSA is likely a combination of the size-dependence (discussed above for PFCAs) and the ion charge being more delocalized across SO₃⁻ headgroup compared to the species with CO₂⁻ headgroups (see **Figure A.1**). As a consequence of this delocalization PFSA exhibit relatively weak interactions with the IPA modifier, which leads to an overall reduction in dynamic clustering and smaller differences in ion mobility between the high- and low-field conditions across the SV duty cycle. Thus, relatively small CV corrections are required to ensure PFSA ion transmission.

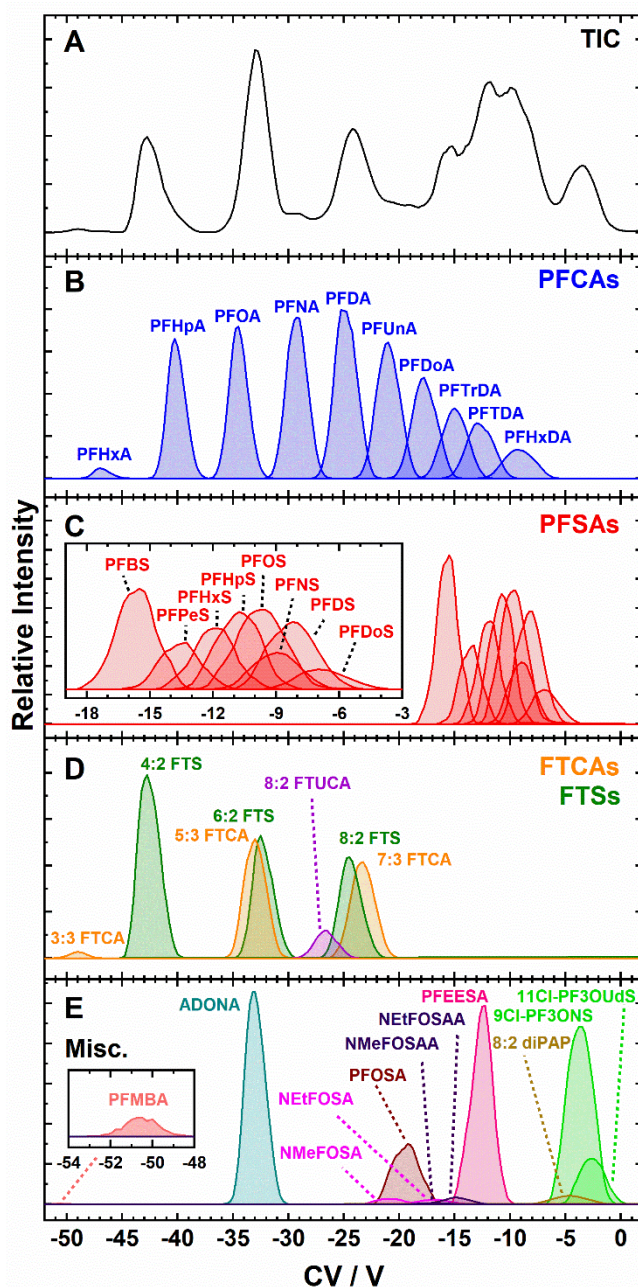


Figure 4.3. Ionograms taken at an SV of 3800 V showing the separation of (A) the 34 detected PFAS by monitoring total ion current, (B) the PFCA species, (C) the PFSA species, (D) the FTCA and FTS species, and (E) eleven PFAS from other chemical classes. Note that the intensity scales are not equal across panels.

Multiple peaks were observed for PFHxS, PFHpS, and PFOS in LC experiments, and these were attributed to the presence branched isomers in the standards. The relative abundances of these species

align with literature expectations; *ca.* 22% branched chain species for PFHxS, 11% for PFHpS, and 32% for PFOS.⁹ Interestingly, DMS measurements yield only a single, but relatively broad peak for each of these analytes. This suggests that the differences in dynamic CCS between the linear and branched species are not sufficient for DMS separation, and that the single peak observed for each molecule is with a convolution of all isomeric forms. Given the relatively poor DMS separation of PFSA homologues, it is reasonable to expect that CCS differences associated with the repositioning of a CF₃ group in one particular PFSA (*i.e.*, branched versus linear isomers) would have only a minor impact on the differential mobility.

4.3.3 LC×DMS-MS² Separation

When coupling LC with DMS, I observed significant CV shifts from the expected centroid based on direct infusion DMS measurements. The CV centroids in the LC×DMS experiments were shifted for nearly all the observed compounds, some by more than 2 V. Interestingly, analytes containing sulfate and sulfonamide headgroups were affected to a much greater extent than those containing carboxylate and sulfonamidoacetic acid headgroups. On average, carboxylate-containing analytes shifted by 0.36 V ± 0.46 V at SV = 3800 V. In comparison, analytes containing sulfate and sulfonamide groups exhibited an average CV shift of 1.36 V ± 0.39 V at SV = 3800 V. A full list of CV shifts can be found in **Table A.5**. I hypothesize that these CV shifts arise from a combination of the LC flow rate, which was 23 times greater than direct infusion DMS experiments (thereby introducing significantly more solvent vapor to the system), and the ACN content within MPB, which impacts dynamic ion-solvent clustering within the DMS cell. Bissonette and coworkers previously described a preferential solvation effect that occurs in mixed-modifier DMS environments, specifically highlighting that ACN dominates dynamic clustering even when present in much smaller amounts than other modifiers.¹⁰⁰ In the case of the PFAS molecules studied here, I suspect that some amount of ACN from the mobile phase enters the DMS cell via the carrier gas and disrupts analyte clustering with IPA. To test this hypothesis, direct infusion DMS experiments were rerun while T-infusing the LC mobile phase (350 μL min⁻¹). The mobile phase

composition was varied between runs to match the expected composition at the elution times for the sulfonate containing analytes. For example, PFBS elutes at 4.30 min which, when considering the solvent delay of *ca.* 2.00 min, corresponds to an ACN composition of $\sim 15\%$ MPB. DMS experiments with five different mobile phase compositions corresponding to 15%, 22%, 27%, 40%, and 46% MPB were conducted to explore the solvent-induced CV shifts. **Figure 4.4** shows the ionograms for PFOA and PFOS in each of the five experiments. The ionogram peak positions of PFOA are relatively consistent, despite the 30% difference in MPB across the five experiments. The ionogram peak position for PFOA is centered around -34.0 V, which is slightly shifted from the value of -34.5 V observed during direct infusion DMS experiments. This CV shift of *ca.* 0.5 V between direct infusion and T-infusion experiments (*ca.* 0.5 V) was observed for all PFCAs and FOSAAs, which exhibited negligible MPB-dependent CV shifts. In contrast, the ionogram peak position for PFOS shifted from CV = -9.0 V (with 15% MPB T-infused) to CV = -7.8 V (with 46% MPB T-infused), which is significantly different from the value of CV = -9.7 V observed in direct infusion experiments. A similar increase in optimal CV with increasing MPB composition was observed for all sulfonate and sulfonamide compounds. Having identified the MPB-dependence of ionogram peak positions, I could then estimate the optimal CV values in LC \times DMS experiments. For example, the RT of 15.76 min for PFOS corresponds to an MPB composition of *ca.* 40% (accounting for the dead volume), which yields a $CV_{opt} = -8.6$ V. This procedure allowed us to reoptimize CV centroid values for all compounds.

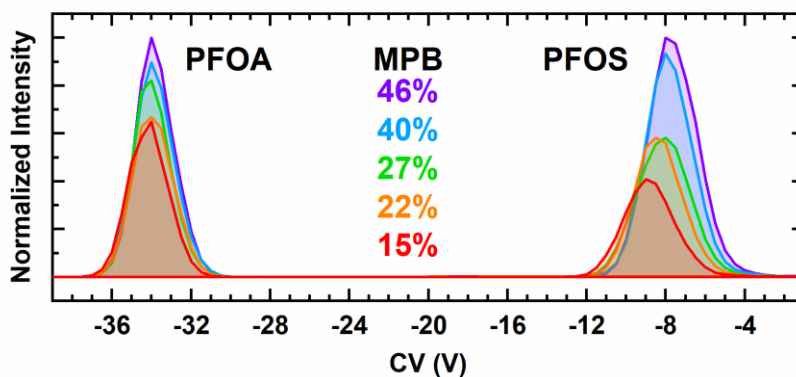


Figure 4.4. Ionograms measured at $SV = 3800$ V for PFOA (left) and PFOS (right) with varying mobile phase B (MPB) composition. The optimal CV value for PFOA remains relatively constant as MPB increases, whereas that of PFOS gradually shifts to more positive values.

Figure 4.5 shows the 2D LC×DMS plot for 34 PFAS compounds. Seven compounds from the standard mixture were undetected owing to ionization efficiency and thermodynamic stability issues. Of the 34 detected species, only two instances of coelution are observed; 8:2 FTUCA and PFNA, and 7:3 FTCA, 8:2 FTS and PFDA. In other words, implementation of 2D LC×DMS resulted in the baseline separation of 29 unique species. In addition to the enhanced resolving power, the 2D LC×DMS method exhibits obvious trends for PFAS subclasses. For example, a clear distinction can be made between the PFCA and PFSA classes (see **Figure 4.5**; highlighted in blue and red, respectively); one could potentially leverage these 2D LC×DMS trends to predict the optimal CV and retention time of PFCAs and PFSA not explicitly measured in this study. The FTCA and FTS classes (see **Figure 4.5**; highlighted in orange and green, respectively) also exhibit a clear trend in the 2D separation space, close to that of the PFCAs. The trends for the FTS and PFCA species converge with increasing chain length, finally overlapping near perfluorodecanoic acid. It is interesting that, although the PFSA and FTSs contain sulfonate headgroups, the two classes occupy distinct regions of the 2D separation space and exhibit different trends from one another with respect to (RT, CV) dependence. I attribute this behaviour to the methylene (*i.e.*, $-\text{CH}_2-$) groups that are present in the FTS compounds. Whereas the electron withdrawing fluorine atoms on the α and β carbons remove electron density from the

headgroup in the PFASs, the methylene carbons of the FTSs do not as strongly affect the charge density of the SO_3^- headgroup. Consequently, the FTS species exhibit much stronger interactions with the IPA modifier than do the PFASs.

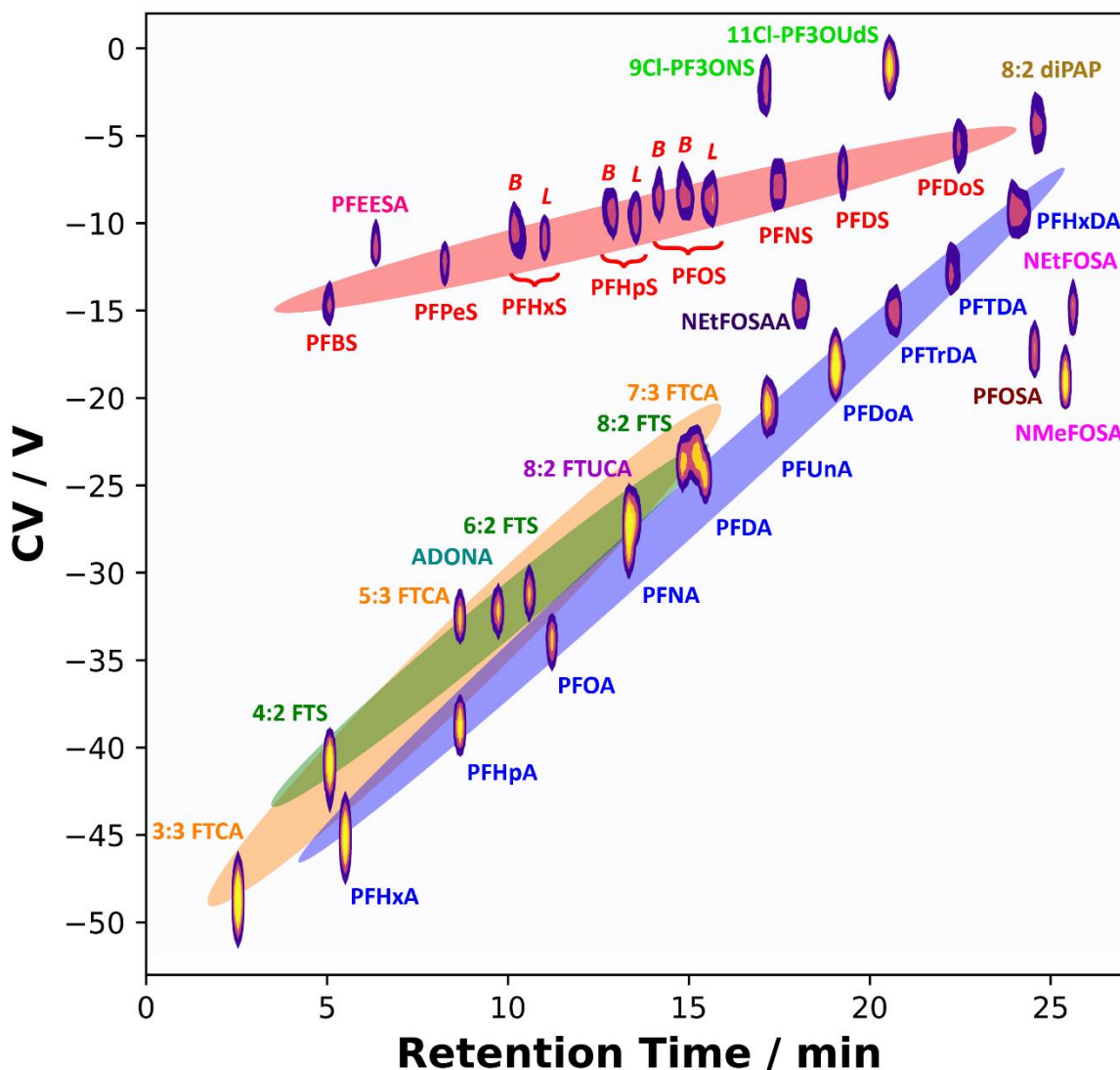


Figure 4.5. 2D LCx DMS plot showing the separation for 34 PFAS compounds. The ovals are a guide to the eye which highlight the approximate trend lines for the PFSA species (red), the PFCA species (blue), the FTS species (green), and the FTCA species (orange). Features corresponding to branched isomers (denoted by *B*) of three PFASs (PFHxS, PFHps, and PFOS) are distinguishable from the linear species (denoted by *L*).

In **Figure 4.5** I observe multiple features for three compounds: PFHxS, PFHpS, and PFOS. These features, for which visibility was improved by peak-specific normalization, are associated with different isomeric species. Peak-specific normalization involved identifying the isomer peaks and normalizing the individual signals for each feature to unity. Thus, branched isomers (denoted by *B* in **Figure 4.5**) become more obvious on the plot. Interestingly, the isomer peaks appear to be slightly shifted in CV space relative to the linear species, showing that there is in fact some separation in the DMS cell. This interpretation is further supported by plotting the ionogram peak FWHM for the PFSA homologous series measured by DMS-MS² (see **Figure 4.6**). In this plot, a relatively consistent increase in peak FWHM is observed as the fluorocarbon chain length increases. However, PFOS is a clear outlier for this trend, having a much larger FWHM than the other members of the homologous series. The DMS-MS² ionogram peak for PFHpS, which exhibits two resolved isomer features in the 2D LC×DMS plot, also exhibits a relatively large FWHM (though somewhat less so than PFOS). However, in the case of PFHxS, which also exhibits two resolved isomer features in the 2D LC×DMS plot, the DMS-MS² ionogram peak FWHM increase is approximately the same as that of PFBS and PFPeS. This variability in ionogram FWHM reflects the relative abundance of the branched isomers for these species and the differences in their differential mobility behaviour.

Although baseline separation of isomers is not achieved in CV space, there is a slight trend in CV space for isomeric species that is apparent in the 2D LC×DMS plot – branched isomers transmit at a slightly more positive CV than do linear isomers. Given that higher SVs can sometimes enhance DMS resolution, an obvious question is: what happens to resolution in CV space when higher SVs are applied? Unfortunately, in this gaseous environment, field-induced dissociation impacts ion signal above $SV = 3800$ V. However, I am currently exploring the impact of introducing additional “protective” gases to the DMS environment, and preliminary work suggests this may be a beneficial approach.

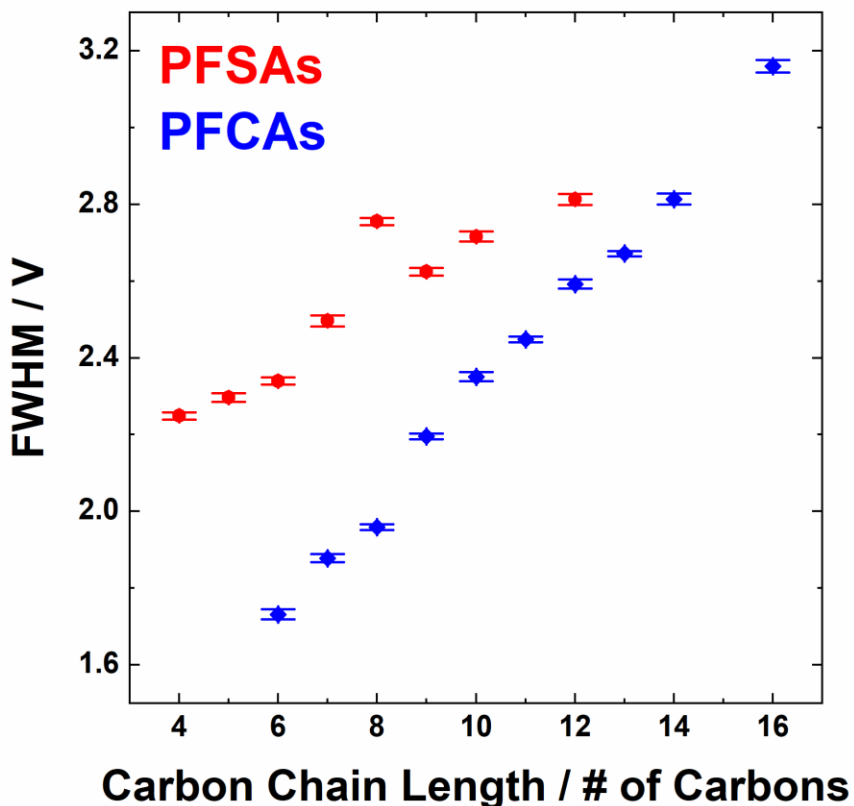


Figure 4.6. Full width at half maximum (FWHM) values for ionograms of the PFCA species (blue) and the PFSA species (red) as a function of chain length. Note that there is a linear increase in FWHM for the PFCA species, however there is a significant outlier in the PFSA trend. This outlier occurs at the 8 carbon-long chain (i.e. PFOS) and is attributed to the presence of multiple isomers which are slightly separated in DMS measurements.

4.3.4 Instrument Quantitation Limits

To assess the feasibility of employing 2D LC×DMS-MS² to quantify PFAS in targeted analyses, I determined the limits of quantitation (LOQ) for the PFAS species in the mixtures of standards. Standard solutions ranging in concentration from 1 ng mL⁻¹ up to 1000 ng mL⁻¹ were prepared in MeOH and were analysed seven times each in order of increasing concentration. Analyte peak areas were measured and then compared to a blank sample to determine the signal-to-noise ratio (S/N). The compound specific LOQs reported are the concentrations corresponding to an average S/N > 10 with an RSD < 20% for the replicates. In some cases, the reported LOQ is relatively high because, although the S/N

for the measurement was relatively high, the RSDs of replicates measured at lower concentrations exceeded 20%. A description of the data-processing workflow is provided in the supporting information. **Table 4.2** provides the LOQs for 33 of the PFAS that I measured; the LOQ for PFHxS is not reported because the RSD for replicates at all concentrations was > 20%.

Table 4.2 Instrument LOQs for 33 PFAS as determined for the 2D LC×DMS-MS² method. LOQs were determined via seven replicate measurements.

Compound	LOQ (ng mL ⁻¹)	S/N	RSD (%)
PFHpA	20	15.3	17.0
PFOA	75	28.9	13.9
PFNA	10	10.9	10.9
PFDA	20	29.6	16.0
PFUnA	20	44.7	14.8
PFDoA	20	28.1	16.1
PFTTrDA	30	25.5	18.5
PFTDA	50	67.6	10.7
PFHxDA	75	36.7	10.9
PFBS	20	10.9	5.9
PFPS	10	12.3	15.2
PFHxS	20	18.5	10.6
PFHpS	7.5	52.9	6.0
PFOS	5	15.9	15.4
PFNS	7.5	67.1	14.9
PFDS	5	12.7	16.7
PFDoS	7.5	49.6	13.1
3:3FTCA	300	15.4	13.9
5:3FTCA	7.5	80.0	6.4
7:3FTCA	3	25.7	14.7
4:2FTS	75	52.0	13.4
6:2FTS	5	14.1	12.3
8:2FTS	5	13.1	5.8
8:2diPAP	75	33.3	12.2
8:2FTUCA	30	41.7	15.2
9Cl-PF3ONS	1	10.3	17.6
11Cl-PF3OUdS	5	14.1	18.2
NMeFOSA	50	283.7	19.0
NEtFOSA	75	436.1	5.4
NEtFOSAA	30	15.2	16.8
ADONA	5	14.3	20.0

PFEESA	20	14.1	12.5
PFOSA	10	93.4	15.6
Average	33	51.0	13.5
STD	54	85	4

Note: the LOQ for PFHxA is not reported because the RSDs for replicates at all concentrations were > 20%.

The LOQs reported in **Table 4.2** are determined for the instrument measurement method. These quantitation limits could be lowered substantially by introducing a preconcentration step into the analytical workflow. For example, pre-concentrating samples *via* SPE could lower LOQs by three orders of magnitude, enabling measurements of concentrations on the order of ng L⁻¹ (*i.e.*, parts-per-trillion). Thus, introducing an SPE preconcentration, as is done in EPA PFAS analysis methods, can facilitate 2D LC×DMS-MS² analysis with LOQs that approach the current state-of-the-art targeted analyses.^{33,43,117,118}

4.4 Conclusions

Separation of 34 PFAS compounds was improved by incorporating DMS into an existing LC-MS² workflow. Baseline resolution for 29 of the 34 measured PFAS was achieved in the 2D LC×DMS space; 2 and 3 PFAS coeluted in (RT, CV) space, respectively. In 1D LC measurements, only 5 compounds are baseline resolved from all other compounds in the mixture. The introduction of DMS provided an orthogonal separation dimension complementary to LC. For example, PFOA and PFHxS coelute in the LC dimension, but have a 24.0 V difference in the DMS CV dimension. Similarly, PFHxS and PFHxDA have overlapping CVs but exhibit a retention time difference of *ca.* 11 minutes. These separations were achieved without increasing the time required and are approaching the LOQs expected for a 1D LC-MS² method.

Also encouraging is the fact that a plot of the 2D LC×DMS data revealed distinct trends for various PFAS subclasses. These distinct trends arise owing to the differences between chemical subclasses with respect to dynamic ion-solvent clustering, and thus differences in effective ion CCS, within the DMS cell. The subclass trends in the 2D LC×DMS space, which converge at low CV and high RT, could

provide predictability with respect to the identity of unknowns, or at least the class to which they belong. To advance research in this direction, full CV scans and non-targeted analysis are necessary, and could be accomplished using a qToF mass spectrometer.¹¹⁶ An interesting additional possibility is the application of machine learning to enable prediction of physicochemical properties using the 2D LC×DMS data. Recent studies have demonstrated that accurate predictive ML models that use only DMS or LC data are possible.^{101,119} Combining DMS and LC data in a single model might improve accuracy and precision.

For three of the PFSA species investigated – PFHxS, PFHpS, and PFOS – both branched and linear isomers were present in the chemical standards. Although separation of various isomers was not dramatically improved by the 2D LC×DMS compared to conventional LC-MS² analysis (*e.g.*, between the right-most and middle features of PFOS $R = 1.36$ in the 2D measurement compared to $R = 1.29$ in 1D LC), the 2D data did reveal that the branched and linear species do separate slightly in the CV space (*i.e.*, branched isomers elute at slightly more positive CVs than do linear isomers). Whether resolution can be improved in the CV dimension is an open question. Such an improvement might be limited by the fact that higher SVs, which in principle could result in improved resolving power, also result in ion fragmentation.

Ultimately, this work demonstrates the efficacy of targeted 2D LC×DMS-MS² analysis. By taking advantage of two orthogonal separation techniques prior to MS detection, ion suppression and chemical noise are substantially reduced. This diminished background could be particularly useful when analysing species present in (or extracted from) complex matrices since it is unlikely that isobaric interferences would transmit with RTs and CVs identical to those of the target analytes. Investigating the performance of the 2D LC×DMS-MS² method for analysing PFAS in environmental samples or for analysing another class of molecules (*e.g.*, various types of pharmaceuticals) are interesting future research directions.

Chapter 5

Conclusions and Outlook

Chemical separation *via* differential mobility spectrometry was optimized for 41 PFAS compounds. This was accomplished by measuring analyte dispersion in the following DMS environments: a pure N₂ carrier gas, N₂ doped with MeOH, and N₂ doped with IPA. The observed behaviour of PFAS in these environments facilitates determining ideal separation conditions and provides insight on their physicochemical properties. The choice of chemical modifier yields dramatically different dispersion behaviour of individual PFAS classes, owing to the strength and extent of ion-solvent clustering. Previous work has demonstrated the correlation between ion-solvent clustering, Log *P*, and Log *S*.¹⁰¹ This indicates that different PFAS classes likely have varying solubility and octanol-water partition, and thus should interact differently within the body. Since the physicochemical principles that underpin DMS separation are different than those underpinning LC, I aimed to enhance chemical separation by combining orthogonal LC and DMS dimensions.

In **Chapter 3**, I describe the behaviour of anions in a variety of DMS environments. Anion behaviour depends on multiple variables, which include the composition of the carrier gas, the interaction strength of ions and collision gases, and the apparent change to ion CCS upon clustering and de-clustering with solvent molecules. I highlighted the case of deprotonated 4-mercaptobenzoic acid, which exhibits two unique DMS dispersion curves associated with two different sites of deprotonation (*i.e.*, the -COOH and -SH groups). These two deprotomers are separable in a pure N₂ environment, indicating that they exhibit differences in their field dependent mobilities. That such subtle differences may be resolved by DMS is a testament to its power as a technique for analytical separations. The major goals of this work were twofold: (1) to expand our understanding of (and database for) ion behaviour in dynamic DMS environments by considering anionic species, and (2) to explore the DMS behaviour of deprotonated PFAS species, in anticipation of developing a two-dimensional (2D) hybrid LC×DMS-MS^N technique. With respect to PFAS separation by DMS, employing a MeOH-modified environment yielded

reasonable separation of the PFCAs but the PFSAAs remained unresolved. To improve PFSA separation, I explored the use of an IPA modifier. This approach further enhanced the resolution of the PFCAs, but only slightly improved PFSA separation. These results demonstrate that PFSAAs cluster extremely weakly with alcohols, and future efforts to improve their DMS separation should focus on non-protic modifiers. Despite the relatively poor resolution of the PFSAAs, I felt that the improvement afforded by introducing the IPA modifier was sufficient for the purposes of this work.

In **Chapter 4** I describe the integration of DMS technology within an LC-MS workflow. The 2D separation of PFAS compounds is explored as a test case. Of the 41 targeted PFAS species, I was able to detect 34. Some of the PFAS compounds were susceptible to field-induced fragmentation within the DMS cell (*i.e.*, PFBA, PFPeA, GenX, NFDHA, PFMPA, PFMBA, and NMeFOSAA). Of the 34 detected species, 29 were baseline resolved; of the remaining five, a group of two compounds co-eluted and a group of three compounds co-eluted. When considering only the LC dimension, it is possible to baseline resolve only five of the PFAS compounds. The PFSA species elute within a narrow CV window, meaning their trend in the 2D space is distinct from that of the PFCAs and fluorotelomers. These trends facilitate non-target analyses, as a compound's position in the 2D space provides an extra classifier for identification. While DMS is known to reduce ion signal intensity, it also can reduce chemical noise. Owing to this, the quantitation limits for this 2D method approach state-of-the-art LC-MS² methods if samples were to be pre-concentrated *via* SPE.^{33,43,117,118} I found that CV_{opt} values for sulfonate-containing PFAS tended to increase with greater ACN content in the mobile phase. It is interesting that the ACN seems to have no effect on carboxylate-containing PFAS. Further investigation of this phenomenon is required. In principle, DMS operates on a millisecond timescale, however when monitoring several MRM channels over a large CV window, the full scan time is on the order of a few minutes. The differences in timescales prevented the direct coupling of LC to DMS and required the use of CV-labeled MRM channels for 2D data acquisition. These challenges highlight the difficulty in combining the LC and DMS methods on the triple-quadrupole system.

This thesis leads to numerous directions for future research. The LC×DMS method should be tested on environmental samples to gauge its efficacy. The complexity of real-world samples often results in heightened chemical noise, and with it, high limits of quantitation. DMS can reduce chemical noise, as any isobaric interferences are unlikely to share an optimal CV with the analyte of interest. My method can easily be applied for targeted studies of environmental samples but its application for non-target analysis requires some careful thought. Ideally, one could monitor the precursors of common fragments or neutral losses belonging to various PFAS classes (SO_3^- , C_2F_5^- , HF, CO_2 , *etc.*) at all CVs in a scan. The position of these features in the resultant 2D plot would aid in compound identification. For example, a compound which produces an HSO_3^- fragment is likely a fluorotelomer sulfonate (FTS). Its position relative to known FTS compounds, along with its mass, then indicates its length and size. Alternatively, a qToF detector would be highly useful, as it allows for continuous, rapid cycling of large CV windows throughout the duration of an LC method.¹¹⁶ This setup could yield entire ionograms for each point in the LC measurement and would circumvent the need for fragment monitoring. These dimensions could then be filtered based on mass and mass defect to aid in PFAS identification.

Another direction for future work involves the generation of predictive machine learning models. The data collected in **Chapter 3** will serve as a foundation for the prediction of PFAS dispersion behaviour. Ideally, a user could provide a PFAS candidate structure, and the model would yield the predicted dispersion curve. The prediction could then be used as an additional classifier in compound identification, or it may narrow scan windows in non-target analyses. Given the suspected thousands of PFAS compounds – and the few dozen available chemical standards – the current experimental set of PFAS represents a miniscule proportion of training data for predictive models. Future work should focus on the DMS measurement of other PFAS and PFAS-like compounds to diversify the data for machine learning.

In this thesis I occasionally observed the field-induced dissociation of certain PFAS species at relatively low separation voltages, preventing their detection at ideal separation conditions. To address

this problem, one could use protective gases within the DMS cell to increase survival yields of fragile ions. A member of the Hopkins Lab is currently investigating CO₂ as a protective gas for the GenX species. Their work has shown that introducing as little as 10% CO₂ into the DMS carrier gas increases GenX signal intensity by nearly two orders of magnitude. This would be useful for enabling the detection of fragile compounds at high SVs and lowering quantitation limits in LC×DMS-MS^N analysis.

While this thesis focuses on PFAS, it is worth stating the generalizability of the LC×DMS-MS^N method. Aside from PFAS, my method may be applied to other pollutants such as disinfection by-products (DBPs), drug metabolites, and even pharmaceuticals. It should also be noted that the method is applicable to anions or cations. Ultimately, this work demonstrates the efficacy of combined LC×DMS as an analytical tool while exploring the separation of PFAS within a mixture.

References

- (1) Wang, Z.; Dewitt, J. C.; Higgins, C. P.; Cousins, I. T. A Never-Ending Story of Per- and Polyfluoroalkyl Substances (PFASs)? *Environ Sci Technol* 2017, 51 (5), 2508–2518. <https://doi.org/10.1021/acs.est.6b04806>.
- (2) Rayne, S.; Forest, K. Perfluoroalkyl Sulfonic and Carboxylic Acids: A Critical Review of Physicochemical Properties, Levels and Patterns in Waters and Wastewaters, and Treatment Methods. *Journal of Environmental Science and Health Part A* 2009, 44 (12), 1145–1199. <https://doi.org/10.1080/10934520903139811>.
- (3) Leung, S. C. E.; Wanninayake, D.; Chen, D.; Nguyen, N. T.; Li, Q. Physicochemical Properties and Interactions of Perfluoroalkyl Substances (PFAS) - Challenges and Opportunities in Sensing and Remediation. *Science of The Total Environment* 2023, 905, 166764. <https://doi.org/10.1016/J.SCITOTENV.2023.166764>.
- (4) Government of Canada. Per- and Polyfluoroalkyl Substances (PFAS). July 29, 2021. <https://www.canada.ca/en/health-canada/services/chemical-substances/other-chemical-substances-interest/per-polyfluoroalkyl-substances.html> (accessed 2022-12-01).
- (5) Kishi, T.; Arai, M. Study on the Generation of Perfluorooctane Sulfonate from the Aqueous Film-Forming Foam. *J Hazard Mater* 2008, 159 (1), 81–86. <https://doi.org/10.1016/j.jhazmat.2007.09.122>.
- (6) Banzhaf, S.; Filipovic, M.; Lewis, J.; Sparrenbom, C. J.; Barthel, R. A Review of Contamination of Surface-, Ground-, and Drinking Water in Sweden by Perfluoroalkyl and Polyfluoroalkyl Substances (PFASs). *Ambio*. Springer Netherlands April 1, 2017, pp 335–346. <https://doi.org/10.1007/s13280-016-0848-8>.
- (7) Health Canada. *Water talk: Summary of drinking water values for PFOS, PFOA and other PFAS*. Government of Canada. <https://www.canada.ca/en/services/health/publications/healthy->

living/water-talk-drinking-water-screening-values-perfluoroalkylated-substances.html (accessed 2024-03-18).

(8) Health Canada. *Draft objective for per- and polyfluoroalkyl substances in Canadian drinking water: Overview*. Government of Canada. <https://www.canada.ca/en/health-canada/programs/consultation-draft-objective-per-polyfluoroalkyl-substances-canadian-drinking-water/overview.html> (accessed 2024-04-08).

(9) Mu, H.; Wang, J.; Chen, L.; Hu, H.; Wang, J.; Gu, C.; Ren, H.; Wu, B. Identification and Characterization of Diverse Isomers of Per- and Polyfluoroalkyl Substances in Chinese Municipal Wastewater. *Water Res* 2023, 230, 119580. <https://doi.org/10.1016/J.WATRES.2023.119580>.

(10) Pérez, F.; Nadal, M.; Navarro-Ortega, A.; Fàbrega, F.; Domingo, J. L.; Barceló, D.; Farré, M. Accumulation of Perfluoroalkyl Substances in Human Tissues. 2013. <https://doi.org/10.1016/j.envint.2013.06.004>.

(11) NORDBY, G. L.; LUCK, J. M. Perfluorooctanoic Acid Interactions with Human Serum Albumin. *J Biol Chem* 1956, 219 (1), 399–404. [https://doi.org/10.1016/s0021-9258\(18\)65805-3](https://doi.org/10.1016/s0021-9258(18)65805-3).

(12) De Silva, A. O.; Armitage, J. M.; Bruton, T. A.; Dassuncao, C.; Heiger-Bernays, W.; Hu, X. C.; Kärrman, A.; Kelly, B.; Ng, C.; Robuck, A.; Sun, M.; Webster, T. F.; Sunderland, E. M. PFAS Exposure Pathways for Humans and Wildlife: A Synthesis of Current Knowledge and Key Gaps in Understanding. *Environmental Toxicology and Chemistry*. Wiley Blackwell March 1, 2021, pp 631–657. <https://doi.org/10.1002/etc.4935>.

(13) Chu, K.; Lu, Y.; Hua, Z.; Liu, Y.; Ma, Y.; Gu, L.; Gao, C.; Yu, L.; Wang, Y. Perfluoroalkyl Acids (PFAAs) in the Aquatic Food Web of a Temperate Urban Lake in East China: Bioaccumulation, Biomagnification, and Probabilistic Human Health Risk. *Environmental Pollution* 2022, 296, 118748. <https://doi.org/10.1016/J.ENVPOL.2021.118748>.

(14) Cara, B.; Lies, T.; Thimo, G.; Robin, L.; Lieven, B. Bioaccumulation and Trophic Transfer of Perfluorinated Alkyl Substances (PFAS) in Marine Biota from the Belgian North Sea: Distribution and

Human Health Risk Implications. *Environmental Pollution* 2022, 311, 119907. <https://doi.org/10.1016/J.ENVPOL.2022.119907>.

(15) Statistics Canada. *Canadian Health Measures Survey: Environmental Laboratory Data, 2016 and 2017*; 2019. <https://www150.statcan.gc.ca/n1/daily-quotidien/191113/dq191113a-eng.htm> (accessed 2024-07-08).

(16) Yu, N.; Wang, X.; Zhang, B.; Yang, J.; Li, M.; Li, J.; Shi, W.; Wei, S.; Yu, H. Distribution of Perfluorooctane Sulfonate Isomers and Predicted Risk of Thyroid Hormonal Perturbation in Drinking Water. *Water Res* 2015, 76, 171–180. <https://doi.org/10.1016/j.watres.2015.02.047>.

(17) Kärrman, A.; Langlois, I.; Bavel, B. van; Lindström, G.; Oehme, M. Identification and Pattern of Perfluorooctane Sulfonate (PFOS) Isomers in Human Serum and Plasma. *Environ Int* 2007, 33 (6), 782–788. <https://doi.org/10.1016/j.envint.2007.02.015>.

(18) Coperchini, F.; Croce, L.; Denegri, M.; Pignatti, P.; Agozzino, M.; Netti, G. S.; Imbriani, M.; Rotondi, M.; Chiovato, L. Adverse Effects of in Vitro GenX Exposure on Rat Thyroid Cell Viability, DNA Integrity and Thyroid-Related Genes Expression. *Environmental Pollution* 2020, 264. <https://doi.org/10.1016/j.envpol.2020.114778>.

(19) Liang, L.; Pan, Y.; Bin, L.; Liu, Y.; Huang, W.; Li, R.; Lai, K. P. Immunotoxicity Mechanisms of Perfluorinated Compounds PFOA and PFOS. *Chemosphere*. Elsevier Ltd March 1, 2022. <https://doi.org/10.1016/j.chemosphere.2021.132892>.

(20) Rickard, B. P.; Rizvi, I.; Fenton, S. E. Per- and Poly-Fluoroalkyl Substances (PFAS) and Female Reproductive Outcomes: PFAS Elimination, Endocrine-Mediated Effects, and Disease. *Toxicology* 2022, 465. <https://doi.org/10.1016/j.tox.2021.153031>.

(21) Schmidt, C. W. Reduced Bone Mineral Density in Children: Another Potential Health Effect of PFAS. *Environmental Health Perspectives*. Public Health Services, US Dept of Health and Human Services April 1, 2020, pp 1–2. <https://doi.org/10.1289/EHP6519>.

- (22) Bell, E. M.; De Guise, S.; McCutcheon, J. R.; Lei, Y.; Levin, M.; Li, B.; Rusling, J. F.; Lawrence, D. A.; Cavallari, J. M.; O'Connell, C.; Javidi, B.; Wang, X.; Ryu, H. Exposure, Health Effects, Sensing, and Remediation of the Emerging PFAS Contaminants – Scientific Challenges and Potential Research Directions. *Science of the Total Environment*. Elsevier B.V. August 1, 2021. <https://doi.org/10.1016/j.scitotenv.2021.146399>.
- (23) Szilagyi, J. T.; Avula, V.; Fry, R. C. Perfluoroalkyl Substances (PFAS) and Their Effects on the Placenta, Pregnancy, and Child Development: A Potential Mechanistic Role for Placental Peroxisome Proliferator–Activated Receptors (PPARs). *Current Environmental Health Reports*. Springer September 1, 2020, pp 222–230. <https://doi.org/10.1007/s40572-020-00279-0>.
- (24) United States Environmental Protection Agency. *Key EPA Actions to Address PFAS*. United States Environmental Protection Agency. <https://www.epa.gov/pfas/key-epa-actions-address-pfas> (accessed 2024-03-18).
- (25) Justice Laws Website. *Prohibition of Certain Toxic Substances Regulations, 2012*. Government of Canada. <https://laws-lois.justice.gc.ca/eng/regulations/SOR-2012-285/page-4.html#h-788616> (accessed 2024-03-18).
- (26) Canadian Food Inspection Agency. *Notice to industry – Intent to engage on implementing an interim standard for per- and polyfluoroalkyl substances (PFAS) in biosolids*. Government of Canada. <https://inspection.canada.ca/en/plant-health/fertilizers/notices-industry/2023-05-19> (accessed 2024-07-08).
- (27) *Perfluoroalkyl and Polyfluoroalkyl Substances (PFAS)*. National Institute of Environmental Health Sciences. <https://www.niehs.nih.gov/health/topics/agents/pfc/index.cfm> (accessed 2022-12-01).
- (28) Charbonnet, J. A.; McDonough, C. A.; Xiao, F.; Schwichtenberg, T.; Cao, D.; Kaserzon, S.; Thomas, K. V.; Dewapriya, P.; Place, B. J.; Schymanski, E. L.; Field, J. A.; Helbling, D. E.; Higgins, C. P. Communicating Confidence of Per- and Polyfluoroalkyl Substance Identification via High-

Resolution Mass Spectrometry. *Environmental Science and Technology Letters*. American Chemical Society June 14, 2022, pp 473–481. <https://doi.org/10.1021/acs.estlett.2c00206>.

(29) Munoz, G.; Michaud, A. M.; Liu, M.; Vo Duy, S.; Montenach, D.; Resseguier, C.; Watteau, F.; Sappin-Didier, V.; Feder, F.; Morvan, T.; Houot, S.; Desrosiers, M.; Liu, J.; Sauv e, S. Target and Nontarget Screening of PFAS in Biosolids, Composts, and Other Organic Waste Products for Land Application in France. *Environ Sci Technol* 2021. <https://doi.org/10.1021/acs.est.1c03697>.

(30) Taylor, R. B.; Sapozhnikova, Y. Comparison and Validation of the QuEChERSER Mega-Method for Determination of per- and Polyfluoroalkyl Substances in Foods by Liquid Chromatography with High-Resolution and Triple Quadrupole Mass Spectrometry. *Anal Chim Acta* 2022, 1230, 340400. <https://doi.org/10.1016/J.ACA.2022.340400>.

(31) Lu, Y.; Meng, L.; Ma, D.; Cao, H.; Liang, Y.; Liu, H.; Wang, Y.; Jiang, G. The Occurrence of PFAS in Human Placenta and Their Binding Abilities to Human Serum Albumin and Organic Anion Transporter 4. *Environmental Pollution* 2021, 273, 116460. <https://doi.org/10.1016/J.ENVPOL.2021.116460>.

(32) Lorenzo, M.; Campo, J.; Farr e, M.; P erez, F.; Pic o, Y.; Barcel o, D. Perfluoroalkyl Substances in the Ebro and Guadalquivir River Basins (Spain). *Science of The Total Environment* 2016, 540, 191–199. <https://doi.org/10.1016/J.SCITOTENV.2015.07.045>.

(33) Miserli, K.; Boti, V.; Konstantinou, I. Analysis of Perfluorinated Compounds in Sewage Sludge and Hydrochar by UHPLC LTQ/Orbitrap MS and Removal Assessment during Hydrothermal Carbonization Treatment. *Science of The Total Environment* 2024, 929, 172650. <https://doi.org/10.1016/J.SCITOTENV.2024.172650>.

(34) Borrull, J.; Colom, A.; Fabregas, J.; Pocurull, E.; Borrull, F. A Liquid Chromatography Tandem Mass Spectrometry Method for Determining 18 Per- and Polyfluoroalkyl Substances in Source and Treated Drinking Water. *J Chromatogr A* 2020, 1629, 461485. <https://doi.org/10.1016/J.CHROMA.2020.461485>.

- (35) Bartolomé, M.; Gallego-Picó, A.; Huetos, O.; Lucena, M. Á.; Castañó, A. A Fast Method for Analysing Six Perfluoroalkyl Substances in Human Serum by Solid-Phase Extraction on-Line Coupled to Liquid Chromatography Tandem Mass Spectrometry. *Anal Bioanal Chem* 2016, 408 (8), 2159–2170. <https://doi.org/10.1007/S00216-016-9319-0>.
- (36) Wang, X. F.; Wang, Q.; Li, Z. G.; Huang, K.; Li, L. D.; Zhao, D. H. Determination of 23 Perfluorinated Alkylated Substances in Water and Suspended Particles by Ultra-Performance Liquid Chromatography/Tandem Mass Spectrometry. *Journal of Environmental Science and Health, Part A* 2018, 53 (14), 1277–1283. <https://doi.org/10.1080/10934529.2018.1528042>.
- (37) Mullin, L.; Katz, D. R.; Riddell, N.; Plumb, R.; Burgess, J. A.; Yeung, L. W. Y.; Jogsten, I. E. Analysis of Hexafluoropropylene Oxide-Dimer Acid (HFPO-DA) by Liquid Chromatography-Mass Spectrometry (LC-MS): Review of Current Approaches and Environmental Levels. *TrAC Trends in Analytical Chemistry* 2019, 118, 828–839. <https://doi.org/10.1016/J.TRAC.2019.05.015>.
- (38) Szostek, B.; Prickett, K. B.; Buck, R. C. Determination of Fluorotelomer Alcohols by Liquid Chromatography/Tandem Mass Spectrometry in Water. *Rapid Communications in Mass Spectrometry* 2006, 20 (19), 2837–2844. <https://doi.org/10.1002/RCM.2667>.
- (39) Berger, U.; Langlois, I.; Oehme, M.; Kallenborn, R. Comparison of Three Types of Mass Spectrometer for High-Performance Liquid Chromatography/Mass Spectrometry Analysis of Perfluoroalkylated Substances and Fluorotelomer Alcohols. <http://dx.doi.org/10.1255/ejms.679> 2004, 10 (5), 579–588. <https://doi.org/10.1255/EJMS.679>.
- (40) Piva, E.; Fais, P.; Cecchetto, G.; Montisci, M.; Viel, G.; Pascali, J. P. Determination of Perfluoroalkyl Substances (PFAS) in Human Hair by Liquid Chromatography-High Accurate Mass Spectrometry (LC-QTOF). *Journal of Chromatography B* 2021, 1172, 122651. <https://doi.org/10.1016/J.JCHROMB.2021.122651>.
- (41) Perovani, I. S.; Barbetta, M. F. S.; Duarte, L. O.; de Oliveira, A. R. M. Determination of Polyfluoroalkyl Substances in Biological Matrices by Chromatography Techniques: A Review Focused

on the Sample Preparation Techniques - Review. *Journal of Chromatography Open* 2023, 3. <https://doi.org/10.1016/j.jcoa.2023.100082>.

(42) Saito, K.; Uemura, E.; Ishizaki, A.; Kataoka, H. Determination of Perfluorooctanoic Acid and Perfluorooctane Sulfonate by Automated In-Tube Solid-Phase Microextraction Coupled with Liquid Chromatography-Mass Spectrometry. *Anal Chim Acta* 2010, 658 (2), 141–146. <https://doi.org/10.1016/j.aca.2009.11.004>.

(43) United States Environmental Protection Agency. *Method 1633 Analysis of Per- and Polyfluoroalkyl Substances (PFAS) in Aqueous, Solid, Biosolids, and Tissue Samples by LC-MS/MS*; 2024. www.epa.gov.

(44) Kirkwood-Donelson, K. I.; Dodds, J. N.; Schnetzer, A.; Hall, N.; Baker, E. S. Uncovering Per- and Polyfluoroalkyl Substances (PFAS) with Nontargeted Ion Mobility Spectrometry–Mass Spectrometry Analyses. *Sci Adv* 2023, 9 (43). <https://doi.org/10.1126/SCIADV.ADJ7048>.

(45) Luo, Y. S.; Aly, N. A.; McCord, J.; Strynar, M. J.; Chiu, W. A.; Dodds, J. N.; Baker, E. S.; Rusyn, I. Rapid Characterization of Emerging Per- And Polyfluoroalkyl Substances in Aqueous Film-Forming Foams Using Ion Mobility Spectrometry-Mass Spectrometry. *Environ Sci Technol* 2020, 54 (23), 15024–15034. <https://doi.org/10.1021/acs.est.0c04798>.

(46) Dodds, J. N.; Hopkins, Z. R.; Knappe, D. R. U.; Baker, E. S. Rapid Characterization of Per- And Polyfluoroalkyl Substances (PFAS) by Ion Mobility Spectrometry-Mass Spectrometry (IMS-MS). *Anal Chem* 2020, 92 (6), 4427–4435. <https://doi.org/10.1021/acs.analchem.9b05364>.

(47) Foster, M.; Rainey, M.; Watson, C.; Dodds, J. N.; Kirkwood, K. I.; Fernández, F. M.; Baker, E. S. Uncovering PFAS and Other Xenobiotics in the Dark Metabolome Using Ion Mobility Spectrometry, Mass Defect Analysis, and Machine Learning. *Environ Sci Technol* 2022, 56 (12), 9133–9143. <https://doi.org/10.1021/acs.est.2c00201>.

(48) Valdiviezo, A.; Aly, N. A.; Luo, Y. S.; Cordova, A.; Casillas, G.; Foster, M. K.; Baker, E. S.; Rusyn, I. Analysis of Per- and Polyfluoroalkyl Substances in Houston Ship Channel and Galveston Bay

Following a Large-Scale Industrial Fire Using Ion-Mobility-Spectrometry-Mass Spectrometry. *J Environ Sci (China)* 2021, *115*, 350–362. <https://doi.org/10.1016/j.jes.2021.08.004>.

(49) Mullin, L.; Jobst, K.; DiLorenzo, R. A.; Plumb, R.; Reiner, E. J.; Yeung, L. W. Y.; Jogsten, I. E. Liquid Chromatography-Ion Mobility-High Resolution Mass Spectrometry for Analysis of Pollutants in Indoor Dust: Identification and Predictive Capabilities. *Anal Chim Acta* 2020, *1125*, 29–40. <https://doi.org/10.1016/J.ACA.2020.05.052>.

(50) Vera, P.; Canellas, E.; Dreolin, N.; Goshawk, J.; Nerín, C. The Analysis of the Migration of per and Poly Fluoroalkyl Substances (PFAS) from Food Contact Materials Using Ultrahigh Performance Liquid Chromatography Coupled to Ion-Mobility Quadrupole Time-of-Flight Mass Spectrometry (UPLC-IMS-QTOF). *Talanta* 2024, *266*, 124999. <https://doi.org/10.1016/J.TALANTA.2023.124999>.

(51) Díaz-Galiano, F. J.; Murcia-Morales, M.; Monteau, F.; Le Bizec, B.; Dervilly, G. Collision Cross-Section as a Universal Molecular Descriptor in the Analysis of PFAS and Use of Ion Mobility Spectrum Filtering for Improved Analytical Sensitivities. *Anal Chim Acta* 2023, *1251*, 341026. <https://doi.org/10.1016/J.ACA.2023.341026>.

(52) Lougkovois, R.; Parinos, K.; Gkotsis, G.; Nika, M.-C.; Thomaidis, N.; Pavlidou, A.; Hatzianestis, I. Monitoring the Presence of Priority Pollutants and Emerging Contaminants at Pagasitikos Gulf, Greece, Following “Daniel” and “Elias” Storm Events, Utilizing the Technique of LC-VIP-HESI-TIMS-HRMS. *EGU24* 2024. <https://doi.org/10.5194/EGUSPHERE-EGU24-7985>.

(53) Bodendiek, S.; Wendt, K.; Kiehne, A.; Daltonik GmbH, B. *FlashNote Environmental screening via timsTOF MS: A new dimension for discrimination and improved sensitivity in the detection of PFOS pollutants*. Bruker. <https://www.bruker.com/en/landingpages/bams/nacrw.html> (accessed 2024-06-30).

- (54) Reynolds, A. J.; Smith, A. M.; Qiu, T. A. Detection, Quantification, and Isomer Differentiation of Per- and Polyfluoroalkyl Substances (PFAS) Using MALDI-TOF with Trapped Ion Mobility. *J Am Soc Mass Spectrom* 2024, 35 (2), 317–325. <https://doi.org/10.1021/JASMS.3C00369>.
- (55) Ahmed, E.; Mohibul Kabir, K. M.; Wang, H.; Xiao, D.; Fletcher, J.; Donald, W. A. Rapid Separation of Isomeric Perfluoroalkyl Substances by High-Resolution Differential Ion Mobility Mass Spectrometry. *Anal Chim Acta* 2019, 1058, 127–135. <https://doi.org/10.1016/j.aca.2019.01.038>.
- (56) United States Environmental Protection Agency. *CompTox Chemicals Dashboard / PFASMASTER Chemicals*. <https://comptox.epa.gov/dashboard/chemical-lists/pfasmaster> (accessed 2024-07-14).
- (57) Gathungu, R. M.; Kautz, R.; Kristal, B. S.; Bird, S. S.; Vouros, P. The Integration of LC-MS and NMR for the Analysis of Low Molecular Weight Trace Analytes in Complex Matrices. *Mass Spectrom Rev* 2020, 39 (1–2), 35–54. <https://doi.org/10.1002/MAS.21575>.
- (58) Makey, D. M.; Shchurik, V.; Wang, H.; Lhotka, H. R.; Stoll, D. R.; Vazhentsev, A.; Mangion, I.; Regalado, E. L.; Ahmad, I. A. H. Mapping the Separation Landscape in Two-Dimensional Liquid Chromatography: Blueprints for Efficient Analysis and Purification of Pharmaceuticals Enabled by Computer-Assisted Modeling. *Anal Chem* 2021, 93 (2), 964–972. <https://doi.org/10.1021/ACS.ANALCHEM.0C03680>.
- (59) Fouad, A.; El-Sayed, D. H.; Salman, B. E.; Bakr, H. H.; Adel, S. E.; Alzarak, T. M.; Mahmoud, A. Macrocyclic Antibiotics as Effective Chiral Selectors in Liquid Chromatography for Enantiomeric Separation of Pharmaceutical Compounds: A Review. *Crit Rev Anal Chem* 2023. <https://doi.org/10.1080/10408347.2023.2224442>.
- (60) Kimura, R.; Tsujimura, H.; Tsuchiya, M.; Soga, S.; Ota, N.; Tanaka, A.; Kim, H. Development of a Cognitive Function Marker Based on D-Amino Acid Proportions Using New Chiral Tandem LC-MS/MS Systems. *Scientific Reports* 2020 10:1 2020, 10 (1), 1–12. <https://doi.org/10.1038/s41598-020-57878-y>.

- (61) Li, P.; Wu, D.-R.; Yip, S. H.; Sun, D.; Pawluczyk, J.; Smith, A.; Kempson, J.; Mathur, A. Large-Scale Purification of a Deprotected Macrocyclic Peptide by Supercritical Fluid Chromatography (SFC) Integrated with Liquid Chromatography in Discovery Chemistry. *J Chromatogr A* 2024, 1730, 465112. <https://doi.org/10.1016/J.CHROMA.2024.465112>.
- (62) De Luca, C.; Lievore, G.; Bozza, D.; Buratti, A.; Cavazzini, A.; Ricci, A.; Macis, M.; Cabri, W.; Felletti, S.; Catani, M. Downstream Processing of Therapeutic Peptides by Means of Preparative Liquid Chromatography. *Molecules* 2021, Vol. 26, Page 4688 2021, 26 (15), 4688. <https://doi.org/10.3390/MOLECULES26154688>.
- (63) Ogata, K.; Ishihama, Y. Extending the Separation Space with Trapped Ion Mobility Spectrometry Improves the Accuracy of Isobaric Tag-Based Quantitation in Proteomic LC/MS/MS. *Anal Chem* 2020, 92 (12), 8037–8040. <https://doi.org/10.1021/ACS.ANALCHEM.0C01695>.
- (64) Camperi, J.; Goyon, A.; Guillarme, D.; Zhang, K.; Stella, C. Multi-Dimensional LC-MS: The next Generation Characterization of Antibody-Based Therapeutics by Unified Online Bottom-up, Middle-up and Intact Approaches. *Analyst* 2021, 146 (3), 747–769. <https://doi.org/10.1039/D0AN01963A>.
- (65) Li, C.; Nielsen, S. B.; Engholm-Keller, K.; Lund, M. N. Oxidation of Whey Proteins during Thermal Treatment Characterized by a Site-Specific LC-MS/MS-Based Proteomic Approach. *J Agric Food Chem* 2022, 70 (14), 4391–4406. <https://doi.org/10.1021/ACS.JAFC.1C07946>.
- (66) Miranda, G.; Bianchi, L.; Krupova, Z.; Trossat, P.; Martin, P. An Improved LC–MS Method to Profile Molecular Diversity and Quantify the Six Main Bovine Milk Proteins, Including Genetic and Splicing Variants as Well as Post-Translationally Modified Isoforms. *Food Chem X* 2020, 5. <https://doi.org/10.1016/j.fochx.2020.100080>.
- (67) Huang, H. J.; Ye, Z. X.; Lu, G.; Zhang, C. X.; Chen, J. P.; Li, J. M. Identification of Salivary Proteins in the Whitefly Bemisia Tabaci by Transcriptomic and LC–MS/MS Analyses. *Insect Sci* 2021, 28 (5), 1369–1381. <https://doi.org/10.1111/1744-7917.12856>.

- (68) Hearn, M. T. High-Performance Liquid Chromatography and Its Application to Protein Chemistry. *Adv Chromatogr* 1982, 20, 1–82. <https://doi.org/10.1201/9781003209706-1/HIGH>.
- (69) Jennings, M. E.; Silveira, J. R.; Treier, K. M.; Tracy, P. B.; Matthews, D. E. Total Retention Liquid Chromatography-Mass Spectrometry to Achieve Maximum Protein Sequence Coverage. *Anal Chem* 2021, 93 (12), 5054–5060. <https://doi.org/10.1021/ACS.ANALCHEM.0C04292>.
- (70) Sadiq, N. W.; Beauchemin, D. Liquid Chromatography. *Sample Introduction Systems in ICPMS and ICPOES* 2020, 213–254. <https://doi.org/10.1016/B978-0-444-59482-2.00004-X>.
- (71) Moldoveanu, S.; David, V. Introductory Information Regarding HPLC. *Essentials in Modern HPLC Separations* 2022, 3–20. <https://doi.org/10.1016/B978-0-323-91177-1.00006-5>.
- (72) Raynie, D. E. Practical Understanding of Partition Coefficients. *LC-GC North America* 2023, 41 (3). <https://doi.org/10.56530/LCGC.NA.TC297005>.
- (73) Jandera, P.; Churáček, J. Gradient Elution in Liquid Chromatography : I. The Influence of the Composition of the Mobile Phase on the Capacity Ratio (Retention Volume, Band Width, and Resolution) in Isocratic Elution — Theoretical Considerations. *J Chromatogr A* 1974, 91 (C), 207–221. [https://doi.org/10.1016/S0021-9673\(01\)97901-4](https://doi.org/10.1016/S0021-9673(01)97901-4).
- (74) Wang, H.; Helliwell, K.; You, X. *Analytical, Nutritional and Clinical Methods Section Isocratic Elution System for the Determination of Catechins, Caffeine and Gallic Acid in Green Tea Using HPLC*; 2000. [https://doi.org/S0308-8146\(99\)00179-X](https://doi.org/S0308-8146(99)00179-X).
- (75) Schellinger, A. P.; Carr, P. W. Isocratic and Gradient Elution Chromatography: A Comparison in Terms of Speed, Retention Reproducibility and Quantitation. *J Chromatogr A* 2006, 1109 (2), 253–266. <https://doi.org/10.1016/J.CHROMA.2006.01.047>.
- (76) Metwally, H.; McAllister, R. G.; Konermann, L. Exploring the Mechanism of Salt-Induced Signal Suppression in Protein Electrospray Mass Spectrometry Using Experiments and Molecular Dynamics Simulations. *Anal Chem* 2015, 87 (4), 2434–2442. <https://doi.org/10.1021/AC5044016>.

- (77) King, R.; Bonfiglio, R.; Fernandez-Metzler, C.; Miller-Stein, C.; Olah, T. Mechanistic Investigation of Ionization Suppression in Electrospray Ionization. *J Am Soc Mass Spectrom* 2000, *11* (11), 942–950. [https://doi.org/10.1016/S1044-0305\(00\)00163-X](https://doi.org/10.1016/S1044-0305(00)00163-X).
- (78) Furey, A.; Moriarty, M.; Bane, V.; Kinsella, B.; Lehane, M. Ion Suppression; A Critical Review on Causes, Evaluation, Prevention and Applications. *Talanta* 2013, *115*, 104–122. <https://doi.org/10.1016/J.TALANTA.2013.03.048>.
- (79) Annesley, T. M. Ion Suppression in Mass Spectrometry. *Clin Chem* 2003, *49* (7), 1041–1044. <https://doi.org/10.1373/49.7.1041>.
- (80) Lo, C. W. S.; Hoad, K.; Loh, T. P.; Van Den Berg, S.; Cooke, B. R.; Greaves, R. F.; Hartmann, M. F.; Wudy, S. A.; Ho, C. S. Endogenous Isobaric Interference on Serum 17 Hydroxyprogesterone by Liquid Chromatography-Tandem Mass Spectrometry Methods. *Clin Chem Lab Med* 2023, *61* (3), E64–E66. <https://doi.org/10.1515/CCLM-2022-1086>.
- (81) Maroto, A.; Fouque, D. J. dit; Lartia, R.; Memboeuf, A. LC-MS Accurate Quantification of a Tryptic Peptide Co-Eluted with an Isobaric Interference by Using in-Source Collisional Purification. *Anal Bioanal Chem* 2023, *415* (29–30), 7211–7221. <https://doi.org/10.1007/S00216-023-04989-W>.
- (82) Qi, Y.; Geib, T.; Schorr, P.; Meier, F.; Volmer, D. A. On the Isobaric Space of 25-Hydroxyvitamin D in Human Serum: Potential for Interferences in Liquid Chromatography/Tandem Mass Spectrometry, Systematic Errors and Accuracy Issues. *Rapid Communications in Mass Spectrometry* 2015, *29* (1), 1–9. <https://doi.org/10.1002/RCM.7075>.
- (83) Danso, D.; Langman, L. J.; Snozek, C. L. H. LC-MS/MS Quantitation of Ribavirin in Serum and Identification of Endogenous Isobaric Interferences. *Clinica Chimica Acta* 2011, *412* (23–24), 2332–2335. <https://doi.org/10.1016/J.CCA.2011.07.016>.
- (84) Gabelica, V.; Marklund, E. Fundamentals of Ion Mobility Spectrometry. *Current Opinion in Chemical Biology*. Elsevier Ltd February 1, 2018, pp 51–59. <https://doi.org/10.1016/j.cbpa.2017.10.022>.

- (85) Gabelica, V.; Shvartsburg, A. A.; Afonso, C.; Barran, P.; Benesch, J. L. P.; Bleiholder, C.; Bowers, M. T.; Bilbao, A.; Bush, M. F.; Campbell, J. L.; Campuzano, I. D. G.; Causon, T.; Clowers, B. H.; Creaser, C. S.; De Pauw, E.; Far, J.; Fernandez-Lima, F.; Fjeldsted, J. C.; Giles, K.; Groessl, M.; Hogan, C. J.; Hann, S.; Kim, H. I.; Kurulugama, R. T.; May, J. C.; McLean, J. A.; Pagel, K.; Richardson, K.; Ridgeway, M. E.; Rosu, F.; Sobott, F.; Thalassinou, K.; Valentine, S. J.; Wyttenbach, T. Recommendations for Reporting Ion Mobility Mass Spectrometry Measurements. *Mass Spectrom Rev* 2019, 38 (3), 291–320. <https://doi.org/10.1002/MAS.21585>.
- (86) Zhou, Z.; Luo, M.; Chen, X.; Yin, Y.; Xiong, X.; Wang, R.; Zhu, Z. J. Ion Mobility Collision Cross-Section Atlas for Known and Unknown Metabolite Annotation in Untargeted Metabolomics. *Nat Commun* 2020, 11 (1). <https://doi.org/10.1038/s41467-020-18171-8>.
- (87) Haack, A.; Ieritano, C.; Hopkins, W. S. MobCal-MPI 2.0: An Accurate and Parallelized Package for Calculating Field-Dependent Collision Cross Sections and Ion Mobilities. *Analyst* 2023, 148 (14), 3257–3273. <https://doi.org/10.1039/D3AN00545C>.
- (88) Ieritano, C.; Lee, A.; Crouse, J.; Bowman, Z.; Mashmouhi, N.; Crossley, P. M.; Friebe, B. P.; Campbell, J. L.; Hopkins, W. S. Determining Collision Cross Sections from Differential Ion Mobility Spectrometry. *Anal Chem* 2021. <https://doi.org/10.1021/acs.analchem.1c01420>.
- (89) Ieritano, C.; Hopkins, W. S. The Hitchhiker’s Guide to Dynamic Ion-Solvent Clustering: Applications in Differential Ion Mobility Spectrometry. *Physical Chemistry Chemical Physics*. Royal Society of Chemistry August 22, 2022. <https://doi.org/10.1039/d2cp02540j>.
- (90) Campbell, J. L.; Le Blanc, J. Y.; Kibbey, R. G. Differential Mobility Spectrometry: A Valuable Technology for Analyzing Challenging Biological Samples. *Bioanalysis* 2015, 7 (7), 853. <https://doi.org/10.4155/BIO.15.14>.
- (91) Shvartsburg, A. A.; Creese, A. J.; Smith, R. D.; Cooper, H. J. Separation of Peptide Isomers with Variant Modified Sites by High-Resolution Differential Ion Mobility Spectrometry. *Anal Chem* 2010, 82 (19), 8327–8334. <https://doi.org/10.1021/ac101878a>.

- (92) Haack, A.; Bissonnette, J. R.; Ieritano, C.; Hopkins, W. S. Improved First-Principles Model of Differential Mobility Using Higher Order Two-Temperature Theory. *J Am Soc Mass Spectrom* 2022, 33 (3), 535–547. <https://doi.org/10.1021/JASMS.1C00354>.
- (93) Krylov, E. V.; Coy, S. L.; Nazarov, E. G. Temperature Effects in Differential Mobility Spectrometry. *Int J Mass Spectrom* 2009, 279 (2–3), 119–125. <https://doi.org/10.1016/j.ijms.2008.10.025>.
- (94) Hopkins, W. S. Dynamic Clustering and Ion Microsolvation. *Comprehensive Analytical Chemistry* 2019, 83, 83–122. <https://doi.org/10.1016/BS.COAC.2018.10.002>.
- (95) Mashmoushi, N.; Juhász, D. R.; Coughlan, N. J. A.; Schneider, B. B.; Le Blanc, Y.; Guna, M.; Ziegler, B. E.; Campbell, J. L.; Hopkins, W. S. UVPD Spectroscopy of Differential Mobility-Selected Prototropic Isomers of Rivaroxaban. *J. Phys. Chem. A* 2021, 125, 8195. <https://doi.org/10.1021/acs.jpca.1c05564>.
- (96) Mashmoushi, N.; Larry Campbell, J.; di Lorenzo, R.; Scott Hopkins, W. Rapid Separation of Cannabinoid Isomer Sets Using Differential Mobility Spectrometry and Mass Spectrometry. *Analyst* 2022, 147 (10), 2198–2206. <https://doi.org/10.1039/D1AN02327F>.
- (97) Haack, A.; Hopkins, W. S. Kinetics in DMS: Modeling Clustering and Declustering Reactions. *Cite This: J. Am. Soc. Mass Spectrom* 2250, 2022. <https://doi.org/10.1021/jasms.2c00224>.
- (98) Ashworth, E. K.; Dezalay, J.; Ryan, C. R. M.; Ieritano, C.; Hopkins, W. S.; Chambrier, I.; Cammidge, A. N.; Stockett, M. H.; Noble, J. A.; Bull, J. N. Protomers of the Green and Cyan Fluorescent Protein Chromophores Investigated Using Action Spectroscopy. *Physical Chemistry Chemical Physics* 2023, 25 (30), 20405–20413. <https://doi.org/10.1039/D3CP02661B>.
- (99) Ryan, C. R. M.; Haack, A.; Hopkins, W. S. Predicting Ion-Solvent Clustering in Differential Mobility Spectrometry Using Anharmonic Thermochemistry. *ChemRxiv* 2023. <https://doi.org/10.26434/CHEMRXIV-2023-BN642>.

- (100) Bissonnette, J. R.; Ryan, C. R. M.; Ieritano, C.; Hopkins, W. S.; Haack, A. First-Principles Modeling of Preferential Solvation in Mixed-Modifier Differential Mobility Spectrometry. *J Am Soc Mass Spectrom* 2023, *34* (7), 1417–1427. <https://doi.org/10.1021/jasms.3c00117>.
- (101) Stienstra, C. M. K.; Ieritano, C.; Haack, A.; Hopkins, W. S. Bridging the Gap between Differential Mobility, Log S, and Log P Using Machine Learning and SHAP Analysis. *Anal Chem* 2023, *95* (27), 10309–10321. <https://doi.org/10.1021/ACS.ANALCHEM.3C00921>.
- (102) Ieritano, C.; Campbell, J. L.; Hopkins, W. S. Predicting Differential Ion Mobility Behaviour: In Silico Using Machine Learning. *Analyst* 2021, *146* (15), 4737–4743. <https://doi.org/10.1039/d1an00557j>.
- (103) Ieritano, C.; Featherstone, J.; Haack, A.; Guna, M.; Campbell, J. L.; Hopkins, W. S. How Hot Are Your Ions in Differential Mobility Spectrometry? *J Am Soc Mass Spectrom* 2020, *31* (3), 582–593. <https://doi.org/10.1021/jasms.9b00043>.
- (104) Campbell, J. L.; Le Blanc, J. C. Y.; Schneider, B. B. Probing Electrospray Ionization Dynamics Using Differential Mobility Spectrometry: The Curious Case of 4-Aminobenzoic Acid. *Anal Chem* 2012, *84* (18), 7857–7864. <https://doi.org/10.1021/ac301529w>.
- (105) Coughlan, N. J. A.; Fu, W.; Guna, M.; Schneider, B. B.; Le Blanc, J. C. Y.; Campbell, J. L.; Hopkins, W. S. Electronic Spectroscopy of Differential Mobility-Selected Prototropic Isomers of Protonatedpara-Aminobenzoic Acid. *Physical Chemistry Chemical Physics* 2021, *23* (36), 20607–20614. <https://doi.org/10.1039/d1cp02120f>.
- (106) Lalli, P. M.; Iglesias, B. A.; Toma, H. E.; De Sa, G. F.; Daroda, R. J.; Silva Filho, J. C.; Szulejko, J. E.; Araki, K.; Eberlin, M. N. Protomers: Formation, Separation and Characterization via Travelling Wave Ion Mobility Mass Spectrometry. *Journal of Mass Spectrometry* 2012, *47* (6), 712–719. <https://doi.org/10.1002/JMS.2999>.

- (107) Bull, J. N.; Coughlan, N. J. A.; Bieske, E. J. Protomer-Specific Photochemistry Investigated Using Ion Mobility Mass Spectrometry. *Journal of Physical Chemistry A* 2017, *121* (32), 6021–6027. <https://doi.org/10.1021/ACS.JPCA.7B05800>.
- (108) Campbell, J. L.; Yang, A. M. C.; Melo, L. R.; Hopkins, W. S. Studying Gas-Phase Interconversion of Tautomers Using Differential Mobility Spectrometry. *J Am Soc Mass Spectrom* 2016, *27* (7), 1277–1284. <https://doi.org/10.1007/S13361-016-1392-2>.
- (109) Walker, S. W. C.; Mark, A.; Verbuyst, B.; Bogdanov, B.; Campbell, J. L.; Hopkins, W. S. Characterizing the Tautomers of Protonated Aniline Using Differential Mobility Spectrometry and Mass Spectrometry. *Journal of Physical Chemistry A* 2018, *122* (15), 3858–3865. <https://doi.org/10.1021/ACS.JPCA.7B10872>.
- (110) Bursch, M.; Mewes, J.-M.; Hansen, A.; Grimme, S. Best-Practice DFT Protocols for Basic Molecular Computational Chemistry**. 2022. <https://doi.org/10.26434/chemrxiv-2022-n304h>.
- (111) Li, W.; Kannan, K. A Simple and Sensitive Method for Simultaneous Analysis of 58 Neutral and Ionic PFAS Using UPLC-MS/MS. *Environ Sci Technol Lett* 2024. <https://doi.org/10.1021/ACS.ESTLETT.4C00146>.
- (112) Young, R. B.; Pica, N. E.; Sharifan, H.; Chen, H.; Roth, H. K.; Blakney, G. T.; Borch, T.; Higgins, C. P.; Kornuc, J. J.; McKenna, A. M.; Blotevogel, J. PFAS Analysis with Ultrahigh Resolution 21T FT-ICR MS: Suspect and Nontargeted Screening with Unrivaled Mass Resolving Power and Accuracy. *Environ Sci Technol* 2022, *56* (4), 2455–2465. <https://doi.org/10.1021/ACS.EST.1C08143>.
- (113) Androulakakis, A.; Alygizakis, N.; Bizani, E.; Thomaidis, N. S. Current Progress in the Environmental Analysis of Poly- and Perfluoroalkyl Substances (PFAS). *Environmental Science: Advances*. Royal Society of Chemistry December 1, 2022, pp 705–724. <https://doi.org/10.1039/d2va00147k>.

- (114) Enders, J. R.; O'Neill, G. M.; Whitten, J. L.; Muddiman, D. C. Understanding the Electrospray Ionization Response Factors of Per- and Poly-Fluoroalkyl Substances (PFAS). *Anal Bioanal Chem* 2022, 414 (3), 1227–1234. <https://doi.org/10.1007/s00216-021-03545-8>.
- (115) Bangma, J.; McCord, J.; Giffard, N.; Buckman, K.; Petali, J.; Chen, C.; Amparo, D.; Turpin, B.; Morrison, G.; Strynar, M. Analytical Method Interferences for Perfluoropentanoic Acid (PFPeA) and Perfluorobutanoic Acid (PFBA) in Biological and Environmental Samples. *Chemosphere* 2023, 315, 137722. <https://doi.org/10.1016/J.CHEMOSPHERE.2022.137722>.
- (116) Ekmekciu, L.; Hopfgartner, G. Liquid Chromatography and Differential Mobility Spectrometry-Data-Independent Mass Spectrometry for Comprehensive Multidimensional Separations in Metabolomics. *Anal Bioanal Chem* 2023, 415 (10), 1905–1915. <https://doi.org/10.1007/S00216-023-04602-0>.
- (117) Pan, Y.; Wang, J.; Yeung, L. W. Y.; Wei, S.; Dai, J. Analysis of Emerging Per- and Polyfluoroalkyl Substances: Progress and Current Issues. *TrAC Trends in Analytical Chemistry* 2020, 124, 115481. <https://doi.org/10.1016/J.TRAC.2019.04.013>.
- (118) Shen, Y.; Wang, L.; Ding, Y.; Liu, S.; Li, Y.; Zhou, Z.; Liang, Y. Trends in the Analysis and Exploration of Per-and Polyfluoroalkyl Substances (PFAS) in Environmental Matrices: A Review. *Crit Rev Anal Chem* 2023. <https://doi.org/10.1080/10408347.2023.2231535>.
- (119) Win, Z. M.; Cheong, A. M. Y.; Hopkins, W. S. Using Machine Learning To Predict Partition Coefficient (Log P) and Distribution Coefficient (Log D) with Molecular Descriptors and Liquid Chromatography Retention Time. *J Chem Inf Model* 2023, 63 (7), 1906–1913. <https://doi.org/10.1021/ACS.JCIM.2C01373>.

Appendix A Supplementary Information

Table A.1 List of anion compound names, molecular weights, parent and fragment m/z and dispersion behaviour measured in N₂ or MeOH.

Name	MW	m/z (parent)	m/z (fragment 1)	^a m/z (fragment 2)	^b Dispersion in	
					N ₂	MeOH
DL-Aspartic Acid	133	132	115	88	x	
D-Leucine	131	130	131	-	x	x
DL-Serine	105	104	74	72	x	x
L-Phenylalanine	165	164	147	103	x	x
L-Proline	115	114	114	-	x	x
D-Valine	117	116	116	-	x	x
L-Glutamine	146	145	59	-	x	x
L-Methionine	149	148	100	-	x	x
L-Threonine	119	118	100	74	x	x
L-Tyrosine	181	180	163	119	x	x
Naproxen	230	229	185	170	x	x
Nicotinic acid	123	122	78	-	x	x
Methyl red	268	267	250	218	x	x
Adenine	135	134	107	92	x	x
Ibuprofen	206	205	161	159	x	x
Maleic acid	116	115	71	-	x	x
Malonic acid	104	103	59	-	x	
Cannabichromene	315	313	191	313	x	x
Cannabidiol	315	313	179	245	x	x
Cannabidiolic Acid	358	357	245	339	x	x
Cannabidivarin	286	285	217	285	x	x
Cannabigerol	317	315	136	315	x	x
Cannabigerolic acid	361	359	341	315	x	x
Tetrahydrocannabivarin	286	285	163	151	x	x
Cannabinol	310	309	279	171	x	x
2,2-difluoropropanoic acid	110	109	65	109	x	
2,3,3,3-tetrafluoropropanoic acid	146	145	101	81	x	
3,3,3-trifluoropropanoic acid	128	127	83	63	x	
Ferulic Acid	194	193	178	134	x	
Pentafluoropropanoic acid	163	162	118	-	x	
Taurocholic Acid	515	514	514	-	x	x
acetaminophen	151	150	107	-	x	x
glucose	179	178	59	-	x	
gly-pro	172	171	114	-	x	x
chelidamic acid	182	181	94	-	x	

3-hydroxy-1,2-dimethyl-4(1H)-pyridone	138	137	138	-	x	
HBDI	216	215	200	131	x	x
Resveratrol	228	227	227	184	x	x
Pterostilbene	256	255	240	197	x	x
γ -Aminobutyric acid	103	102	102	-	x	x
2-Aminonicotinic acid	138	137	66	93	x	x
3-Aminobenzoic acid	137	136	92	136	x	x
4-Aminobenzoic acid	137	136	92	136	x	x
Ethylmalonic acid	132	131	131	-	x	
Hexanoic acid	116	115	71	115	x	x
Crotonic acid	86	85	85	-	x	x
Heptanoic acid	130	129	85	129		x
Isonicotinic acid	123	122	78	122	x	x
Isovaleric acid	102	101	101	-	x	x
Valeric acid	102.13	101	101	-		x
2-Tert-butyl-4-methoxyphenol	180	179	164	149	x	x
Congo Red	697	696	81	-	x	x
2-methylphenol	108	107	107	-	x	x
Corticosterone	345	344	241	327	x	x
Hydrocortisone	362	361	282	331	x	x
Sodium Deoxycholate	392.6	393	345	327	x	x
Folic acid	441	440	132	440	x	x
Cholic acid	409	408	289	407	x	x
Carvedilol	407	405	405	181	x	x
Ranitidine	314	313	142	170	x	x
Sodium Dodecyl Sulfate	266	265	80	97	x	x
Gemfibrozil	250	249	121	249	x	x
Minoxidil	209	208	208	-	x	x
2,3,4,5-Tetrafluorobenzoic Acid	194	193	129	149	x	x
Gallic acid	170	169	169	-	x	
4-(1H-Pyrrol-1-yl)phenol	159	158	157	118	x	x
Allantoin	158	157	157	139	x	x
Mandelic acid	152	151	151	107	x	x
D-Tartaric Acid	150	149	129	149	x	x
trans-Cinnamic acid	148	147	147	103	x	x
4-Fluorobenzoic acid	140	139	95	139	x	x
Malic Acid	134	133	115	71	x	x
5-Hydroxyindole	133	132	104	131	x	x
Fumaric Acid	116	115	71	115	x	x
(Aminomethyl) phosphonic acid	111	110	79	63	x	x

3-amino-2-fluoropropionic acid	107	106	86	106	x	x
Inosine	268	267	135	267	x	x
Palmitic acid	256	255	237	255	x	x
Hypoxanthine	136	135	92	135	x	
L-Pyroglutamic acid	129	128	82	128	x	x
Hypotaurine	109	108	64	108	x	x
2-Phenyl-5-benzimidazole sulfonic acid	274	273	193	273	x	x
atenolol	266	265	97	219	x	x
2,2',4,4'-Tetrahydroxybenzophenone	246	245	109	135	x	x
2,4-Dichlorophenoxyacetic acid	221	220	134	220	x	x
2,4 - Dihydroxybenzophenone	214	213	91	135	x	x
2,(4-Isobutylphenyl)propanoic acid	206	205	205	159	x	x
Atrazine-2-hydroxy	197	196	83	196	x	x
Atrazine- desethyl-2-hydroxy	169	168	83	168	x	x
8-Aminocaprylic acid	159	158	158	-	x	x
Irgasan	290	288	255	289	x	
(+/-)-4-methyloctanoic acid	158	157	157	-	x	
Isophthalic acid	166.13	165	121	165	x	x
1,5-Naphthalenedisulfonic acid, disodium salt	332	331	207	287	x	x
Stearic Acid	285	283	265	283	x	x
9-phenanthrol	194	193	165	193	x	x
2-hydroxyfluorene 98%	182	181	181	-	x	x
2-aminoterephthalic acid	181	180	92	136	x	x
Sodium-p-toluenesulphonate	194	193	80	107	x	x
2,4-Dichlorophenol	163	162	89	163	x	x
Vanillin	152	151	136	92	x	x
1-Naphthol	144	143	115	143	x	x
Sodium octanoate	143	142	143	-	x	x
2-nitrophenol	139	138	108	138	x	x
3-Hydroxybenzoic acid	138	137	93	137	x	x
Salicylic acid	138	137	93	137	x	x
Cyanuric acid anhydrous	129	128	85	128	x	x
Hydroquinone	110	109	77	109	x	x
Media Dye, Blue (brilliant blue)	793	373	170	373	x	x
Media Dye, Red (Erythrosine)	880	417	127	417	x	x
Media Dye, Yellow (Tartrazine)	534	155	137	155	x	x
Indole-3-butyric acid	203	202	158	116	x	
Glutathione	307	306	143	306	x	
Phloroglucinol	126	125	57	125	x	x

L-asparagine	132	131	113	131	x	x
Tetracycline	444	443	358	443	x	
Novobiocin	613	612	205	611	x	
trans-4-aminomethyl- cyclohexanecarboxylic acid	157	156	138	156	x	x
ethylenediaminetetraacetic acid (EDTA)	292	291	159	-	x	
chlorogenic acid	354	353	191	353	x	x
5-chloro-2-(2,4 dichlorophenoxy)phenol	290	288	255	288	x	x
cadolylic acid sodium salt	160	159	107	137	x	x
terephthalic acid	166	165	121	165	x	x
Ellagic acid	302	301	284	301	x	x
sodium 2-naphthalene	230	207	80	207	x	x
dodecylbenzene sulfonic acid	327	325	197	325	x	x
8-aminocaprylic acid	159	158	140	158	x	x
2-acrylamido-2-methyl-1- propanesulfonic acid	207	206	80	206	x	x
nafcillin sodium salt monohydrate	455	453	243	413	x	
oxalic acid	90	89	89	-	x	x
nonanoic acid	158	157	157	-	x	
Perfluorobethanesulfonic Acid (PFBS)	300	299	80	99	x	x
Perfluoropentanesulfonic Acid (PFPS)	350	349	80	99	x	x
Perfluorohexanesulfonic Acid (PFHxS)	400	399	80	99	x	x
Perfluoroheptanesulfonic Acid (PFHpS)	450	449	80	99	x	x
Perfluorooctanesulfonic Acid (PFOS)	500	499	80	99	x	x
Perfluoroheptanesulfonic Acid (PFNS)	550	549	80	99	x	x
Perfluorodecanesulfonic Acid (PFDS)	600	599	80	99	x	x
Perfluorododecanesulfonic Acid (PFDoS)	700	699	80	99	x	x
4:2 FTS	328	327	307	81	x	x
6:2 FTS	428	427	407	81	x	x
8:2 FTS	528	527	507	81	x	x
GenX	330	285	185	169	x	x
PFMPA	230	229	85	135	x	x
PFMOBA	280	279	85	97	x	x
NFDHA	296	295	201	85	x	x
9Cl-PF3ONS	532/534	531/533	351	353	x	x
11Cl	632/634	631/633	451	453	x	x
PFEESA	316	315	135	83	x	x
3:3 FTCA	242	241	177	117	x	x

5:3 FTCA	342	341	217	237	x	x
7:3 FTCA	442	441	317	337	x	x
ADONA	378	377	251	85	x	x
PFBA	214	213	169	-	x	x
Perfluoropentanoic Acid (PFPA)	264	263	219	-	x	x
Perfluorohexanoic Acid (PFHxA)	314	313	269	119	x	x
Perfluoroheptanoic Acid (PFHpA)	364	363	319	169	x	x
Perfluorooctanoic Acid (PFOA)	414	413	369	169	x	x
Perfluorononanoic Acid (PFNA)	464	463	419	219	x	x
Perfluorodecanoic Acid (PFDA)	514	513	469	219	x	x
Perfluoroundecanoic Acid (PFUnA)	564	563	519	269	x	x
Perfluorododecanoic Acid (PFDoA)	614	613	569	319	x	x
Perfluorotridecanoic Acid (PFTrA)	664	663	619	169	x	x
PFTeA	714	713	669	169	x	x
PFHxDA	814	813	769	169	x	x
PFODA	914	913	369	413	x	x
PFOSA	499	498	78	169	x	x
NMeFOSA	513	512	169	219	x	x
NEtFOSA	527	526	169	219	x	x
NMeFOSAA	571	570	319	169	x	x
NEtFOSAA	585	584	526	483	x	x
8:2 FTUCA	458	457	393	343	x	x
8:2 diPAP	990	989	543	79	x	x
sulfamethazine	278.33	277	106	122	x	x
aztreonam	435.4	434	80	96	x	x
Acid Black 1	616.5	285	80	164	x	x
Acid Red 151	454.4	431	275	156	x	x
Acid Red 88	400.4	377	221	143	x	x
acid orange 7	350.3	327	171	156	x	x
amaranth	604.5	268	80	268	x	
cis-aconitic acid	174.11	173	129	173	x	x
furosemide	330.7	329	205	285	x	x
indoprofen	281.3	280	236	280	x	x
fosinopril	563.7	562.3	220.4	416	x	x
orotic acid	156.1	155	111	155	x	x
5-Fluorouracil	130.08	129	129	59	x	x
b-Estradiol-3-sulfate	374.4	373.4	271	351	x	x
warfarin	308.3	307	161	250	x	x
glafenine	372.8	371	253	297	x	x

2-(methylamino)benzoic acid	151.16	150	150	106	x	x
2-(4-butylphenyl)propanoic acid	206.28	205	205	159	x	x
1-cyclohexylcyclohexane-1-carboxylic acid	210.3	209	209	-	x	x
3-(4-Isobutylphenyl)propanoic acid	206.28	205	205	161	x	x
(2S)-2-[4-(2-methylpropyl)phenyl]propanoic acid	206.28	205	159	205		x
Diphenylacetic acid	212.24	211	211	157	x	x
9H-fluorene-2-carboxylic acid	210.23	209	209	165	x	x
9-Anthracenecarboxylic acid	222.24	221	177	221	x	x
4'-Hydroxy-4-biphenylcarboxylic acid	214.22	213	169	213	x	x
(1R,4aR,4bR,10aR)-1,4a-dimethyl-7-propan-2-yl-2,3,4,4b,5,6,10,10a-octahydrophenanthrene-1-carboxylic acid	302.5	301	301	-	x	x
linoleic acid	280	279	279	177	x	x
Oleic Acid	282.5	281	281	-	x	x
alpha-Phenylcinnamic acid	224.25	223	179	223	x	x
Pelubiprofen	258.31	257	257	-	x	x
3-Iodoprop-2-enoic acid	197.96	196	164	196	x	x
3,3-Dibromoacrylic acid	229.85	228	228	211	x	x
(Isopropylthio)acetic acid	134.2	133	133	-	x	x
2-(Tert-butoxy)acetic acid	132.16	131	75	131	x	x
4-Mercaptobenzoic acid	154.19	153	109	153	x	x
4-Bromo-2-methylbenzoic acid	215	214	214	170	x	x
2,5-Diodobenzoic acid	373.91	372	127	373	x	x
4-Acetylbenzoic acid	164.16	163	119	163	x	x
4-Fluoro-3,5-dimethylbenzoic acid	168.16	167	123	167	x	x
4-(Pentafluorosulfanyl)benzoic acid	248.17	247	127	247		x
4-Octylbenzoic acid	234.33	233	233	189		x
4-[4-(Methoxycarbonyl)phenyl]benzoic acid	256.25	255	255	211		x
Ricinoleic acid	298.5	297	297	183		x
3,4,5-trihydroxybenzoic acid	170	169	125	169	x	x
9,12-Octadecadienoic acid, sodium salt	302	279	178	235	x	x
Lauric Acid	200	199	199	-	x	x
Potassium 1-carboxyvinyl hydrogenphosphate	206	205	161	205	x	x
3-Mercaptopropionic acid	106	105	105	75	x	
4,4,4-Trifluorobutanamide	141	140	120	100	x	x

3-Iodobut-2-enoic acid	212	211	127	211	x	x
HO-Peg3-CH2cooh	208	207	207	105	x	x

^aNote that the second fragment m/z is not always shown. In these cases, the ion did not fragment and thus only the parent–parent transition was monitored.

^bNote that the total number of compounds listed to have been measured in either DMS environment may not be the same as that mentioned in **Section 3.3.1**; certain compounds which were measured were susceptible to field-induced fragmentation at high SV, and thus the dispersion type could not be assigned.

Table A.2 List of PFAS compound classes, names, abbreviations, and which chemical standard(s) each compound is found in.

Class	Name	Abbrev.	Contained in Standard(s)
Perfluorocarboxylic acids (PFCAs)	Perfluorobutanoic acid	PFBA	Native
	Perfluoropentanoic acid	PFPeA	Native
	Perfluorohexanoic acid	PFHxA	Native
	Perfluoroheptanoic acid	PFHpA	Native
	Perfluorooctanoic acid	PFOA	Native
	Perfluorononanoic acid	PFNA	Native
	Perfluorodecanoic acid	PFDA	Native
	Perfluoroundecanoic acid	PFUnA	Native
	Perfluorododecanoic acid	PFDoA	Native
	Perfluorotridecanoic acid	PFTrDA	Native
	Perfluorotetradecanoic acid	PFTDA	Native
Perfluorosulfonic acids (PFSAs)	Perfluorohexadecanoic acid	PFHxDA	Native
	Perfluorobutanesulfonic acid	PFBS	Native, 1633–2
	Perfluoropentanesulfonic acid	PFPeS	1633–2
	Perfluorohexanesulfonic acid	PFHxS	Native
	Perfluoroheptanesulfonic acid	PFHpS	Native
	Perfluorooctanesulfonic acid	PFOS	Native
	Perfluorononanesulfonic acid	PFNS	1633–2
	Perfluorodecanesulfonic acid	PFDS	Native
Fluorotelomer carboxylic acids (FTCAs)	Perfluorododecanesulfonic acid	PFDoS	1633–2
	3:3 Fluorotelomer carboxylic acid	3:3 FTCA	1633–4
	5:3 Fluorotelomer carboxylic acid	5:3 FTCA	1633–4
	7:3 Fluorotelomer carboxylic acid	7:3 FTCA	1633–4
Fluorotelomer sulfonic acids (FTSs)	8:2 Fluorotelomer unsaturated carboxylic acid	8:2 FTUCA	Native
	4:2 Fluorotelomer sulfonic acid	4:2 FTS	1633–2
	6:2 Fluorotelomer sulfonic acid	6:2 FTS	Native, 1633–2
Perfluorosulfonamides (FOSAs)	8:2 Fluorotelomer sulfonic acid	8:2 FTS	Native, 1633–2
	N–Methylperfluoro–1–octanesulfonamide	NMeFOSA	Native
	N–Ethylperfluoro–1–octanesulfonamide	NEtFOSA	Native
Perfluorosulfonamido acetic acids (FOSAAs)	Perfluorooctanesulfonamide	PFOSA	Native
	N–Methylperfluoro–1–octanesulfonamido acetic acid	NMeFOSAA	Native
Chlorinated ether sulfonic acids	N–Ethylperfluoro–1–octanesulfonamido acetic acid	NEtFOSAA	Native
	9–chlorohexadecafluoro–3–oxanone–1–sulfonic acid	9Cl-PF3ONS	Native, 1633–4
Miscellaneous ether containing PFAS	11–chloroeicosafluoro–3–oxaundecane–1–sulfonic acid	11Cl-PF3OUdS	1633–4
	Nonafluoro–3,6–dioxahexanoic acid	NFDHA	1633–4
	4,8–Dioxa–3H–perfluorononanoic acid	ADONA	Native, 1633–4
	2,3,3,3–Tetrafluoro–2–(heptafluoropropoxy)propanoic acid	HFPO-DA (GenX)	Native, 1633–4
	1,1,2,2–Tetrafluoro–2–(perfluoroethoxy)ethanesulfonic acid	PFEESA	1633–4
	2,2,3,3,4,4–Hexafluoro–4–(trifluoromethoxy)butanoic acid	PFMBA	1633–4
	2,2,3,3–tetrafluoro–3–(trifluoromethoxy)propanoic acid	PFMPA	1633–4
Fluorotelomer phosphate diester	8:2 Fluorotelomer phosphate diester	8:2 diPAP	Native

Table A.3 Multiple Reaction Monitoring (MRM) table of PFAS for DMS and LC experiments.

Q1 Mass (Da)	Q3 Mass (Da)	Dwell Time (ms)	ID ^a	Declustering Potential (V)	Entrance Potential (V)	Collision Energy (V)	Cell Exit Potential (V)
213	169	50	PFBA	-20	-9	-13	-20
263	219	50	PFPA	-15	-7	-10	-23
313	269	50	PFHxA	-60	-2	-13	-52
313	119	50	PFHxA_q	-60	-2	-28	-52
363	319	50	PFHpA	-40	-2	-14	-15
363	169	50	PFHpA_q	-40	-2	-22	-21
413	369	50	PFOA	-20	-10	-14	-18
413	169	50	PFOA_q	-20	-10	-23	-22
463	419	50	PFNA	-25	-10	-14	-20
463	219	50	PFNA_q	-25	-10	-24	-25
513	469	50	PFDA	-25	-10	-16	-22
513	219	50	PFDA_q	-25	-10	-26	-11
563	519	50	PFUnA	-20	-10	-17	-25
563	269	50	PFUnA_q	-20	-10	-25	-27
613	569	50	PFDoA	-30	-10	-19	-28
613	319	50	PFDoA_q	-30	-10	-26	-15
663	619	50	PFTrDA	-40	-10	-17	-30
663	169	50	PFTrDA_q	-40	-10	-38	-23
713	669	50	PFTeDA	-50	-10	-21	-30
713	169	50	PFTeDA_q	-50	-10	-36	-18
813	769	50	PFHxDA	-50	-6	-18	-37
813	169	50	PFHxDA_q	-50	-6	-40	-18
913	369	50	PFODA	-50	-7	-30	-19
913	413	50	PFODA_q	-50	-7	-13	-20
241	177	50	3:3FTCA	-50	-10	-11	-15
241	117	50	3:3FTCA_q	-50	-10	-40	-15
341	217	50	5:3FTCA	-50	-2	-32	-22
341	237	50	5:3FTCA_q	-50	-2	-18	-22
441	317	50	7:3FTCA	-50	-10	-27	-16
441	337	50	7:3FTCA_q	-50	-10	-18	-16
457	393	50	8:2FTUCA	-15	-6	-15	-20
457	343	50	8:2FTUCA_q	-15	-6	-50	-17
570	319	50	NMeFOSAA	-60	-10	-26	-15
570	169	50	NMeFOSAA_q	-60	-10	-30	-20
584	526	50	NEtFOSAA	-60	-10	-30	-25
584	483	50	NEtFOSAA_q	-60	-10	-22	-24
329	185	50	HFPO-DA (GenX)	-60	-10	-22	-30
329	169	50	HFPO-DA (GenX)_q	-60	-10	-11	-20
377	251	50	ADONA	-30	-2	-17	-24
377	85	50	ADONA_q	-30	-2	-40	-20
295	201	50	NFDHA	-20	-6	-11	-10
295	85	50	NFDHA_q	-20	-6	-30	-18
229	85	50	PFMPA	-25	-10	-17	-15
279	85	50	PFMBA	-30	-5	-16	-15
299	80	50	PFBS	-60	-2	-63	-15
299	99	50	PFBS_q	-60	-2	-40	-50
349	80	50	PFPS	-70	-4	-70	-15
349	99	50	PFPS_q	-70	-4	-70	-13
399	80	50	PFHxS	-90	-10	-87	-20

399	99	50	PFHxS_q	-90	-10	-75	-18
449	80	50	PFHpS	-100	-2	-95	-18
449	99	50	PFHpS_q	-100	-2	-85	-12
499	80	50	PFOS	-50	-6	-110	-19
499	99	50	PFOS_q	-50	-6	-90	-24
549	80	50	PFNS	-80	-2	-110	-15
549	99	50	PFNS_q	-80	-2	-100	-15
599	80	50	PFDS	-80	-2	-120	-15
599	99	50	PFDS_q	-80	-2	-110	-15
699	80	50	PFDoS	-80	-4	-130	-18
699	99	50	PFDoS_q	-80	-4	-140	-20
327	307	50	4:2FTS	-50	-6	-30	-16
327	81	50	4:2FTS_q	-50	-6	-55	-16
427	407	50	6:2FTS	-70	-6	-32	-20
427	81	50	6:2FTS_q	-70	-6	-65	-15
527	507	50	8:2FTS	-80	-6	-38	-24
527	81	50	8:2FTS_q	-80	-6	-90	-20
315	135	50	PFEESA	-50	-3	-28	-15
315	83	50	PFEESA_q	-50	-3	-24	-14
531	351	50	9Cl-PF3ONS	-50	-4	-40	-18
533	353	50	9Cl-PF3ONS_q	-70	-5	-37	-17
631	451	50	11Cl-PF3OUdS	-60	-10	-38	-22
633	453	50	11Cl-PF3OUdS_q	-70	-5	-41	-20
498	78	50	PFOSA	-70	-6	-80	-18
498	169	50	PFOSA_q	-70	-6	-38	-17
512	169	50	NMeFOSA	-60	-6	-35	-19
512	219	50	NMeFOSA_q	-60	-6	-33	-24
526	169	50	NEtFOSA	-60	-6	-36	-20
526	219	50	NEtFOSA_q	-60	-6	-35	-25
989	543	50	8:2diPAP	-50	-6	-35	-28
989	79	50	8:2diPAP_q	-50	-6	-140	-20

^aIDs with the “_q” suffix represent the secondary (qualifier) fragment used for compound monitoring.

Table A.4 CV-labeled MRM transitions of PFAS for LC×DMS experiments.

Q1 Mass (Da)	Q3 Mass (Da)	Dwell Time (ms)	ID ^a	Declustering Potential (V)	Entrance Potential (V)	Collision Energy (V)	Cell Exit Potential (V)	Compensation Voltage (V)
631	451	5	11Cl-PF3OUdS Q101	-60	-10	-38	-22	-3.7
631	451	5	11Cl-PF3OUdS Q102	-60	-10	-38	-22	-3.2
631	451	5	11Cl-PF3OUdS Q103	-60	-10	-38	-22	-2.7
631	451	5	11Cl-PF3OUdS Q104	-60	-10	-38	-22	-2.2
631	451	5	11Cl-PF3OUdS Q105	-60	-10	-38	-22	-1.7
631	451	5	11Cl-PF3OUdS Q106	-60	-10	-38	-22	-1.2
631	451	5	11Cl-PF3OUdS Q107	-60	-10	-38	-22	-0.7
631	451	5	11Cl-PF3OUdS Q108	-60	-10	-38	-22	-0.2
631	451	5	11Cl-PF3OUdS Q109	-60	-10	-38	-22	0.3
631	451	5	11Cl-PF3OUdS Q110	-60	-10	-38	-22	0.8
631	451	5	11Cl-PF3OUdS Q111	-60	-10	-38	-22	1.3
631	451	5	11Cl-PF3OUdS Q112	-60	-10	-38	-22	1.8
631	451	5	11Cl-PF3OUdS Q113	-60	-10	-38	-22	2.3
241	177	5	3:3FTCA Q101	-50	-10	-11	-15	-52
241	177	5	3:3FTCA Q102	-50	-10	-11	-15	-51.5
241	177	5	3:3FTCA Q103	-50	-10	-11	-15	-51
241	177	5	3:3FTCA Q104	-50	-10	-11	-15	-50.5
241	177	5	3:3FTCA Q105	-50	-10	-11	-15	-50
241	177	5	3:3FTCA Q106	-50	-10	-11	-15	-49.5
241	177	5	3:3FTCA Q107	-50	-10	-11	-15	-49
241	177	5	3:3FTCA Q108	-50	-10	-11	-15	-48.5
241	177	5	3:3FTCA Q109	-50	-10	-11	-15	-48
241	177	5	3:3FTCA Q110	-50	-10	-11	-15	-47.5
241	177	5	3:3FTCA Q111	-50	-10	-11	-15	-47
241	177	5	3:3FTCA Q112	-50	-10	-11	-15	-46.5
241	177	5	3:3FTCA Q113	-50	-10	-11	-15	-46
327	307	5	4:2FTS Q101	-50	-6	-30	-16	-44.5
327	307	5	4:2FTS Q102	-50	-6	-30	-16	-44
327	307	5	4:2FTS Q103	-50	-6	-30	-16	-43.5
327	307	5	4:2FTS Q104	-50	-6	-30	-16	-43
327	307	5	4:2FTS Q105	-50	-6	-30	-16	-42.5
327	307	5	4:2FTS Q106	-50	-6	-30	-16	-42
327	307	5	4:2FTS Q107	-50	-6	-30	-16	-41.5
327	307	5	4:2FTS Q108	-50	-6	-30	-16	-41
327	307	5	4:2FTS Q109	-50	-6	-30	-16	-40.5
327	307	5	4:2FTS Q110	-50	-6	-30	-16	-40
327	307	5	4:2FTS Q111	-50	-6	-30	-16	-39.5
327	307	5	4:2FTS Q112	-50	-6	-30	-16	-39
327	307	5	4:2FTS Q113	-50	-6	-30	-16	-38.5
341	217	5	5:3FTCA Q101	-50	-2	-32	-22	-36.3
341	217	5	5:3FTCA Q102	-50	-2	-32	-22	-35.8
341	217	5	5:3FTCA Q103	-50	-2	-32	-22	-35.3
341	217	5	5:3FTCA Q104	-50	-2	-32	-22	-34.8
341	217	5	5:3FTCA Q105	-50	-2	-32	-22	-34.3
341	217	5	5:3FTCA Q106	-50	-2	-32	-22	-33.8
341	217	5	5:3FTCA Q107	-50	-2	-32	-22	-33.3
341	217	5	5:3FTCA Q108	-50	-2	-32	-22	-32.8
341	217	5	5:3FTCA Q109	-50	-2	-32	-22	-32.3
341	217	5	5:3FTCA Q110	-50	-2	-32	-22	-31.8
341	217	5	5:3FTCA Q111	-50	-2	-32	-22	-31.3
341	217	5	5:3FTCA Q112	-50	-2	-32	-22	-30.8
341	217	5	5:3FTCA Q113	-50	-2	-32	-22	-30.3
427	407	5	6:2FTS Q101	-70	-6	-32	-20	-34.4
427	407	5	6:2FTS Q102	-70	-6	-32	-20	-33.9

427	407	5	6:2FTS Q103	-70	-6	-32	-20	-33.4
427	407	5	6:2FTS Q104	-70	-6	-32	-20	-32.9
427	407	5	6:2FTS Q105	-70	-6	-32	-20	-32.4
427	407	5	6:2FTS Q106	-70	-6	-32	-20	-31.9
427	407	5	6:2FTS Q107	-70	-6	-32	-20	-31.4
427	407	5	6:2FTS Q108	-70	-6	-32	-20	-30.9
427	407	5	6:2FTS Q109	-70	-6	-32	-20	-30.4
427	407	5	6:2FTS Q110	-70	-6	-32	-20	-29.9
427	407	5	6:2FTS Q111	-70	-6	-32	-20	-29.4
427	407	5	6:2FTS Q112	-70	-6	-32	-20	-28.9
427	407	5	6:2FTS Q113	-70	-6	-32	-20	-28.4
441	317	5	7:3FTCA Q101	-50	-10	-27	-16	-26.6
441	317	5	7:3FTCA Q102	-50	-10	-27	-16	-26.1
441	317	5	7:3FTCA Q103	-50	-10	-27	-16	-25.6
441	317	5	7:3FTCA Q104	-50	-10	-27	-16	-25.1
441	317	5	7:3FTCA Q105	-50	-10	-27	-16	-24.6
441	317	5	7:3FTCA Q106	-50	-10	-27	-16	-24.1
441	317	5	7:3FTCA Q107	-50	-10	-27	-16	-23.6
441	317	5	7:3FTCA Q108	-50	-10	-27	-16	-23.1
441	317	5	7:3FTCA Q109	-50	-10	-27	-16	-22.6
441	317	5	7:3FTCA Q110	-50	-10	-27	-16	-22.1
441	317	5	7:3FTCA Q111	-50	-10	-27	-16	-21.6
441	317	5	7:3FTCA Q112	-50	-10	-27	-16	-21.1
441	317	5	7:3FTCA Q113	-50	-10	-27	-16	-20.6
989	543	5	8:2diPAP Q101	-50	-6	-35	-28	-7.9
989	543	5	8:2diPAP Q102	-50	-6	-35	-28	-7.4
989	543	5	8:2diPAP Q103	-50	-6	-35	-28	-6.9
989	543	5	8:2diPAP Q104	-50	-6	-35	-28	-6.4
989	543	5	8:2diPAP Q105	-50	-6	-35	-28	-5.9
989	543	5	8:2diPAP Q106	-50	-6	-35	-28	-5.4
989	543	5	8:2diPAP Q107	-50	-6	-35	-28	-4.9
989	543	5	8:2diPAP Q108	-50	-6	-35	-28	-4.4
989	543	5	8:2diPAP Q109	-50	-6	-35	-28	-3.9
989	543	5	8:2diPAP Q110	-50	-6	-35	-28	-3.4
989	543	5	8:2diPAP Q111	-50	-6	-35	-28	-2.9
989	543	5	8:2diPAP Q112	-50	-6	-35	-28	-2.4
989	543	5	8:2diPAP Q113	-50	-6	-35	-28	-1.9
527	507	5	8:2FTS Q101	-80	-6	-38	-24	-26.7
527	507	5	8:2FTS Q102	-80	-6	-38	-24	-26.2
527	507	5	8:2FTS Q103	-80	-6	-38	-24	-25.7
527	507	5	8:2FTS Q104	-80	-6	-38	-24	-25.2
527	507	5	8:2FTS Q105	-80	-6	-38	-24	-24.7
527	507	5	8:2FTS Q106	-80	-6	-38	-24	-24.2
527	507	5	8:2FTS Q107	-80	-6	-38	-24	-23.7
527	507	5	8:2FTS Q108	-80	-6	-38	-24	-23.2
527	507	5	8:2FTS Q109	-80	-6	-38	-24	-22.7
527	507	5	8:2FTS Q110	-80	-6	-38	-24	-22.2
527	507	5	8:2FTS Q111	-80	-6	-38	-24	-21.7
527	507	5	8:2FTS Q112	-80	-6	-38	-24	-21.2
527	507	5	8:2FTS Q113	-80	-6	-38	-24	-20.7
457	393	5	8:2FTUCA Q101	-15	-6	-15	-20	-29.7
457	393	5	8:2FTUCA Q102	-15	-6	-15	-20	-29.2
457	393	5	8:2FTUCA Q103	-15	-6	-15	-20	-28.7
457	393	5	8:2FTUCA Q104	-15	-6	-15	-20	-28.2
457	393	5	8:2FTUCA Q105	-15	-6	-15	-20	-27.7
457	393	5	8:2FTUCA Q106	-15	-6	-15	-20	-27.2
457	393	5	8:2FTUCA Q107	-15	-6	-15	-20	-26.7
457	393	5	8:2FTUCA Q108	-15	-6	-15	-20	-26.2

457	393	5	8:2FTUCA Q109	-15	-6	-15	-20	-25.7
457	393	5	8:2FTUCA Q110	-15	-6	-15	-20	-25.2
457	393	5	8:2FTUCA Q111	-15	-6	-15	-20	-24.7
457	393	5	8:2FTUCA Q112	-15	-6	-15	-20	-24.2
457	393	5	8:2FTUCA Q113	-15	-6	-15	-20	-23.7
531	351	5	9Cl-PF3ONS Q101	-50	-4	-40	-18	-4.5
531	351	5	9Cl-PF3ONS Q102	-50	-4	-40	-18	-4
531	351	5	9Cl-PF3ONS Q103	-50	-4	-40	-18	-3.5
531	351	5	9Cl-PF3ONS Q104	-50	-4	-40	-18	-3
531	351	5	9Cl-PF3ONS Q105	-50	-4	-40	-18	-2.5
531	351	5	9Cl-PF3ONS Q106	-50	-4	-40	-18	-2
531	351	5	9Cl-PF3ONS Q107	-50	-4	-40	-18	-1.5
531	351	5	9Cl-PF3ONS Q108	-50	-4	-40	-18	-1
531	351	5	9Cl-PF3ONS Q109	-50	-4	-40	-18	-0.5
531	351	5	9Cl-PF3ONS Q110	-50	-4	-40	-18	0
531	351	5	9Cl-PF3ONS Q111	-50	-4	-40	-18	0.5
531	351	5	9Cl-PF3ONS Q112	-50	-4	-40	-18	1
531	351	5	9Cl-PF3ONS Q113	-50	-4	-40	-18	1.5
377	251	5	ADONA Q101	-30	-2	-17	-24	-36
377	251	5	ADONA Q102	-30	-2	-17	-24	-35.5
377	251	5	ADONA Q103	-30	-2	-17	-24	-35
377	251	5	ADONA Q104	-30	-2	-17	-24	-34.5
377	251	5	ADONA Q105	-30	-2	-17	-24	-34
377	251	5	ADONA Q106	-30	-2	-17	-24	-33.5
377	251	5	ADONA Q107	-30	-2	-17	-24	-33
377	251	5	ADONA Q108	-30	-2	-17	-24	-32.5
377	251	5	ADONA Q109	-30	-2	-17	-24	-32
377	251	5	ADONA Q110	-30	-2	-17	-24	-31.5
377	251	5	ADONA Q111	-30	-2	-17	-24	-31
377	251	5	ADONA Q112	-30	-2	-17	-24	-30.5
377	251	5	ADONA Q113	-30	-2	-17	-24	-30
526	169	5	NEtFOSA Q101	-60	-6	-36	-20	-16.3
526	169	5	NEtFOSA Q102	-60	-6	-36	-20	-15.8
526	169	5	NEtFOSA Q103	-60	-6	-36	-20	-15.3
526	169	5	NEtFOSA Q104	-60	-6	-36	-20	-14.8
526	169	5	NEtFOSA Q105	-60	-6	-36	-20	-14.3
526	169	5	NEtFOSA Q106	-60	-6	-36	-20	-13.8
526	169	5	NEtFOSA Q107	-60	-6	-36	-20	-13.3
526	169	5	NEtFOSA Q108	-60	-6	-36	-20	-12.8
526	169	5	NEtFOSA Q109	-60	-6	-36	-20	-12.3
526	169	5	NEtFOSA Q110	-60	-6	-36	-20	-11.8
526	169	5	NEtFOSA Q111	-60	-6	-36	-20	-11.3
526	169	5	NEtFOSA Q112	-60	-6	-36	-20	-10.8
526	169	5	NEtFOSA Q113	-60	-6	-36	-20	-10.3
584	526	5	NEtFOSAA Q101	-60	-10	-30	-25	-18
584	526	5	NEtFOSAA Q102	-60	-10	-30	-25	-17.5
584	526	5	NEtFOSAA Q103	-60	-10	-30	-25	-17
584	526	5	NEtFOSAA Q104	-60	-10	-30	-25	-16.5
584	526	5	NEtFOSAA Q105	-60	-10	-30	-25	-16
584	526	5	NEtFOSAA Q106	-60	-10	-30	-25	-15.5
584	526	5	NEtFOSAA Q107	-60	-10	-30	-25	-15
584	526	5	NEtFOSAA Q108	-60	-10	-30	-25	-14.5
584	526	5	NEtFOSAA Q109	-60	-10	-30	-25	-14
584	526	5	NEtFOSAA Q110	-60	-10	-30	-25	-13.5
584	526	5	NEtFOSAA Q111	-60	-10	-30	-25	-13
584	526	5	NEtFOSAA Q112	-60	-10	-30	-25	-12.5
584	526	5	NEtFOSAA Q113	-60	-10	-30	-25	-12
512	169	5	NMeFOSA Q101	-60	-6	-35	-19	-20.3

512	169	5	NMeFOSA_Q102	-60	-6	-35	-19	-19.8
512	169	5	NMeFOSA_Q103	-60	-6	-35	-19	-19.3
512	169	5	NMeFOSA_Q104	-60	-6	-35	-19	-18.8
512	169	5	NMeFOSA_Q105	-60	-6	-35	-19	-18.3
512	169	5	NMeFOSA_Q106	-60	-6	-35	-19	-17.8
512	169	5	NMeFOSA_Q107	-60	-6	-35	-19	-17.3
512	169	5	NMeFOSA_Q108	-60	-6	-35	-19	-16.8
512	169	5	NMeFOSA_Q109	-60	-6	-35	-19	-16.3
512	169	5	NMeFOSA_Q110	-60	-6	-35	-19	-15.8
512	169	5	NMeFOSA_Q111	-60	-6	-35	-19	-15.3
512	169	5	NMeFOSA_Q112	-60	-6	-35	-19	-14.8
512	169	5	NMeFOSA_Q113	-60	-6	-35	-19	-14.3
299	80	5	PFBS_Q101	-60	-2	-63	-15	-17.6
299	80	5	PFBS_Q102	-60	-2	-63	-15	-17.1
299	80	5	PFBS_Q103	-60	-2	-63	-15	-16.6
299	80	5	PFBS_Q104	-60	-2	-63	-15	-16.1
299	80	5	PFBS_Q105	-60	-2	-63	-15	-15.6
299	80	5	PFBS_Q106	-60	-2	-63	-15	-15.1
299	80	5	PFBS_Q107	-60	-2	-63	-15	-14.6
299	80	5	PFBS_Q108	-60	-2	-63	-15	-14.1
299	80	5	PFBS_Q109	-60	-2	-63	-15	-13.6
299	80	5	PFBS_Q110	-60	-2	-63	-15	-13.1
299	80	5	PFBS_Q111	-60	-2	-63	-15	-12.6
299	80	5	PFBS_Q112	-60	-2	-63	-15	-12.1
299	80	5	PFBS_Q113	-60	-2	-63	-15	-11.6
513	469	5	PFDA_Q101	-25	-10	-16	-22	-28
513	469	5	PFDA_Q102	-25	-10	-16	-22	-27.5
513	469	5	PFDA_Q103	-25	-10	-16	-22	-27
513	469	5	PFDA_Q104	-25	-10	-16	-22	-26.5
513	469	5	PFDA_Q105	-25	-10	-16	-22	-26
513	469	5	PFDA_Q106	-25	-10	-16	-22	-25.5
513	469	5	PFDA_Q107	-25	-10	-16	-22	-25
513	469	5	PFDA_Q108	-25	-10	-16	-22	-24.5
513	469	5	PFDA_Q109	-25	-10	-16	-22	-24
513	469	5	PFDA_Q110	-25	-10	-16	-22	-23.5
513	469	5	PFDA_Q111	-25	-10	-16	-22	-23
513	469	5	PFDA_Q112	-25	-10	-16	-22	-22.5
513	469	5	PFDA_Q113	-25	-10	-16	-22	-22
613	569	5	PFDaA_Q101	-30	-10	-19	-28	-21
613	569	5	PFDaA_Q102	-30	-10	-19	-28	-20.5
613	569	5	PFDaA_Q103	-30	-10	-19	-28	-20
613	569	5	PFDaA_Q104	-30	-10	-19	-28	-19.5
613	569	5	PFDaA_Q105	-30	-10	-19	-28	-19
613	569	5	PFDaA_Q106	-30	-10	-19	-28	-18.5
613	569	5	PFDaA_Q107	-30	-10	-19	-28	-18
613	569	5	PFDaA_Q108	-30	-10	-19	-28	-17.5
613	569	5	PFDaA_Q109	-30	-10	-19	-28	-17
613	569	5	PFDaA_Q110	-30	-10	-19	-28	-16.5
613	569	5	PFDaA_Q111	-30	-10	-19	-28	-16
613	569	5	PFDaA_Q112	-30	-10	-19	-28	-15.5
613	569	5	PFDaA_Q113	-30	-10	-19	-28	-15
699	80	5	PFDoS_Q101	-80	-4	-130	-18	-7.6
699	80	5	PFDoS_Q102	-80	-4	-130	-18	-7.1
699	80	5	PFDoS_Q103	-80	-4	-130	-18	-6.6
699	80	5	PFDoS_Q104	-80	-4	-130	-18	-6.1
699	80	5	PFDoS_Q105	-80	-4	-130	-18	-5.6
699	80	5	PFDoS_Q106	-80	-4	-130	-18	-5.1
699	80	5	PFDoS_Q107	-80	-4	-130	-18	-4.6

699	80	5	PFDoS Q108	-80	-4	-130	-18	-4.1
699	80	5	PFDoS Q109	-80	-4	-130	-18	-3.6
699	80	5	PFDoS Q110	-80	-4	-130	-18	-3.1
699	80	5	PFDoS Q111	-80	-4	-130	-18	-2.6
699	80	5	PFDoS Q112	-80	-4	-130	-18	-2.1
699	80	5	PFDoS Q113	-80	-4	-130	-18	-1.6
599	80	5	PFDS Q101	-80	-2	-120	-15	-8.8
599	80	5	PFDS Q102	-80	-2	-120	-15	-8.3
599	80	5	PFDS Q103	-80	-2	-120	-15	-7.8
599	80	5	PFDS Q104	-80	-2	-120	-15	-7.3
599	80	5	PFDS Q105	-80	-2	-120	-15	-6.8
599	80	5	PFDS Q106	-80	-2	-120	-15	-6.3
599	80	5	PFDS Q107	-80	-2	-120	-15	-5.8
599	80	5	PFDS Q108	-80	-2	-120	-15	-5.3
599	80	5	PFDS Q109	-80	-2	-120	-15	-4.8
599	80	5	PFDS Q110	-80	-2	-120	-15	-4.3
599	80	5	PFDS Q111	-80	-2	-120	-15	-3.8
599	80	5	PFDS Q112	-80	-2	-120	-15	-3.3
599	80	5	PFDS Q113	-80	-2	-120	-15	-2.8
315	135	5	PFEESA Q101	-50	-3	-28	-15	-14.6
315	135	5	PFEESA Q102	-50	-3	-28	-15	-14.1
315	135	5	PFEESA Q103	-50	-3	-28	-15	-13.6
315	135	5	PFEESA Q104	-50	-3	-28	-15	-13.1
315	135	5	PFEESA Q105	-50	-3	-28	-15	-12.6
315	135	5	PFEESA Q106	-50	-3	-28	-15	-12.1
315	135	5	PFEESA Q107	-50	-3	-28	-15	-11.6
315	135	5	PFEESA Q108	-50	-3	-28	-15	-11.1
315	135	5	PFEESA Q109	-50	-3	-28	-15	-10.6
315	135	5	PFEESA Q110	-50	-3	-28	-15	-10.1
315	135	5	PFEESA Q111	-50	-3	-28	-15	-9.6
315	135	5	PFEESA Q112	-50	-3	-28	-15	-9.1
315	135	5	PFEESA Q113	-50	-3	-28	-15	-8.6
363	319	5	PFHpA Q101	-40	-2	-14	-15	-42.4
363	319	5	PFHpA Q102	-40	-2	-14	-15	-41.9
363	319	5	PFHpA Q103	-40	-2	-14	-15	-41.4
363	319	5	PFHpA Q104	-40	-2	-14	-15	-40.9
363	319	5	PFHpA Q105	-40	-2	-14	-15	-40.4
363	319	5	PFHpA Q106	-40	-2	-14	-15	-39.9
363	319	5	PFHpA Q107	-40	-2	-14	-15	-39.4
363	319	5	PFHpA Q108	-40	-2	-14	-15	-38.9
363	319	5	PFHpA Q109	-40	-2	-14	-15	-38.4
363	319	5	PFHpA Q110	-40	-2	-14	-15	-37.9
363	319	5	PFHpA Q111	-40	-2	-14	-15	-37.4
363	319	5	PFHpA Q112	-40	-2	-14	-15	-36.9
363	319	5	PFHpA Q113	-40	-2	-14	-15	-36.4
449	80	5	PFHpS Q101	-100	-2	-95	-18	-13
449	80	5	PFHpS Q102	-100	-2	-95	-18	-12.5
449	80	5	PFHpS Q103	-100	-2	-95	-18	-12
449	80	5	PFHpS Q104	-100	-2	-95	-18	-11.5
449	80	5	PFHpS Q105	-100	-2	-95	-18	-11
449	80	5	PFHpS Q106	-100	-2	-95	-18	-10.5
449	80	5	PFHpS Q107	-100	-2	-95	-18	-10
449	80	5	PFHpS Q108	-100	-2	-95	-18	-9.5
449	80	5	PFHpS Q109	-100	-2	-95	-18	-9
449	80	5	PFHpS Q110	-100	-2	-95	-18	-8.5
449	80	5	PFHpS Q111	-100	-2	-95	-18	-8
449	80	5	PFHpS Q112	-100	-2	-95	-18	-7.5
449	80	5	PFHpS Q113	-100	-2	-95	-18	-7

449	80	5	PFHpS Q114	-100	-2	-95	-18	-6.5
449	80	5	PFHpS Q115	-100	-2	-95	-18	-6
449	80	5	PFHpS Q116	-100	-2	-95	-18	-5.5
449	80	5	PFHpS Q117	-100	-2	-95	-18	-5
449	80	5	PFHpS Q118	-100	-2	-95	-18	-4.5
449	80	5	PFHpS Q119	-100	-2	-95	-18	-4
313	269	5	PFHxA Q101	-60	-2	-13	-52	-49.5
313	269	5	PFHxA Q102	-60	-2	-13	-52	-49
313	269	5	PFHxA Q103	-60	-2	-13	-52	-48.5
313	269	5	PFHxA Q104	-60	-2	-13	-52	-48
313	269	5	PFHxA Q105	-60	-2	-13	-52	-47.5
313	269	5	PFHxA Q106	-60	-2	-13	-52	-47
313	269	5	PFHxA Q107	-60	-2	-13	-52	-46.5
313	269	5	PFHxA Q108	-60	-2	-13	-52	-46
313	269	5	PFHxA Q109	-60	-2	-13	-52	-45.5
313	269	5	PFHxA Q110	-60	-2	-13	-52	-45
313	269	5	PFHxA Q111	-60	-2	-13	-52	-44.5
313	269	5	PFHxA Q112	-60	-2	-13	-52	-44
313	269	5	PFHxA Q113	-60	-2	-13	-52	-43.5
813	769	5	PFHxDA Q101	-50	-6	-18	-37	-12.3
813	769	5	PFHxDA Q102	-50	-6	-18	-37	-11.8
813	769	5	PFHxDA Q103	-50	-6	-18	-37	-11.3
813	769	5	PFHxDA Q104	-50	-6	-18	-37	-10.8
813	769	5	PFHxDA Q105	-50	-6	-18	-37	-10.3
813	769	5	PFHxDA Q106	-50	-6	-18	-37	-9.8
813	769	5	PFHxDA Q107	-50	-6	-18	-37	-9.3
813	769	5	PFHxDA Q108	-50	-6	-18	-37	-8.8
813	769	5	PFHxDA Q109	-50	-6	-18	-37	-8.3
813	769	5	PFHxDA Q110	-50	-6	-18	-37	-7.8
813	769	5	PFHxDA Q111	-50	-6	-18	-37	-7.3
813	769	5	PFHxDA Q112	-50	-6	-18	-37	-6.8
813	769	5	PFHxDA Q113	-50	-6	-18	-37	-6.3
399	80	5	PFHxS Q101	-90	-10	-87	-20	-14.2
399	80	5	PFHxS Q102	-90	-10	-87	-20	-13.7
399	80	5	PFHxS Q103	-90	-10	-87	-20	-13.2
399	80	5	PFHxS Q104	-90	-10	-87	-20	-12.7
399	80	5	PFHxS Q105	-90	-10	-87	-20	-12.2
399	80	5	PFHxS Q106	-90	-10	-87	-20	-11.7
399	80	5	PFHxS Q107	-90	-10	-87	-20	-11.2
399	80	5	PFHxS Q108	-90	-10	-87	-20	-10.7
399	80	5	PFHxS Q109	-90	-10	-87	-20	-10.2
399	80	5	PFHxS Q110	-90	-10	-87	-20	-9.7
399	80	5	PFHxS Q111	-90	-10	-87	-20	-9.2
399	80	5	PFHxS Q112	-90	-10	-87	-20	-8.7
399	80	5	PFHxS Q113	-90	-10	-87	-20	-8.2
399	80	5	PFHxS Q114	-90	-10	-87	-20	-7.7
399	80	5	PFHxS Q115	-90	-10	-87	-20	-7.2
399	80	5	PFHxS Q116	-90	-10	-87	-20	-6.7
399	80	5	PFHxS Q117	-90	-10	-87	-20	-6.2
399	80	5	PFHxS Q118	-90	-10	-87	-20	-5.7
399	80	5	PFHxS Q119	-90	-10	-87	-20	-5.2
279	85	5	PFMBA Q101	-30	-5	-16	-15	-53
279	85	5	PFMBA Q102	-30	-5	-16	-15	-52.5
279	85	5	PFMBA Q103	-30	-5	-16	-15	-52
279	85	5	PFMBA Q104	-30	-5	-16	-15	-51.5
279	85	5	PFMBA Q105	-30	-5	-16	-15	-51
279	85	5	PFMBA Q106	-30	-5	-16	-15	-50.5
279	85	5	PFMBA Q107	-30	-5	-16	-15	-50

279	85	5	PFMBA Q108	-30	-5	-16	-15	-49.5
279	85	5	PFMBA Q109	-30	-5	-16	-15	-49
279	85	5	PFMBA Q110	-30	-5	-16	-15	-48.5
279	85	5	PFMBA Q111	-30	-5	-16	-15	-48
279	85	5	PFMBA Q112	-30	-5	-16	-15	-47.5
279	85	5	PFMBA Q113	-30	-5	-16	-15	-47
463	419	5	PFNA Q101	-25	-10	-14	-20	-32.5
463	419	5	PFNA Q102	-25	-10	-14	-20	-32
463	419	5	PFNA Q103	-25	-10	-14	-20	-31.5
463	419	5	PFNA Q104	-25	-10	-14	-20	-31
463	419	5	PFNA Q105	-25	-10	-14	-20	-30.5
463	419	5	PFNA Q106	-25	-10	-14	-20	-30
463	419	5	PFNA Q107	-25	-10	-14	-20	-29.5
463	419	5	PFNA Q108	-25	-10	-14	-20	-29
463	419	5	PFNA Q109	-25	-10	-14	-20	-28.5
463	419	5	PFNA Q110	-25	-10	-14	-20	-28
463	419	5	PFNA Q111	-25	-10	-14	-20	-27.5
463	419	5	PFNA Q112	-25	-10	-14	-20	-27
463	419	5	PFNA Q113	-25	-10	-14	-20	-26.5
549	80	5	PFNS Q101	-80	-2	-110	-15	-9.6
549	80	5	PFNS Q102	-80	-2	-110	-15	-9.1
549	80	5	PFNS Q103	-80	-2	-110	-15	-8.6
549	80	5	PFNS Q104	-80	-2	-110	-15	-8.1
549	80	5	PFNS Q105	-80	-2	-110	-15	-7.6
549	80	5	PFNS Q106	-80	-2	-110	-15	-7.1
549	80	5	PFNS Q107	-80	-2	-110	-15	-6.6
549	80	5	PFNS Q108	-80	-2	-110	-15	-6.1
549	80	5	PFNS Q109	-80	-2	-110	-15	-5.6
549	80	5	PFNS Q110	-80	-2	-110	-15	-5.1
549	80	5	PFNS Q111	-80	-2	-110	-15	-4.6
549	80	5	PFNS Q112	-80	-2	-110	-15	-4.1
549	80	5	PFNS Q113	-80	-2	-110	-15	-3.6
413	369	5	PFOA Q101	-20	-10	-14	-18	-37.5
413	369	5	PFOA Q102	-20	-10	-14	-18	-37
413	369	5	PFOA Q103	-20	-10	-14	-18	-36.5
413	369	5	PFOA Q104	-20	-10	-14	-18	-36
413	369	5	PFOA Q105	-20	-10	-14	-18	-35.5
413	369	5	PFOA Q106	-20	-10	-14	-18	-35
413	369	5	PFOA Q107	-20	-10	-14	-18	-34.5
413	369	5	PFOA Q108	-20	-10	-14	-18	-34
413	369	5	PFOA Q109	-20	-10	-14	-18	-33.5
413	369	5	PFOA Q110	-20	-10	-14	-18	-33
413	369	5	PFOA Q111	-20	-10	-14	-18	-32.5
413	369	5	PFOA Q112	-20	-10	-14	-18	-32
413	369	5	PFOA Q113	-20	-10	-14	-18	-31.5
499	80	5	PFOS Q101	-50	-6	-110	-19	-14.6
499	80	5	PFOS Q102	-50	-6	-110	-19	-14.1
499	80	5	PFOS Q103	-50	-6	-110	-19	-13.6
499	80	5	PFOS Q104	-50	-6	-110	-19	-13.1
499	80	5	PFOS Q105	-50	-6	-110	-19	-12.6
499	80	5	PFOS Q106	-50	-6	-110	-19	-12.1
499	80	5	PFOS Q107	-50	-6	-110	-19	-11.6
499	80	5	PFOS Q108	-50	-6	-110	-19	-11.1
499	80	5	PFOS Q109	-50	-6	-110	-19	-10.6
499	80	5	PFOS Q110	-50	-6	-110	-19	-10.1
499	80	5	PFOS Q111	-50	-6	-110	-19	-9.6
499	80	5	PFOS Q112	-50	-6	-110	-19	-9.1
499	80	5	PFOS Q113	-50	-6	-110	-19	-8.6

499	80	5	PFOS Q114	-50	-6	-110	-19	-8.1
499	80	5	PFOS Q115	-50	-6	-110	-19	-7.6
499	80	5	PFOS Q116	-50	-6	-110	-19	-7.1
499	80	5	PFOS Q117	-50	-6	-110	-19	-6.6
499	80	5	PFOS Q118	-50	-6	-110	-19	-6.1
499	80	5	PFOS Q119	-50	-6	-110	-19	-5.6
498	78	5	PFOSA Q101	-70	-6	-80	-18	-18.4
498	78	5	PFOSA Q102	-70	-6	-80	-18	-17.9
498	78	5	PFOSA Q103	-70	-6	-80	-18	-17.4
498	78	5	PFOSA Q104	-70	-6	-80	-18	-16.9
498	78	5	PFOSA Q105	-70	-6	-80	-18	-16.4
498	78	5	PFOSA Q106	-70	-6	-80	-18	-15.9
498	78	5	PFOSA Q107	-70	-6	-80	-18	-15.4
498	78	5	PFOSA Q108	-70	-6	-80	-18	-14.9
498	78	5	PFOSA Q109	-70	-6	-80	-18	-14.4
498	78	5	PFOSA Q110	-70	-6	-80	-18	-13.9
498	78	5	PFOSA Q111	-70	-6	-80	-18	-13.4
498	78	5	PFOSA Q112	-70	-6	-80	-18	-12.9
498	78	5	PFOSA Q113	-70	-6	-80	-18	-12.4
349	80	5	PFPS Q101	-70	-4	-70	-15	-14.8
349	80	5	PFPS Q102	-70	-4	-70	-15	-14.3
349	80	5	PFPS Q103	-70	-4	-70	-15	-13.8
349	80	5	PFPS Q104	-70	-4	-70	-15	-13.3
349	80	5	PFPS Q105	-70	-4	-70	-15	-12.8
349	80	5	PFPS Q106	-70	-4	-70	-15	-12.3
349	80	5	PFPS Q107	-70	-4	-70	-15	-11.8
349	80	5	PFPS Q108	-70	-4	-70	-15	-11.3
349	80	5	PFPS Q109	-70	-4	-70	-15	-10.8
349	80	5	PFPS Q110	-70	-4	-70	-15	-10.3
349	80	5	PFPS Q111	-70	-4	-70	-15	-9.8
349	80	5	PFPS Q112	-70	-4	-70	-15	-9.3
349	80	5	PFPS Q113	-70	-4	-70	-15	-8.8
713	669	5	PFTDA Q101	-50	-10	-21	-30	-15.5
713	669	5	PFTDA Q102	-50	-10	-21	-30	-15
713	669	5	PFTDA Q103	-50	-10	-21	-30	-14.5
713	669	5	PFTDA Q104	-50	-10	-21	-30	-14
713	669	5	PFTDA Q105	-50	-10	-21	-30	-13.5
713	669	5	PFTDA Q106	-50	-10	-21	-30	-13
713	669	5	PFTDA Q107	-50	-10	-21	-30	-12.5
713	669	5	PFTDA Q108	-50	-10	-21	-30	-12
713	669	5	PFTDA Q109	-50	-10	-21	-30	-11.5
713	669	5	PFTDA Q110	-50	-10	-21	-30	-11
713	669	5	PFTDA Q111	-50	-10	-21	-30	-10.5
713	669	5	PFTDA Q112	-50	-10	-21	-30	-10
713	669	5	PFTDA Q113	-50	-10	-21	-30	-9.5
663	619	5	PFTTrDA Q101	-40	-10	-17	-30	-18.5
663	619	5	PFTTrDA Q102	-40	-10	-17	-30	-18
663	619	5	PFTTrDA Q103	-40	-10	-17	-30	-17.5
663	619	5	PFTTrDA Q104	-40	-10	-17	-30	-17
663	619	5	PFTTrDA Q105	-40	-10	-17	-30	-16.5
663	619	5	PFTTrDA Q106	-40	-10	-17	-30	-16
663	619	5	PFTTrDA Q107	-40	-10	-17	-30	-15.5
663	619	5	PFTTrDA Q108	-40	-10	-17	-30	-15
663	619	5	PFTTrDA Q109	-40	-10	-17	-30	-14.5
663	619	5	PFTTrDA Q110	-40	-10	-17	-30	-14
663	619	5	PFTTrDA Q111	-40	-10	-17	-30	-13.5
663	619	5	PFTTrDA Q112	-40	-10	-17	-30	-13
663	619	5	PFTTrDA Q113	-40	-10	-17	-30	-12.5

563	519	5	PFUnA_Q101	-20	-10	-17	-25	-23.5
563	519	5	PFUnA_Q102	-20	-10	-17	-25	-23
563	519	5	PFUnA_Q103	-20	-10	-17	-25	-22.5
563	519	5	PFUnA_Q104	-20	-10	-17	-25	-22
563	519	5	PFUnA_Q105	-20	-10	-17	-25	-21.5
563	519	5	PFUnA_Q106	-20	-10	-17	-25	-21
563	519	5	PFUnA_Q107	-20	-10	-17	-25	-20.5
563	519	5	PFUnA_Q108	-20	-10	-17	-25	-20
563	519	5	PFUnA_Q109	-20	-10	-17	-25	-19.5
563	519	5	PFUnA_Q110	-20	-10	-17	-25	-19
563	519	5	PFUnA_Q111	-20	-10	-17	-25	-18.5
563	519	5	PFUnA_Q112	-20	-10	-17	-25	-18
563	519	5	PFUnA_Q113	-20	-10	-17	-25	-17.5

^a Note that the “_Qxxx” following the compound IDs represent the CV steps, where the IDs labeled “_Q107” correspond to the CV_{opt} for most PFAS. For PFHxS, PFHpS, and PFOS the ID labeled with “_Q110” corresponds to the CV_{opt}, as these compounds contained an extra 6 steps each.

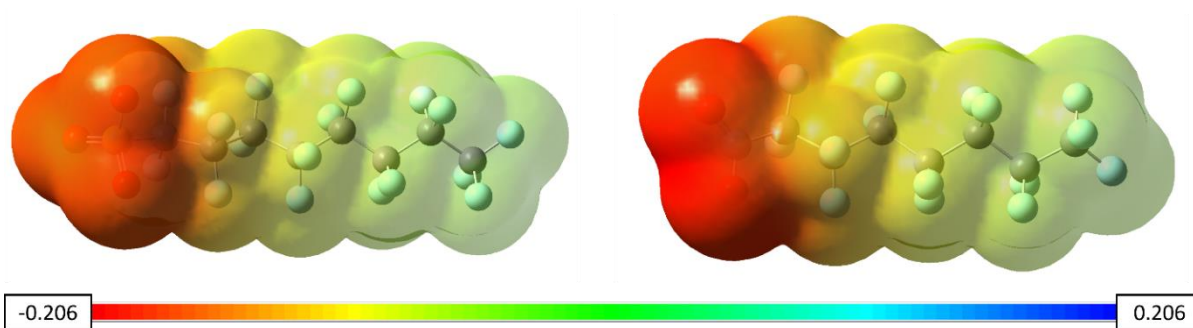


Figure A.1. Electrostatic potential (ESP) surfaces of PFOS (left) and PFOA (right) calculated with Gaussian16 using B3LYP 6-31G(D). Note that the CO₂ headgroup of PFOA exhibits much more electron density (i.e. deeper red) than the SO₃ headgroup of PFOS.

Table A.5 CV shifts of PFAS between LCxDMS and DMS measurements.

Compound	CV _{opt} in DMS (V)	CV _{opt} in LCxDMS (V)	Δ CV _{opt} (V)	% Difference
PFBS	-15.65	-14.53	1.13	7.19
PFPS	-13.57	-12.42	1.16	8.51
PFHxS	-11.93	-10.65	1.28	10.76
PFHpS	-10.77	-9.50	1.27	11.76
PFOS	-9.72	-8.36	1.36	14.03
PFNS	-8.99	-7.69	1.30	14.42
PFDS	-8.24	-7.02	1.21	14.74
PFDoS	-6.83	-5.66	1.18	17.22
PFHxA	-46.87	-45.20	1.67	3.56
PFHpA	-40.14	-38.93	1.22	3.03
PFOA	-34.52	-33.74	0.78	2.27
PFNA	-29.25	-28.79	0.46	1.58
PFDA	-24.84	-24.60	0.25	0.99
PFUnA	-21.01	-20.76	0.25	1.20
PFDoA	-17.74	-17.68	0.06	0.32
PFTTrDA	-14.98	-14.98	0.00	0.02
PFTDA	-12.71	-12.78	-0.06	0.49
PFHxDA	-9.18	-9.22	-0.04	0.46
4:2FTS	-42.61	-40.85	1.76	4.14
6:2FTS	-32.33	-31.20	1.13	3.50
8:2FTS	-24.43	-23.69	0.74	3.04
3:3FTCA	-48.99	-48.77	0.22	0.45
5:3FTCA	-33.02	-32.64	0.38	1.14
7:3FTCA	-23.30	-23.23	0.07	0.32
8:2FTUCA	-26.63	-26.53	0.11	0.11
8:2diPAP	-4.60	-4.35	0.25	0.25
NMeFOSA	-20.85	-18.83	2.03	9.71
NEtFOSA	-16.87	-14.81	2.06	12.21
NEtFOSAA	-14.82	-14.58	0.24	1.59
PFOSA	-19.41	-17.27	2.14	11.04
PFEESA	-12.51	-11.35	1.15	9.20
9Cl-PF3ONS	-3.70	-2.59	1.10	29.87
11Cl-PF3OUdS	-2.60	-1.47	1.14	43.63